Drift tube ion mobility spectrometry laser induced fluorescence detection

zur Erlangung des akademischen Grades eines

Doktors der Naturwissenschaften

– Dr. rer. nat. –

genehmigte Dissertation von

Florian Uteschil

geboren in Siegen

Institut für instrumentelle analytische Chemie

der

Universität Duisburg-Essen

Die vorliegende Arbeit wurde im Zeitraum von April 2013 bis Dezember 2016 im Arbeitskreis von PD Dr. Ursula Telgheder am Institut für instrumentelle analytische Chemie der Universität Duisburg-Essen durchgeführt.

Tag der Disputation: 26.04.2017

Gutachter: PD Dr. Ursula Telgheder

Prof. Dr. Oliver J. Schmitz

Dr. rer. nat. habil. Helko Borsdorf

Vorsitzender: Prof. Dr. Thomas Schrader

Acknowledgements

Abstract

The coupling of ion mobility spectrometry (IMS) and laser-induced fluorescence spectroscopy (LIF) at atmospheric pressure was realized in this work. The construction of a module based drift tube enabled the use of different ionization techniques, as well as the implementation of a laser induced fluorescence detection system and a Faraday plate detector. With the analysis of the ionized dye Rhodamine 6G the system was characterized. For this, a "homemade" electrospray ionization source was used as ion source. At a distance of approximately 9 mm from the ESI tip to the drift tube entrance, a high desolvation rate of gaseous Rhodamine 6G was observed. The length of the drift tube was 3.2 cm. The drift time resolved laser induced fluorescence analysis of ions at ambient conditions on the example of dye Rhodamine 6G was investigated in a simplified IMS drift cell of open design.

Continuous wave radiation at a wavelength of 447 nm and 462 nm was used for excitation. The maxima of the fluorescence were observed at $\lambda = 505$ nm. The drift time resolved fluorescence emission was monitored by a spectrograph in combination with a gated intensified charge coupled device.

The dependencies of Rhodamine 6G fluorescence intensities (continuous ion flow) on the electric fields of both the ion gate field and the drift field were determined at the exit of the 32 mm long drift cell. With increasing gate voltage, the signal intensity decreased. With an electrospray flow rate of 300 nL min^{-1} and a laser diode with 462 nm used as excitation source, a gate voltage of $\geq$ 50 V was required to block or deflect fluorescent ions of Rhodamine 6G in the drift cell. The increase of the fluorescence intensity was proportional to the electric field strength in the range of 510 - 638 V cm^{-1}.

Drift time dependent (pulsed ion flow) LIF analysis was performed under optimized conditions (462 nm, ESI flow rate 300 nL min^{-1}, gate voltage 80 V, ICCD integration time: 100 μs). The drift time spectra produced with both, the Faraday plate detector and the laser induced fluorescence detector showed the same trends. Significantly smaller FWHM were found with the LIF detector as compared to that found with the electrometer.

Based on the findings of the experiments with Rhodamine 6G, the experimental setup for PAH analysis was designed and developed. A unidirectional flow, closed, heated (up to 200° C) drift

tube (length: 16.8 cm) ion mobility spectrometer with photoionization source (VUV Kr, 10.0/10.6 eV) was implemented in a pulsed laser induced fluorescence detection system. With this setup it was possible to investigate the dependence of the fluorescence intensity of selected PAH (continuous ion introduction) on the experimental parameters such as: PID-lamp current, ion gate voltage, electric field strength in the drift tube.

The fluorescence intensity was dependent on the PID lamp current. The rise of both the fluorescence intensity and the continuous ion current with the increase of the PID lamp current was observed. The simultaneous decrease of both the total ion current and the fluorescence intensity with the increase of the ion gate voltage was monitored. The generated by photoionization ions could be transported through the drift region and detected with the laser induced fluorescence monitoring system. The LIF signal intensities increased proportional to the drift field strength in the range of $157 - 265$ V cm^{-1}.

Zusammenfassung

Im Rahmen der Arbeit wurde die Kopplung der Ionenmobilitätsspektrometrie (IMS) und der Laser-induzierten Fluoreszenzspektroskopie (LIF) unter Atmosphärendruck realisiert. Die Konstruktion einer modulartig aufgebauten offenen Driftröhre ermöglicht die flexible Anpassung an unterschiedliche Ionenquellen sowie an die LIF-Zelle und Faraday-Platte als Detektionssysteme. Anhand der Analyse des ionisierten Farbstoffs Rhodamin 6G in der Gasphase konnte das System charakterisiert werden. Für diese Untersuchungen wurde eine „homemade" ESI-Einheit als Ionenquelle eingesetzt. Eine ausreichend hohe Rate desolvatisierter Rhodamin 6G-Ionen wurde mit einer Distanz von 9 mm zwischen ESI-Spitze und Eingang der Driftröhre erreicht. Die Länge der Driftröhre beträgt 3,2 cm.

Die Anregung der Rhodamin 6G-Ionen in der Gasphase erfolgte mit kontinuierlicher Strahlung bei den Wellenlängen $\lambda = 447$ nm und $\lambda = 462$ nm. Die maximale Intensität der Fluoreszenzstrahlung wurde bei $\lambda = 505$ nm gemessen. Die driftzeitaufgelöste Fluoreszenz wurde mittels eines Spektrographen in Kombination mit einer ICCD-Kamera detektiert.

Untersuchungen zur Abhängigkeit der Fluoreszenzintensität bei kontinuierlichem Ioneneintrag von der Gitterspannung und der Driftspannung zeigen, dass mit ansteigender Gitterspannung die Signalintensität abfällt. Bei einer Flussrate von 300 nL min^{-1} und einer Anregungswellenlänge von $\lambda = 462$ nm muss die Gitterspannung größer als 50 V sein, um den generierten Rhodamin 6G-Ionenstrom zu sperren. Bei den genannten Bedingungen verhält sich die Fluoreszenzintensität proportional zur elektrischen Feldstärke in der Driftröhre (510 – 638 V cm^{-1}).

Im gepulsten Betrieb wurde die driftzeitaufgelöste LIF-Analyse unter optimierten Bedingungen ($\lambda = 462$ nm, ESI-Flussrate: 300 nL min^{-1}, Gitterspannung: 80 V, ICCD-Integrationszeit: 100 µs) durchgeführt. Der Vergleich mit Driftzeitspektren, die mittels Faradayplatten-Detektion erhalten wurden, zeigt, dass die Halbwertsbreiten der LIF-generierten Signale signifikant geringer sind, als die mit der Faradayplatten-Detektion generierten Signale.

Die so gewonnenen Erkenntnisse führten zur Entwicklung und Konstruktion des experimentellen Aufbaus für die Detektion von polykondensierten aromatischen Kohlenwasserstoffen (PAH). Für die Untersuchungen wurde eine beheizbare (bis zu T = 200 °C) Driftröhre (Länge: 16.8 cm) mit einer Photoionisationsquelle (VUV Kr, 10.0/10.6 eV) entwickelt. In das geschlossene

Ionenmobilitätsspektrometer wurde ein gepulstes LIF-System integriert. Mit diesem Aufbau war es möglich, die Abhängigkeit der Fluoreszenzintensität ausgewählter PAHs (kontinuierlicher Ionenstrom) von experimentellen Parametern, wie z.B. Lampenstrom (PID), Gitterspannung, elektrische Feldstärke in der Driftröhre, zu untersuchen. Mit zunehmendem Lampenstrom steigen die Fluoreszenzintensität sowie der kontinuierliche Ionenstrom. Mit steigender Gitterspannung nehmen die Fluoreszenzintensität sowie der kontinuierliche Ionenstrom ab. Die Fluoreszenzintensität verhält sich proportional zur elektrischen Feldstärke in der Driftröhre (157 – 265 V cm^{-1}).

Table of Content

1   General introduction

The Ion Mobility Spectrometry (IMS) has shown to be a sensitive analytical method, but the specific information obtained about the analytes is limited. Because IMS is a gas-phase separation technique it is often compared to mass spectrometry (MS). This is unfortunate because when IMS resolution is compared in MS terms, the instruments have a peak position to peak width ratio of around 30.[1] The resolution of commercial available IMS instruments is lower in comparison to e.g. gas-chromatographic techniques. In chromatographic terms, the plate number of IMS instruments is around 5000.[1] Therefore, the Laser Induced Fluorescence (LIF) is a promising technique that can enhance both, the resolution and the sensitivity of IMS instruments. The LIF provides an orthogonal arrangement to IMS. The detection of ions in IMS instruments is conducted with high-gain transimpedance amplifiers. The bandwidth of such operational amplifiers is inversely proportional to the gain and therefore physically limited. The optical-electronic detection is known to be fast up to femtoseconds and there are no limits of amplification due to electronic amplifier. Additionally, emission spectra of the separated ions are obtained by LIF at different excitation wavelengths.

This work demonstrates the feasibility of the coupling of two orthogonal methods, namely drift tube ion mobility spectrometry and laser induced fluorescence spectroscopy. The capability of Ion Mobility Spectrometry with Laser Induced Fluorescence detection (IMS-LIF) is investigated on example of the dye of Rhodamine 6G and polycyclic aromatic hydrocarbons (PAH).

1.1   *Principle of Ion Mobility Spectrometry*

The motion of ions in gases, described by Albritton and McDaniel was further investigated by Karasek and was called plasma chromatography.[2] However, the main working principle of a plasma chromatograph described by Albritton, McDaniel, and Karasek can still be found in state of the art IMS instruments. The main principle is the separation and detection of gaseous organics in form of ions at ambient conditions. The stand-alone IMS instruments are powerful for the rapid and sensitive detection of different substances, acting as a chemical sensor. The technique is advantageous due to its simplicity. Since IMS can work at ambient pressure, high vacuum systems (e.g. used in mass spectrometry) are not necessary. The analysis is typically performed within the time range from several milliseconds (ms) up to several tens of ms resulting in so-called drift time

spectra. Compared to capillary gas chromatography, the separation takes place on a much shorter time scale. Ion mobility spectra are generated by the detection of ion swarms drifting through a bath gas under the influence of an electrical field. After the gaseous sample introduction and ionization, ion injection takes place periodically through a shutter with pulse widths from 50 up to 1000 μs. The ion swarms drift in a gaseous atmosphere (typically nitrogen or ambient air) towards a faraday plate detector driven by voltage gradient. The velocity of the ion swarms can be correlated with their molecular structure, mass, charge, and collision cross section. These parameters can be calculated from the size, mass, charge, position of charge and charge distribution.[3] Due to the differences in these parameters the ion swarms have characteristic drift velocities providing the separation of charged particles.[4] The drift velocity is proportional to the electric field strength (E) and called ion mobility coefficient K:

$$K = v_d E^{-1} [cm^{-1}Vs^{-1}]]$$ (1)

The ion mobility coefficient normalized to ambient conditions with a pressure of 760 Torr (1 atm) and a temperature of 273 K (25° C) is called reduced ion mobility coefficient K_0:

$$K_0 = K \left(\frac{273}{T}\right) \left(\frac{P}{760}\right)$$ (2)

Determination of the chemical identity requires the precise assignment of ion swarm velocities (mobility). The identity of mono- and diatomic gases in pure „bath gases" to mobility coefficients were performed under subambient conditions.[5] Based on these works the ion mobility coefficient was determined as:

$$K = \frac{3_e(2\pi)^{\frac{1}{2}}(1 + \alpha)}{16N(\mu k T_{eff})^{\frac{1}{2}}\Omega_D(T_{eff})} \tag{3}$$

where e is the elementary charge; N (number of density) is the numerical parameter for the gas density of the used neutral (drift) gas in number of molecules per cm³; α is the correction factor; μ is the reduced mass of the ions and the used drift gas molecules; T_{eff} is the effective temperature of the ion in K, (the thermal energy and the received energy from the electric field), and $\Omega_{eff}(T_{eff})$ is the collision cross section in nm² at T_{eff}.[6]

IMS can be used as a pre separation step prior to mass spectrometry. The separation based on size and the subsequent analysis based on mass gives two-dimensional data for each ion. The ratio of the collision cross section to the charge Ω/z is used instead of the mass/charge ratio m/z:

$$\frac{\Omega}{z} = 0.265 \left(\frac{\pi}{kT}\right)^{1/2} \left(\frac{1}{m} + \frac{1}{M}\right)^{1/2} \frac{t_d E}{L} \frac{760}{P} \frac{T}{273} \frac{e}{N_o} \tag{4}$$

where Ω is the collision cross section in A², z is the number of charges of the ion, k is the Boltzmann constant, T is the temperature of the buffer gas, m is the mass of the ion, M is the mass of the buffer gas molecules, t_d is the drift time of the ion in milliseconds, E is the electrical field in the ion mobility drift tube, L is the length of the drift tube in cm, P is the pressure of the buffer gas (in torr) in the drift region, e is the electron charge, and N_o is the number density under standard temperature and pressure conditions.

1.2 *Ion Mobility Spectrometry Instrumentation*

An Ion Mobility Spectrometer consists of three main parts, namely (1) inlet, (2) drift tube, and (3) detector. Each of main parts consists of two or more components: (1) the inlet consists of a sample inlet system and an ionization source; (2) the drift tube consists of an ion injection system, drift rings, and insulator rings; (3) the detector consists of a faraday plate detector and an aperture grid. In the following each of these components will be presented in details.

1.2.1 Sample inlet

Numerous sample inlet constructions are described in the literature. The focus lies on the transfer of the sample into the gas phase (if needed) and the efficient transport to the ionization region of the IMS inlet. Solid, liquid, and gaseous samples can be analyzed using suitable systems for IMS. Solid samples can be thermally desorbed, pyrolized or laser ablated prior to the transfer to the ion source. Introduction of analytes from the liquid phase can be conducted directly using a sample wire, membranes, solid phase micro extraction (SPME), electrospray- or coronaspray ionization, or liquid chromatography. The gaseous sample introduction can be realized directly, through membranes or with a gas chromatograph. The introduction for samples of different aggregate form for IMS analysis is described below in details.

1.2.1.1 Solid samples

Solid samples need to be vaporized or require sample preparation. Either a solid sample is collected from a surface that can be heated to vaporize the sample[7] or the particulate solids get collected from various surfaces with a tube containing a collection mesh and a pump drawing the particulates into the tube.[8] In both cases, heat is applied to the collected material to desorb and/or vaporize the solid sample. During the heating program the carrier gas transports the sample to the ionization source. Another approach is the ablation and ionization with a pulsed laser (266 nm) focused on the solid sample surface (ø 0.2 mm, 6mJ/pulse).[9]

1.2.1.2 Liquid samples

Liquid samples need to be vaporized or the analyte of interest is extracted from the solution. A well applied method is the permeation tube[10] inlet since it is an accepted method for the calibration of instruments that detect or sense gases.[11] The permeation tube method for liquid sample introduction in IMS instruments is suitable for alkanes and aromatic compounds.[12] Headspace sample introduction of aliphatic and aromatic amines has been proven by means of IMS.[13] A typical analytical method to analyze the dissolved compounds of interest is the solid phase extraction of analytes from liquid solution. For example, aqueous solutions of diazepam and cocaine have been extracted by means of solid phase microextraction (SPME) prior to IMS analysis.[14]

The development of alternative ion sources including electrospray and coronaspray, led to the extension of analytes accessible by IMS. Electrospray ionization is the direct ionization from liquid

solution and is therefore a useful method for sample introduction in mass- or ion mobility spectrometers. Electrospray ionization firstly implemented by Dole[15] has been used by several groups as ion source for IMS instruments. The miniaturization of ESI (nano-ESI) was described by Wilm and Mann.[16] The main advantage of nano-ESI as compared to ESI was improved due to lower sample volumes. Liquid chromatography-nESI-IMS was used for analysis of active pharmaceutical ingredients .[17]

1.2.1.3 Gaseous samples

Since the linear range is limited for commonly used radioactive ion sources, dilution methods may be used to reduce the sample concentration in the carrier gas stream.[18] Using purge vessels and glass flasks, dilutions of volatile organic compounds in the gas phase can be realized by means of adjustment of gas flows entering the inlet of an IMS instrument.[19] Headspace analysis require the sample handling at a constant temperature as well as temperature controlled injector and transfer line for the vapor phase.[20] Other gas inlet systems use direct injections with a syringe, a syringe pump or a membrane inlet system[21] which is often equipped with a pump for continuous recirculation of air or other gas of interest. Commercially available IMS instruments are often equipped with a gas chromatograph as pre separation system. Attempts to couple gas chromatography to a bidirectional gas flow IMS were only marginally successful.[1] An interesting approach was the implementation of an unidirectional gas flow to reduce the amount of neutrals swept into the drift region.[22] In this study the IMS was used as a detector for two-dimensional gas chromatography (GC-IMS). The received signals were analyzed by both, a retention time and a drift time.

Ionization sources

1.2.1.4   Radioactive sources

Most of plasma chromatographs or ion mobility spectrometers use ^{63}Ni foil as ionization source. ^{63}Ni and Tritium (^{3}H) are most commonly used β-emitters. ^{63}Ni emits high energy electrons which lose their energy by collisions with drift gas molecules. In nitrogen drift gas, the initially formed N_2^+ initiates a series of reactions resulting in reactant ion positive (RIP) formation:[23]

1. $N_2 + e^-$ $\rightarrow$ $N_2^+ + 2e^-$
2. $N_2^+ + 2N_2$ $\rightarrow$ $N_4^+ + N_2$
3. $N_4^+ + H_2O$ $\rightarrow$ $H_2O^+ + 2 N_2$
4. $H_2O^+ + H_2O$ $\rightarrow$ $H_3O^+ + OH$
5. $H_3O^+ + H_2O + N_2$ $\rightarrow$ $H^+(H_2O)_2 + N_2$
6. $H^+(H_2O)_{n-1} + H_2O + N_2$ $\rightarrow$ $H^+(H_2O)_n + N_2$
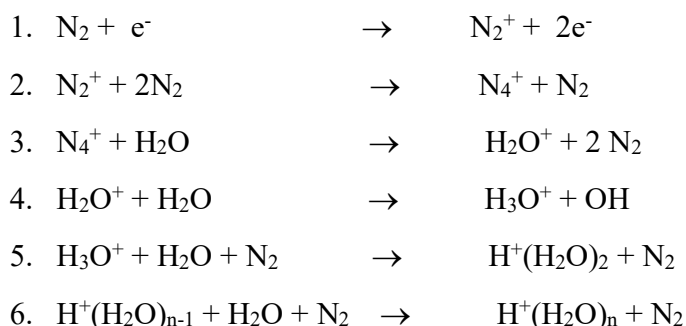
The number of water molecules clustered with the proton (Eq. 6) is determined by the concentration of water molecules in the gas phase, the temperature, and the field strength. Another reactive ion $(H_2O)_yNO^+$ can be formed by the following reactions:[24]

1. $N_2^+ + O$ $\rightarrow$ $NO^+ + N$
2. $NO^+ + yH_2O + N_2$ $\rightarrow$ $(H_2O)_yNO^+ + N_2$
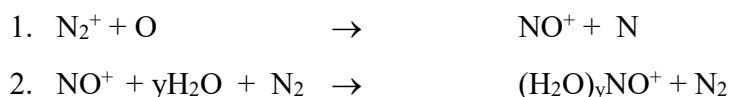
The $H^+(H_2O)_n$ can undergo proton transfer reactions with impurities of high proton affinity e.g ammonia. Origin of the ammonia can be contaminations of the drift gas or outgassing of the used materials.

1. $NH_3 + H^+(H_2O)_n$ $\rightarrow$ $NH_4^+ + nH_2O$
2. $NH_4^+ + H_2O + N_2$ $\rightarrow$ $(H_2O)NH_4^+ + N_2$
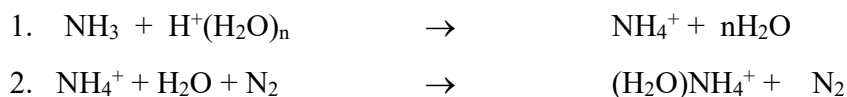
O_2^- clustered with water has been shown to be the negative reactant ion when ionization is performed in presence of oxygen traces.[25] Since the electron affinity of chloride ions is greater than of oxygen, charge transfer from oxygen ion to chlorine neutrals is possible.

1.2.1.5 Photoionization

Excited gases can emit a short-wavelength high frequency irradiation. Tanaka und Zelikoff[26] showed the spectral bands emitted by excited rare gases; for example 123.9 nm und 116.9 nm for krypton. These values are equivalent to 10.0 eV and 10.6 eV. There is a difference between direct current glow discharge (DC) and radio frequency alternating current (RF) gas discharge lamps. In the case of DC-discharge the lamp emits continuously, whereas in the case of the RF-discharge the operating current for excitation and the lamp emission are pulsed within the radio frequency range. The natural resonance frequency of the gas in the lamp is excited by the glow discharge, resulting in very stable, precise photon energy within vacuum ultraviolet range. The Photoionization discharge lamps (PID-lamps) are frequently used in analytical chemistry, e.g in gas chromatography detectors[27], for the mobile detection of volatile organic compounds (VOC) in the atmosphere[28], in instruments for the high performance liquid chromatography (HPLC) coupled to tandem mass spectrometry.[29] Additionally, the dopant-assisted photoionization may improve the sensitivity of the detector and the whole method.[30]

1.2.1.6 Principle of APPI / DA-APPI

When the ionization potential (IP) of a compound M is smaller than the energy of the absorbed radiation, an electron is removed from M resulting in formation of radical-cation

$$M + h\nu \rightarrow M^{+\cdot}$$
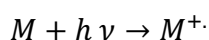
Radical-cations have a free unpaired electron, tending to form bonds with surrounding molecules such as abstracted hydrogen from organic molecules.

$$M^{+\cdot} + RH \rightarrow MH + R^{+\cdot}$$

$$M^{+\cdot} + H\cdot \rightarrow MH^+$$
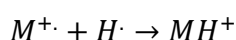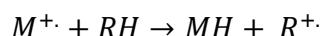
The radical cation in turn can recombine with free electrons and may return to its neutral state

$$M^{+\bullet} + e^- \rightarrow M$$
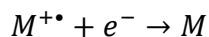
Using dopant-assisted photoionization, a supporting compound with appropriate IP gets ionized and can ionize the compound of interest ($D_{IP} > M_{IP}$)

$$D + h\nu \rightarrow D^{+\cdot} + e^-$$

$$D^{+\cdot} + M \rightarrow D + M^{+\cdot}$$
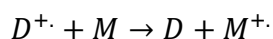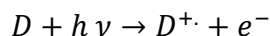
The dopant can react with other dopant molecules via protonation. The dopants provide H and are signed as minus (-) H.

$$D^{+\cdot} + D \rightarrow DH^+ + [D - H]^{\cdot}$$

This has been shown on example of acetone.[31] When the proton affinity (PA) of the analyte is higher than the PA of the protonated dopant, proton transfer reactions can occur.

$$DH^+ + M \rightarrow D + MH^+$$
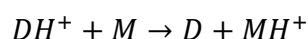
IMS with photoionization has been used to determine methyl-tert-butyl ether, benzene, toluene and *m*-xylene in water.[32] Dopant assisted photoionization IMS in negative mode using acetone and toluene as dopants has been shown to ionize explosives[33]. Ionization proceeds via formation of hydrated CO_3^- clusters in the presence of ~300 mg/L CO_2 in purified air.

In case of the analysis of aldehydes and poly-condensed nitrogen containing heterocyclic compounds the photoionization mechanism is not completely understood.[34]

However, photoionization of aromatic compounds is well suited. The photoionization is favored due to the good charge stabilization by aromatic compounds and proceeds via π-electron systems.[35]

1.2.1.7 *Electrospray ionization*

Gas-phase ion mobility spectrometer has first been coupled to ESI by Chapman 1937.[36] Because of the insufficient ion's desolvation the ESI was found to be useful only for mass spectrometry applications. Attempts to overcome the problem were made by several authors using heated nitrogen as drift gas with an unidirectional flow to increase desolvation efficiency,[37] cooling of the electrospray needle to prevent solvent evaporation in the capillary[38] and additional heated gas flows in the desolvation region.[39] Liquid chromatography effluents (with flow rates up to 200μL min^{-1})

were introduced in an IMS by means of ESI using a t-cylindrical inlet called orthogonal electrostatic ion-deflection device.[40] Due to this inlet system, spectra were less affected by solvent drops generated by the ESI used at continuous sample flow mode. This mode is typical for liquid chromatography (LC). Improved ESI-IMS design enable the analysis of amines, narcotics, pesticides and neurolepticals.[39, 40b]

1.2.2   Ion injection

The first pulsed introductions of charged particles into electric fields have been described by Cravath.[41] The same experimental setup has been used by Bradbury and Nielsen, to determine the mobility of electrons in hydrogen.[42] These publications are fundamental for the usage of ion gates in commercially available IMS coupled with time of flight mass spectrometers (IMS-TOF-MS). An ion shutter according to Bradbury and Nielsen consists of two sets of thin wires in an interdigitated arrangement close to each other. The wires are typically of about 0.05 mm diameter and placed in a distance of about 0.5 mm between the wires centers. The two wire sets are placed in a drift tube perpendicularly to the electric field gradient and are electrically insulated from neighboring ring electrodes. When a potential is applied between two wire sets a closing electric field is generated between the wires. The direction of the closing field is perpendicular to the drift field. Therefore, it is required that one wire set is always held at a potential suited to the electric field gradient generated by the voltage divider. The ion gate setup according to Bradbury and Nielsen are used for pulsed ion injection in TOF-MS.[43] Tadjimukhamedov investigated the electric fields in the drift tube as well as between the gate wires and compared the required ratios between these electric fields according to simulations and experimental data.[44] The deviations between simulations and experimental data were explained by the complicated fabrication of ideal working ion gates.

The switching electronics for the ion injection into a drift tube usually require custom electronics.

The injection systems used in ion mobility spectrometry are described below.

1.2.2.1   *Bradbury-Nielsen-Gate (BNG)*

An ion shutter built according to the design of Bradbury and Nielsen. It consists of two wire sets separated in a non-conductive frame in one plane. This part of an IMS provides periodically working pulsed ion injection into the drift region of an IMS. It transmits small portions of ions

when the potential difference between the grid wires is zero and deflects the ions when the potential difference between the grid wires is applied. Mechanical and electrical isolation especially at high temperatures is difficult due to thermal expansion of the used materials. Wires can be bonded to ceramic frames with high temperature epoxies.[45]

1.2.2.2   Tyndall-Powell-Gate

An ion gate built according to Tyndall and Powell. It consists of two grids with parallel wires placed in separate planes within a distance range of 0.01 – 1 mm to each other. The wires of the grids are arranged in a parallel and interdigitated pattern. The advantage of this ion gate type is the appropriate manufacturing procedure. The main disadvantage is the limited permeability of ions. The permeability of ions is limited by the distance of the two wire sets arranged in the axial plane of the IMS.[46]

The permeability of BNG is usually higher compared to the Tyndall-Powell design. The ions swarms generated with a BNG are usually sharper than those generated with a Tyndall-Powell gate.

1.2.2.3   Ion grid function

"The grid is "on" (ions are transmitted) when the two wire sets are at equal potentials corresponding to the uniform drift-field potential at the location of the grid, and the grid is "off" (ions are not transmitted), when the two sets of wires are at differential potential equally displaced above and below the uniform drift-field potential at the location of the grid. In the "on" condition ions are conducted through the grid, but in the "off" condition ions are not conducted through the grid. The grid is driven by a square pulse generator coupled with opto-isolator circuitry to the high-voltage supply biasing the cell."[47] The voltage difference between the wires establishes an electric field across the drift tube to draw the ions to the wire surfaces, resulting in neutralization of the ions. When the electric field is removed the ions can pass through the grids and ion mobility spectra can be recorded. After a short period of time (typically 100-400 μs) the electric field between the wires is established again and ions are hindered from passing the ion shutter. The example of the voltage control arrangement is shown in Figure 1. There are two possibilities to switch the ion grid. The first possibility is when one wire set is held at constant potential while the other wire set is pulsed from high to low potential. Alternatively, in "off" mode both of wire sets are at potentials equally

displaced above and below the uniform drift-field potential at the location of the grid (Vref+ΔV; Vref-ΔV) and in "on" mode the common gradient potential is applied to the wire sets (Vref).
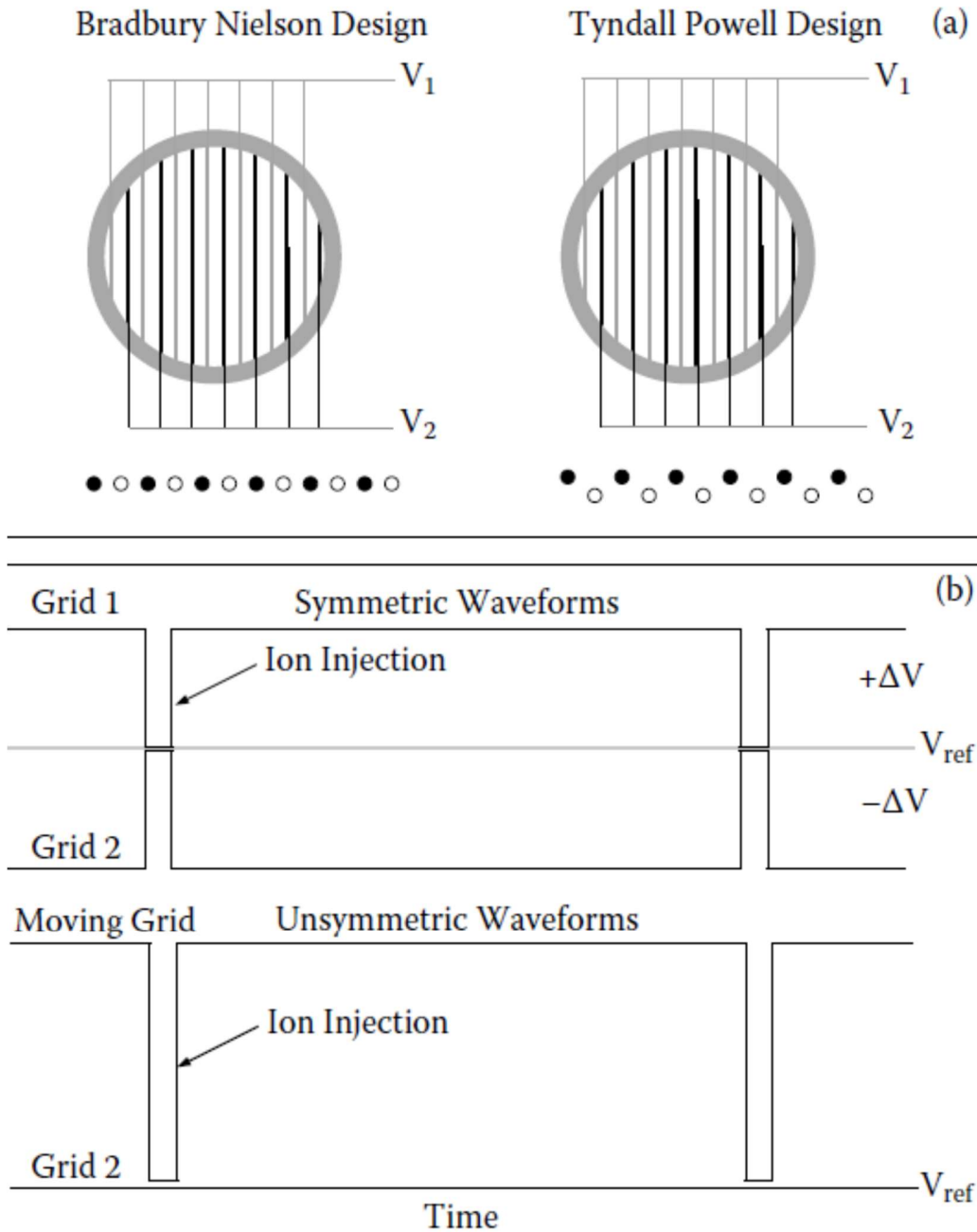
Figure 1 Designs of ion shutters with Bradbury–Nielsen on left and Tyndall–Powell on right with end view and side view (a). Two waveform plans (b); a waveform is applied to each grid. A voltage difference on adjacent wires creates an electric field, and ions are drawn to wires and collide. Resultant neutrals are swept with drift gas from the analyzer. In each plan, wires are brought to a common potential, which is referenced to the voltage divider of the drift tube.[45]

1.2.2.4 Gridless methods for ion injection

The presence of wires inside the cross section of the drift tube drastically complicates the manufacturing of IMS instruments. To overcome these problems other injection methods are proposed e.g. field switching method, mechanical ion injection as well as injections with pulsed ionization source (pulsed corona discharge, xenon-flash lamps, and pulsed laser systems).[48]

1.2.3 Drift Rings

The central component of ion mobility spectrometer is the tubular arrangement of rings forming a drift tube that is supported by other components including the power supplies, shutter controllers, heaters, detector electronics and gas flows. The design of the drift tube separated in sections, e.g. ion source, drift and detection region, is found in almost every classical drift tube ion mobility spectrometer. A stacked tube of an alternating arrangement of conductive and non-conductive rings is the mostly used design for IMS devices with a linear voltage gradient. McDaniel's design of a research grade IMS was based on stacked rings and become the first IMS with a convenient vapor sample inlet.[2b, 49] The stacked ring design was further improved for the coupling of capillary gas chromatography with IMS. The diffusion of neutrals into the IMS and the sample residence time in the ion source and reaction region were reduced by construction of a pneumatically "tight" drift tube and an unidirectional gas flow, respectively.[22] The electric field within the drift region is linear, uniform, and within the range of several 100 V cm^{-1}. However, the electric field straight in the source, reaction and shutter regions can be different to that in the drift region. The homogeneity of the electric field and the effects of drift tube designs (including the source, shutter, and housing components) can be modeled by computer based simulations.[50] The influence of the thickness of drift rings and insulator rings on the homogeneity of the electric field has been investigated by Liu et al.[51] It was found that the homogeneity decreases with increase of the drift rings thickness. Therefore, the drift rings should be infinitely thin. However, the ring thickness is limited by electrical connections and the design of the voltage divider attached to the drift rings. The construction of drift region with rings of very small thickness becomes inconvenient. The compromise is a drift ring with a thin inner electrode part of ~ 1 mm thickness and an outer electrode part of several mm thicknesses to provide an appropriate electrical contact. The insulators can be designed in an interlocking design as shown by Gormally and Philipps.[52] Spangler et al. used a thick film resistor ink layer inside a ceramic tube to provide a total resistivity of 10-20 MΩ.[53]

A comparable technology uses the monolithic resistive glass tube producing a radial homogeneity of the electric fields across the tube.[54]

1.2.4 Ion detection

1.2.4.1 Faraday plate detector

The Faraday cup is the most common ion detector for the detection of ion currents at vacuum. Under vacuum conditions, the energy of ions that hit the plate is high enough to knock the secondary ions or electrons out from the metal surface of the Faraday cup, resulting in decreased ion detection efficiency. To avoid the loss of charged species, the detector has a cup shape to trap the secondary ions and electrons. . At ambient pressure conditions, the energy of the ions is not sufficient to produce secondary ions and the ions can be collected by a flat plate. This fact makes the detector construction and interfacing to the drift tube much easier. When positively charged ions arrive at the detector, electrons from the Faraday plate will be shifted to the detector surface to compensate the positive charge of the ions. This induces a current that will be registered by the electrometer. Because the charged ion swarm produces the electric field, this current may be generated even before the ions arrive at the Faraday plate surface. This results in an earlier response of the electrometer leading to the peak fronting. Therefore, the recorded signals may have a broader peak shape resulting in decreased resolving power. This effect can be avoided by utilization of an aperture grid that prevents the detection of induced charge from ions approaching the detector surface. An aperture grid can be placed in front of the Faraday plate to shield the detector plate from the field induced by approaching ions. In the ideal assembly, the Faraday plate is placed closely between the aperture grid (0.5 – 2 mm distance[18]) and the last ring electrode representing the terminal electrode for the drift gradient. The aperture grid and the last electrode are placed at electrical potential above and below the Faraday plate, respectively. The voltage bias is chosen so that a field of 300-600 V cm^{-1} is established between the aperture grid and the Faraday plate. When ions pass the aperture grid, the aperture grid and the terminal electrode focus the approaching ions onto the Faraday plate. The combination of aperture grid and the detector plate can act as a capacitor. Therefore, a ballast capacitor is added between the aperture grid and the ground potential. This capacitor serves as a source of electrons for the aperture grid. The role of capacitor is to drain the induced current to ground.[55] Spangler described the effects of ionic charge induced current detection in Ion mobility spectrometers:
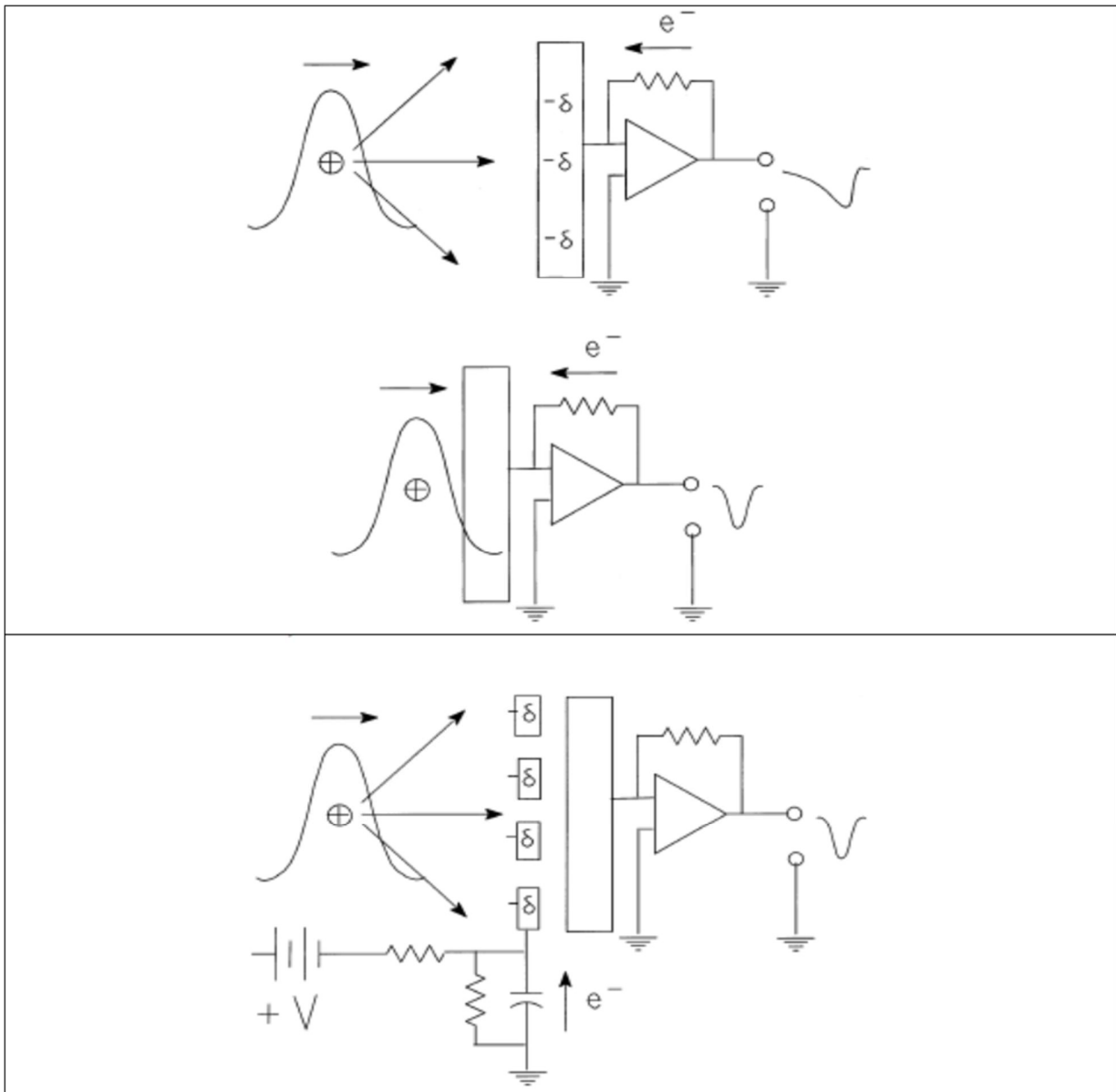
Figure 2 Ionic charges at different detector designs. Adapted from [55] (top figure) Illustration of an ion pulse approaching and hitting the detector of an IMS. The ionic charge induces surface charge on the faraday plate. Electron flow occurs before and after the ion injection hits the faraday plate. (bottom figure) An aperture grid shields the faraday plate from induced charge. A capacitor is used as electron source for the aperture grid

1.2.4.2 Transimpedance amplifier

The detector plate is typically coupled to the inverting input of an operational amplifier. The collision of ions on the detector plate results in a current flow within the range of $10^{-10} - 10^{-11}$ A that is amplified and converted to voltages within the range of $1 - 10$ V.[18] The commercially available Faraday cups are adjusted to the demands of the mass spectrometery. Ion beams in a mass spectrometer can be as low as a few fA (1 fA = 6.242 ions s^{-1}), hence an amplification of $10^9 - 10^{13}$ is necessary. The large feedback resistance required for this gain produces a slow signal accompanied by a high electronic noise.[45]

For ambient pressure applications, only Faraday plate detectors are commonly used, limited by thermal (Johnson) noise from the connected electronic of the instrument. The two commonly used detectors in low pressure or vacuum conditions are the continuous dynode electron multipliers and the multichannel plate detector. The detectors are frequently used in mass analyzers. A selection of ion mobility analyzers coupled to mass spectrometry is described below.

1.2.4.3 IMS-MS

The first investigation of ions drifting in a low electric field at "low" pressures (0.7 torr) by means of magnetic sector mass spectrometry were reported by McDaniel et al 1962.[56] The first drift-tube-IMS-time-of-flight mass spectrometry (TOF-MS) coupling has been reported by McKnight et al.[57] Quadrupole Instruments have been employed as IMS detector by Albritton and McDaniel.[2a, 58] The objective of these first mass-spectrometric to drift tube IMS couplings was the investigation of ion-molecule reactions in specified buffer gas conditions. The first step towards IMS-TOF-MS analysis was the investigation of ion families with multiple charging. IMS spectra are typically recorded on the millisecond time range while mass spectra are usually recorded in microseconds. The drift field used in IMS for accurate calculations of collision cross sections is usually <10 Td to be within the low field conditions. At these conditions the ion mobility is proportional to the electric field strength. The resolving power of an IMS is dependent of the number of collisions. That is why instruments working at reduced pressure have an increased drift tube length. Due to the higher radial diffusion of the ions at atmospheric pressure a larger inner diameter of the drift tube is

required. This increases the size and complexity of the instrument. The advantage of low pressure systems is the possible use of ion trap injection and ion focusing devices e.g. ion funnels.

The first ambient pressure ion mobility drift tube was interfaced to an MS by Cohen.[49] During the following development of IMS as an analytical tool, drift tubes at ambient pressure have been interfaced to a variety of MS. The most frequently used mass spectrometer is the quadrupole mass spectrometer which was firstly interfaced to ambient pressure drift tube IMS instruments by Karasek in cooperation with Franklin GNO corporation.[59] IMS-quadrupole MS can provide a sensitive and mass selective method for the detection of single compounds or target compounds in complex mixtures. With huge effort ESI-IMS has been coupled to high resolution ambient pressure IMS[36-37, 38-40] and initially evaluated by the orthogonal TOF-MS detection.[60] Recently, ambient pressure drift tubes have been coupled to TOF-MS as commercially available instrument (also known as IM-MS).[61] This instrument was used for identification and quantification of specific metabolites (here: E.coli digest with > 100 metabolites detected by IM-MS in seconds).[62] The interfacing between drift tube and MS can be complicated due to the need of ion guide systems that focus selected ions into the mass spectrometer.

Trapping mass spectrometers do not require the pinhole but the so-called two ion gate system needs to be used to select specific mobilities in the trap.

Differential mobility spectrometry (DMS) and field asymmetric IMS (FAIMS) are used as pre-filters for ions in atmospheric pressure ionization mass spectrometry.[63]

1.2.4.4 Optical Detection

An alternative approach for the detection of gas phase ions at ambient pressure is the charged particle detector in form of a modified charge coupled device[64]. The CCD is modified by replacing the photosensitive layer by a metal-oxide semiconductor capacitor[65]. The pixel well is designed to hold up to 1×10^6 electrons producing a maximum voltage of 2 V yielding 2 $\mu V/e^{-66}$.

The presented study starts with the laser induced fluorescence detection of gaseous ions at atmospheric pressure. This novel detection system for ion mobility instruments could pose another

dimension by means of spectral information and is potentially able to detect ions on a faster time-regime than the transimpedance amplifiers used in IMS.

1.3 *Excursion - Laser Induced Fluorescence Emission*

Since nothing has been published of the combination of laser induced fluorescence with drift tube IMS the principles of LIF are brought in the framework.

Fluorescence is the emission of one or more photons by molecules or atoms activated by electromagnetic irradiation. The activating photons with a frequency v will get absorbed when the energy of the photon ($E = h\ v$) corresponds to the atom's excitation energy. The energy is transferred to one of the atom's electrons and the energy excess is dissipated by the emission of another photon of the same or different frequency. The processes occurring from absorption to emission can be given in the Jablonski scheme.

Figure 3 Jablonski scheme from[67]
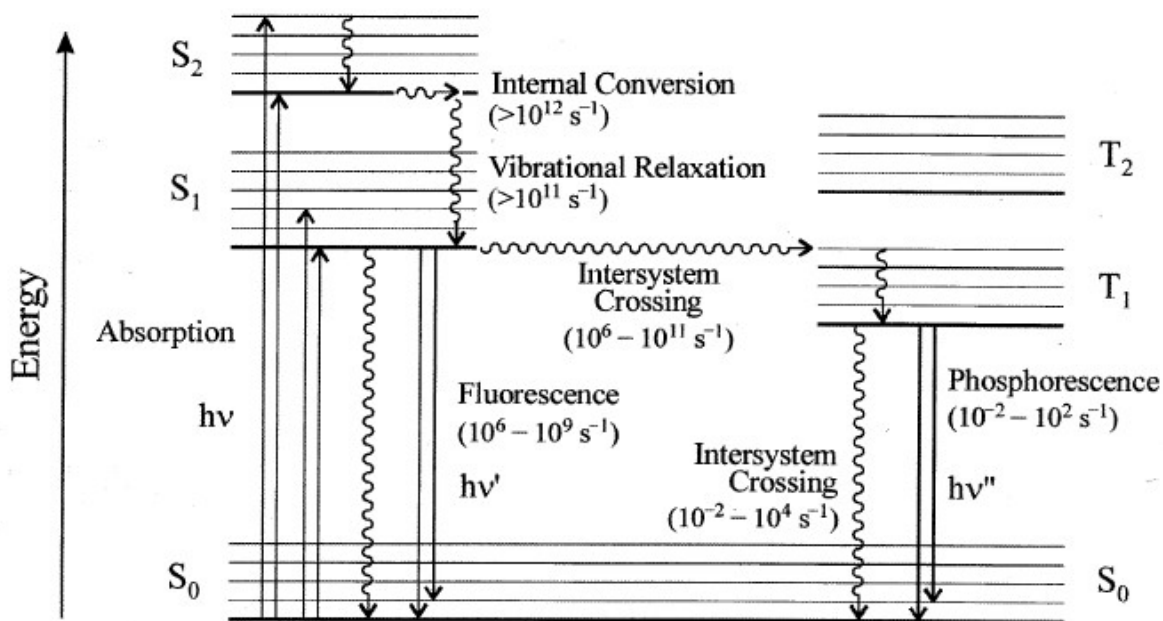
In the diagram, the electronic singlet and triplet states are drawn in two columns. The vibrational sublevels are shown schematically as well. In the ground state the molecule is on the lowest vibrational level of S_0. The degree of the absorbed energy determines the population of the vibrational levels of S_1 or S_2. Vibrational relaxation is the transition from an energy level higher

than the lowest vibrational level of the first electronic state S1 to the 0 vibrational level of S1. This can occur in solution within a time scale of $10^{-13} - 10^{-11}$ s. Internal Conversion is the transition (non-radiative with the same electron spin multiplicity) from higher singlet excited states than S1 towards the 0 vibrational level of the singlet S1 state. The internal conversion from S1 to S0 can occur, but due to the larger energy gap compared to the transition from S2 to S1, this is likely competed with the emission of fluorescence and intersystem crossing to triplet states from which phosphorescence is possibly emitted when returning to the ground state. The intersystem crossing is a non-radiative transition between two energetically equivalent vibrational levels of different electron spin multiplicity. For example, the transition from the 0 vibrational level of S1 to higher vibrational levels of T1 (intersystem crossing) can compete with the transition to the ground state with the emission of fluorescence. The fluorescence process is dependent on fluorescence lifetime and the quantum yield. The emission of fluorescence occurs within 10^{-9} seconds and the lifetime is defined as [68]

$$\tau = \frac{1}{k_f + k_{nr}} \tag{5}$$

Where k_f is rate constant for the transition from S1 to S0 and the k_{nr} is the rate constant for the overall non radiative transitions such as IC, ISC, etc. The quantum yield is the ratio of the number of photons emitted to the number of photons absorbed.

$$\phi = \frac{photons\ emitted}{photons\ absorbed} \tag{6}$$

Fluorescence emission occurs from the lowest vibrational level of S1. After emission the molecule returns to the ground state and the energy is lost to the environment/surroundings. This energy loss is observed in the Stokes shift, representing the gap between the absorption (excitation) maximum and fluorescence emission maximum.

In laser induced fluorescence spectroscopy, the molecule absorbs monochromatic, polarized, coherent light. A selection of systems for light amplification by stimulated emission of radiation (LASER) is presented in the following.

1.3.1 Laser Diodes

Laser diodes use microscopic chips of Gallium-Arsenide or other semiconductors to generate coherent light. The energy gaps between the conduction and the valence band electrons are responsible for the mechanisms of laser action. A laser beam exits the edge of the processed laser diode chip. Most of the laser diodes are also called Fabry-Perot diode lasers.

1.3.2 Pulsed Laser Systems

The shortening of the emission duration can lead to an increased level of power. The realization of that is performed with so-called quality-switches (Q-switches).

Using the laser for fluorescence spectroscopy (e.g. detection of fluorescence lifetimes) the exact pulse of the laser light can be synchronized with a light detection system.

1.3.3 LIF detection of ions in the gas phase

The LIF provides an orthogonal to IMS second dimension of separation/detection. The investigation of gaseous ions by laser induced fluorescence has been performed for several compounds in the past years. A lot of effort has been put into the design and development of different systems to investigate the optical properties of anorganic and organic ions. Laser induced fluorescence of nitrogen cations has been performed firstly in 1975 by Engelking and Smith.[69] LIF emission spectra of CO^+ and CO^{2+} were reported shortly afterwards.[70] The fluorescence emission of fluorinated benzene cations followed a few years later.[71] However these techniques did not use mass selective methods for the investigation of gaseous ions by LIF. The fluorescence spectrum of mass selected CD^+ ions was initially possible in a cylindrical radio frequency quadrupole ion trap.[72] In an ion trap of the same principle (Langmuir) ion-molecule reactions of N_2^+ with Ar and N_2 have been studied.[73] LIF of gas-phase penning trapped organic ions have firstly been investigated by Wang et al.[74] The setup included a Penning trap and a Nd:YAG pumped dye laser to excite ionized hexafluorobenzene. The same group determined the fluorescence lifetimes of pentafluorobenzene and trifluorobenzene radical cations respectively[75] followed by wavelength resolved LIF for trifluorobenzene.[76] The LIF of gas phase radical cations of the Xanthene dye Rhodamine 640 was firstly determined in a linear quadrupole ion trap, designed by Friedrich et al.[77]

The group of Khoury et al. detected the gaseous ionic fluorescence of the organic dyes Rhodamine 640 (Rhodamine 101) and Alexa Fluor 350 in a Paul trap.[78] The photo fragmentation rate was investigated by the temporal decay of the fluorescence emission.

The first systematic study of dispersed (wavelength resolved) fluorescence spectra of Rhodamine ions in the gas phase has been presented by Forbes et al.[79] The previous observed blue shift[78] of the emitted fluorescence light from solution to the gas phase has been shown on three Rhodamine dyes. All three protonated dyes showed smaller stokes shifts in the gas phase than in solution.

Gas-phase conformational changes were the most motivating reasons for the fundamental studies of the fluorescence emission of the ions mentioned above. A trend can be seen from complicated instrumentation (e.g. ion sources, ion traps, fast single photon detection, and so on) to miniaturized systems. This includes the fluorescence detection of the ions at atmospheric pressure.

In conclusion, the discovery of fluorescence emission detection of ions, gives rise to the implementation of gas phase separation systems. The fast separation in drift tube ion mobility spectrometry exploits the ionized state of the molecule and provides analytical information via drift-time measurements. Here, drift tube ion mobility spectrometry demonstrates a method, where ions can be separated at atmospheric pressure by their collision cross section to charge ratio.

The coupling of ion mobility based systems with LIF is so far scarcely described in literature. The drift field LIF coupling was used for investigation of the vibronic excitation mechanisms of N_2^+ .[80] Recently, a LIF signal has been recorded in so called "action spectroscopy". The LIF was analyzed in trapping mass spectrometer after isolation of ions with differential mobility analyzer.[81] The analytes were Rhodamine 6G and the green fluorescent Protein also known as „GFP". Ions were generated with different methods (high vacuum/ambient) and were stored in traps prior to fluorescence spectroscopy and mass spectrometry.[82] Competing attempts were shown by Chingin et al. with the investigation of gaseous Rhodamine 6G ions at ambient conditions.[83] In this work, the IMS contributes with the availability to separate ions in the gas phase and benefits from LIF providing spectral information. The detection of ions in IMS instruments is conducted with high-gain transimpedance amplifiers. The bandwidth of such operational amplifiers is inversely proportional to the gain and therefore physically limited. Special suppression circuitry in transimpedance amplifiers and short ion injection times ~10µs can enhance the resolution and

signal to noise ratio during signal recording in IMS.[84] The Optical detection is known to work down to the femtosecond regime and can potentially overcome the limits of amplification electronics.

2   Aims

Secondary electron multiplier (SEM), microchannel plate (MCP) and Faraday plate are commonly used detectors for ion mobility based separation systems. However, Faraday plate is not selective and SEM/MCP detectors are cost intensive as well as scarcely field deployable. The interest in new, complementary/alternative detection systems for drift tube ion mobility spectrometry has grown in recent years. The use of optical detectors is promising for detection of ions due to the additional information obtained (e.g. wavelength and lifetime of fluorescence). The drift time resolved laser induced fluorescence detection (LIF) in drift tube spectrometers has hitherto not been reported in the literature.

Firstly, the proof of principle of drift tube ion mobility spectrometry and fluorescence detection has to be realized on the example of Xanthene dye ionized by electrospray ionization. For this purpose, high numbers of ions should be generated and efficiently transported into the drift region. To generate drift time resolved fluorescence spectra, the ions need to be injected into the drift field region in form of short swarms. This can be realized by the use of ion shutter according to Bradbury and Nielsen which allow high permeability of ions. The design and development of the ion shutter as well as the influence of the gate field on the ion transmission should be investigated. The pulse of the injection needs to be synchronized with an optical detection system that consists of an excitation source and a fluorescence detector. Since the peak width is expected to be in the range of hundreds-of-milliseconds a faster sampling rate and thus shorter integration time are needed. Spectrograph in combination with a gated intensified charge coupled device (ICCD) can overcome both problems.

With this setup the influence of the main parameters can be investigated. The influence of the electric field strength on signal parameters (intensity, full width at half maximum (FWHM), drift time) analyzed with both the fluorescence detector and electrometer have to be investigated. The dependence of the ion transmission on the perpendicular ion gate field should also be investigated.

After proof of principle measurements, a suitable experimental setup for the analysis of PAH should be developed. Due to the non-efficient ionization of PAH with ESI, the photoionization technique should be used. This method is known for efficient ionization of aromatic compounds. An efficient photoionization of PAH requires a pure and dry atmosphere. Therefore, a closed drift tube ion mobility spectrometer with unidirectional flow design will be constructed.

To avoid condensation of PAH, the ion mobility spectrometer should be heated. To achieve higher resolution, the drift length will be increased. To enable the simultaneous analysis by means of LIF and electrometer detectors, a LIF cell should be integrated into the ion mobility spectrometer.

With the modified experimental setup, the relationship between intensity, FWHM, drift time of the signal and the electric field strength with both the fluorescence detector and electrometer should be investigated. The required lamp discharge current for efficient ion generation should be determined.

3 Method development for drift tube ion mobility spectrometry in combination with laser induced fluorescence detection

The following section describes the instrumentation for the IMS-LIF coupling performed in this study. Firstly, the ionization sources (PI, ESI) are presented. Secondly a detailed description of the IMS components is described. A third section introduces two laser excitation sources (laser diode and Nd:YAG pulsed laser system) used in this work. The fourth section explains the principle of the ICCD camera. Lastly, the experimental setups with both the continuous excitation source and the pulsed laser system are shown.

3.1 *Hardware and Electronics*

This part focusses on the development and implementation of the material and electronics that are required for the coupling of drift tube IMS and LIF. The central components of the drift tube ion mobility spectrometer are not commercially available separately. Many commercially available solutions exist, using drift tube IMS as detection system but the drift tubes are always mechanically integrated to the sample introduction system. Commercially available components do not meet the requirements, such as: the implementation of a single ion gate between an ion source of interest, the mechanical integration of optical components into ion optics working at atmospheric pressure, the Faraday plate detector with aperture and additional integration in commercially available transimpedance amplifiers. The principle of ion injection and drift tube design is not standardized yet. Hence, the manufacturers use in-house methods for the construction of ion gates, drift tubes and Faraday plate detectors. The idea of fluorescence detection of moving ions in an electric field has not been performed yet. The experimental execution of this coupling requires a high degree of mechanical flexibility.

The IMS-LIF coupling is investigated on the design and development of a drift tube ion mobility spectrometer equipped with a fluorescence detection system located at the Faraday plate detector. The components are introduced in the following section and divided into: ion sources, drift tube design and the setup of special components (e.g.: ion gate, aperture grid, important electronic circuits), laser induced fluorescence system (e.g.: laser, ICCD camera)

3.2 *Ion sources*

3.2.1 Photoionization

The ion generation in an IMS is conventionally performed by corona discharge ionization or via β-emitters in form of ^{63}Ni and Tritium (^{3}H). The interest in non-radiative ion sources is still high, since licensing procedures and the transfer of analyzers with radioactive sources is strictly limited. The photoionization discharge (PID) lamps are often used to increase the selectivity for organic compounds such as aromatics, hydrocarbons and alcohols. Additionally, the lamps represent a ready to use ion source that continuously emits photons of high energy. Two geometries of photoionization sources for ion mobility are described in the literature. The perpendicular arrangement of the source window simplifies the mechanical implementation into the ionization region of the drift tube. However, the photoionization source should emit inside the electric field to enhance the ion transmission towards the mobility analyzer. Hence, between the perpendicular positioning of the source, an electric field needs to be established forcing ions towards the ion gate and consecutively into the mobility drift tube. A so-called repeller was added to the drift tube on which the highest drift potential is applied. A detailed description is shown in Figure 4. The electric field applied to the repeller and drift tube forces ions to move towards the ion gate where the initial process of pulsed ion injection for mobility based separation takes place.
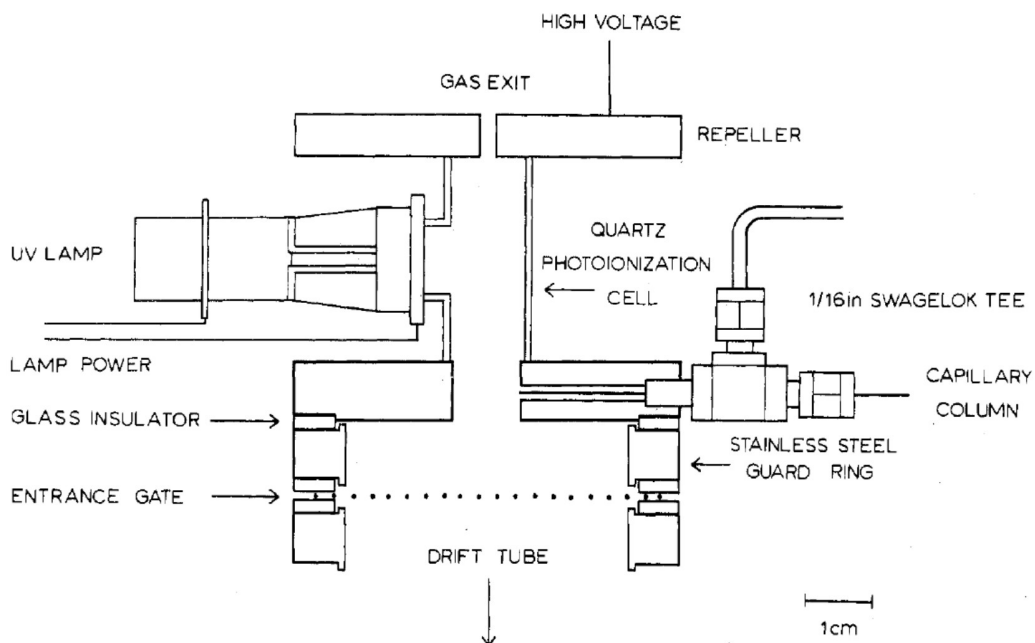
Figure 4 Perpendicular design of the photoionization source for gas-chromatography ion mobility spectrometry from Baim et al.[22]

The axial design was reported with lower detection limits compared to the side-mount design.[85] In case of on axis mounted lamp, the ion source irradiates a higher volume, leading to a higher ionization yield. The ion gate positioning close to the photoionization region can be disadvantageous due to the ionization of sample molecules behind the gate.[86] The literature shows an increasing trend of the adaption of axial mounted photo ionization sources in ion mobility spectrometers.[33, 85b, 87] Efficient transfer of the ions generated by photoionization of sample molecules, requires an electric field between the repeller electrode and the first ring electrode of a drift tube. The high electric field strength with low voltage consumption can be achieved with a close positioning of the electrode towards the drift cell entrance. It was shown that the penetration of UV photons can occur to distances of 2 cm when using pure nitrogen as both, drift and carrier gas.[85a] Using air containing oxygen instead, resulted in quenching of the photons within the first millimeters from the source window.[85a]

An improved design for the atmospheric pressure photoionization was developed by Tabrizchi et al.[85b] The PID lamp was mounted axially and was separated from the IMS inlet region by a metal

disk. The metal disk fulfills two tasks. One is the extraction of ionized sample molecules from the source region by applying a high voltage between the lamp head and the metal disk. Second, the metal disk divides the source region from the IMS inlet region and connects the two regions by a centered hole. The idea of using the PID lamp electrodes as drift electrodes increases the complexity of the required electronic circuits.

The setup of an ion mobility spectrometer with a PID ion source is presented. The simple way of non-radioactive ion generation is the photoionization of volatile organic vapor. The photoionization source chamber was designed to fit in a unidirectional flow IMS. The PID ion source consists of a Heraeus PKS 106 vacuum ultraviolet photoionization discharge lamp. The PID lamp is sealed concentrically onto the ionization chamber with a conical shell of ~ 0.13 mL volume. The sealing is realized with the ion source lamp cover that consists of a metal spring, an electrode terminal and a cover that is mounted onto the ionization source head. The lamp socket represents both, the first ring electrode of the mobility spectrometer and the PID lamp anode. The lamp socket is attached to the electrode terminal via a copper connector and a metal spring. This assembly is diagonally inserted in the lamp cover. The sample can be introduced into the ionization chamber via holes and gas tight screw fittings. A second hole serves the purpose of dopant introduction into the ionization chamber. At the tip of the conical shell, the ionized sample molecules exit through a 1 mm opening. This opening is surrounded by an extraction ring electrode acting as the interface between the ion source chamber and the IMS inlet. The drift gas passes in a unidirectional flow against the ion flow and exits through holes in the extraction electrode and the photoionization source head respectively. A side view of the technical drawing of the ion source assembly is shown in the following drawing.
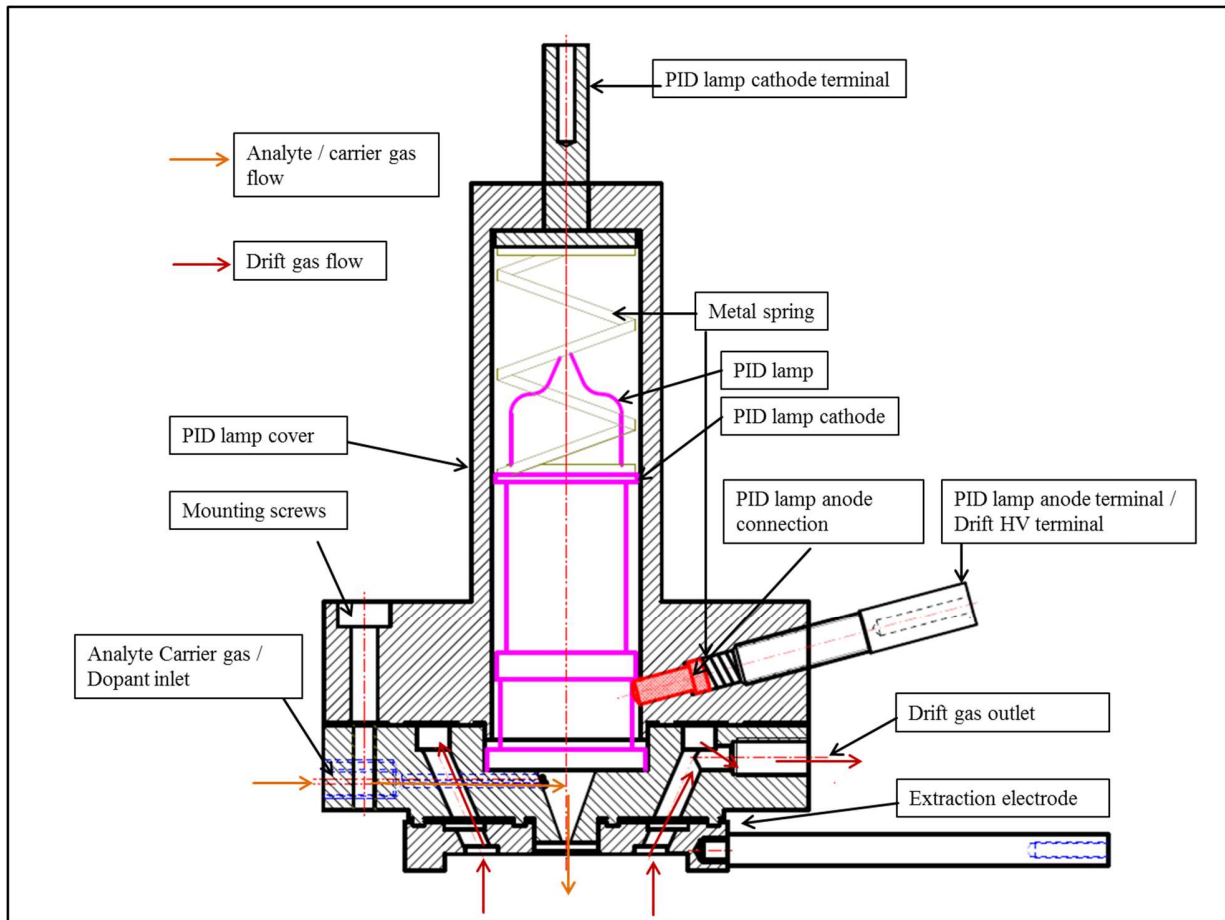
Figure 5 Technical drawing of the photoionization source assembly side view. Printed with the permission of the mechanical workshop TGM University Duisburg-Essen

Method development for drift tube ion mobility spectrometry in combination with laser induced fluorescence detection

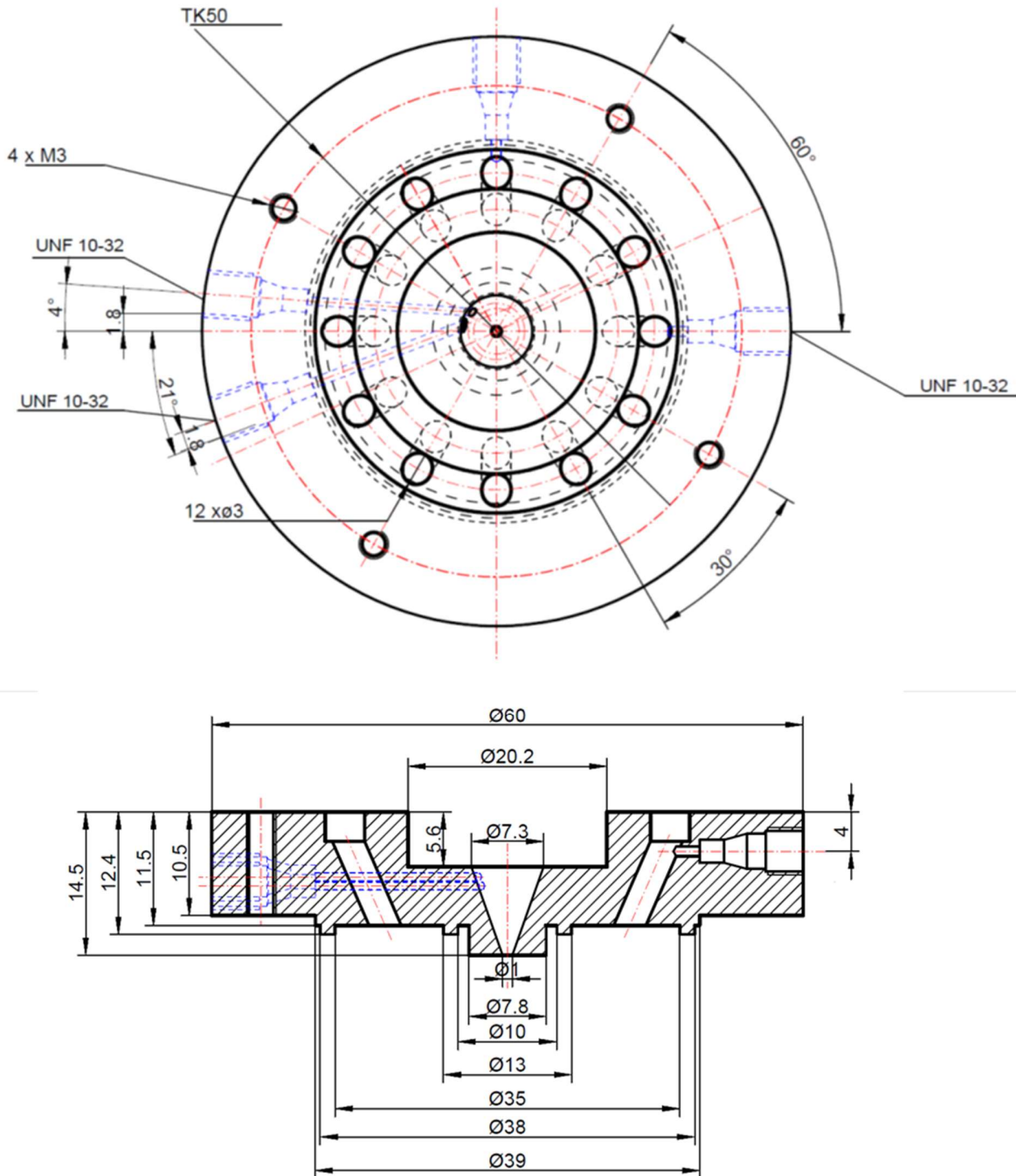The technical drawing of the photoionization source head is shown below.

Figure 6 Technical drawing of the photoionization source head. Printed with the permission of the mechanical workshop TGM University Duisburg-Essen. Material: polyether ether ketone (PEEK); Macor™

3.2.2 Electrospray ionization

In order to provide the ionization of polar compounds, the second ionization source used in this work is the electrospray ionization. When a high voltage potential is applied to an aqueous solution with ionic components or to a conducting surface that is in contact with this solution, it comes to a charge separation at the capillary tip. The cations accumulate on the surface of the solution and get pulled towards the counter electrode (e.g. the entrance of a mass spectrometer - in this case the IMS entrance). The transfer of dissolved analytes from solution into the gas phase occurs with two characteristic phenomena. First, with a threshold level of the electric field strength called electrospray onset[88] the formation of the characteristic Taylor cone[89] takes place. Secondly when the Taylor cone is stable (cone jet mode) the liquid filament (jet) emits small droplets in form of a spray (plume). The addition of organic modifiers (e.g. Methanol or Acetonitrile) decreases the surface tension and lower field strengths are required to perform the spray process. In the negative mode (Solution/capillary on negative potential), undesired corona discharges can occur.[90]
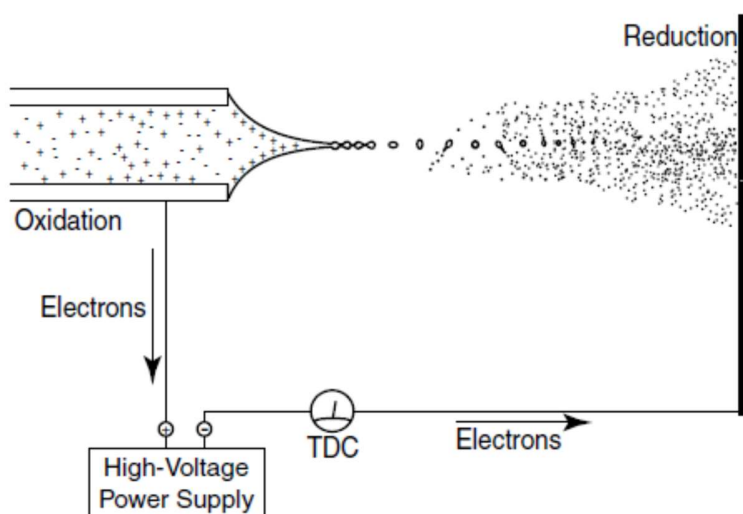

Figure 7 Schematic of the positive mode of electrospray ionization where TDC is the total droplet current. The droplets emitted from the Taylor cone merge into a fine spray towards the counter electrode [91]

The electrospray ion source used in this work consists of the parts from the commercially available nano-spray ion source (nano ESI v 1.0, 2009, Thermo Scientific, Waltham, USA). A scheme of the microcross connection interface is shown below.
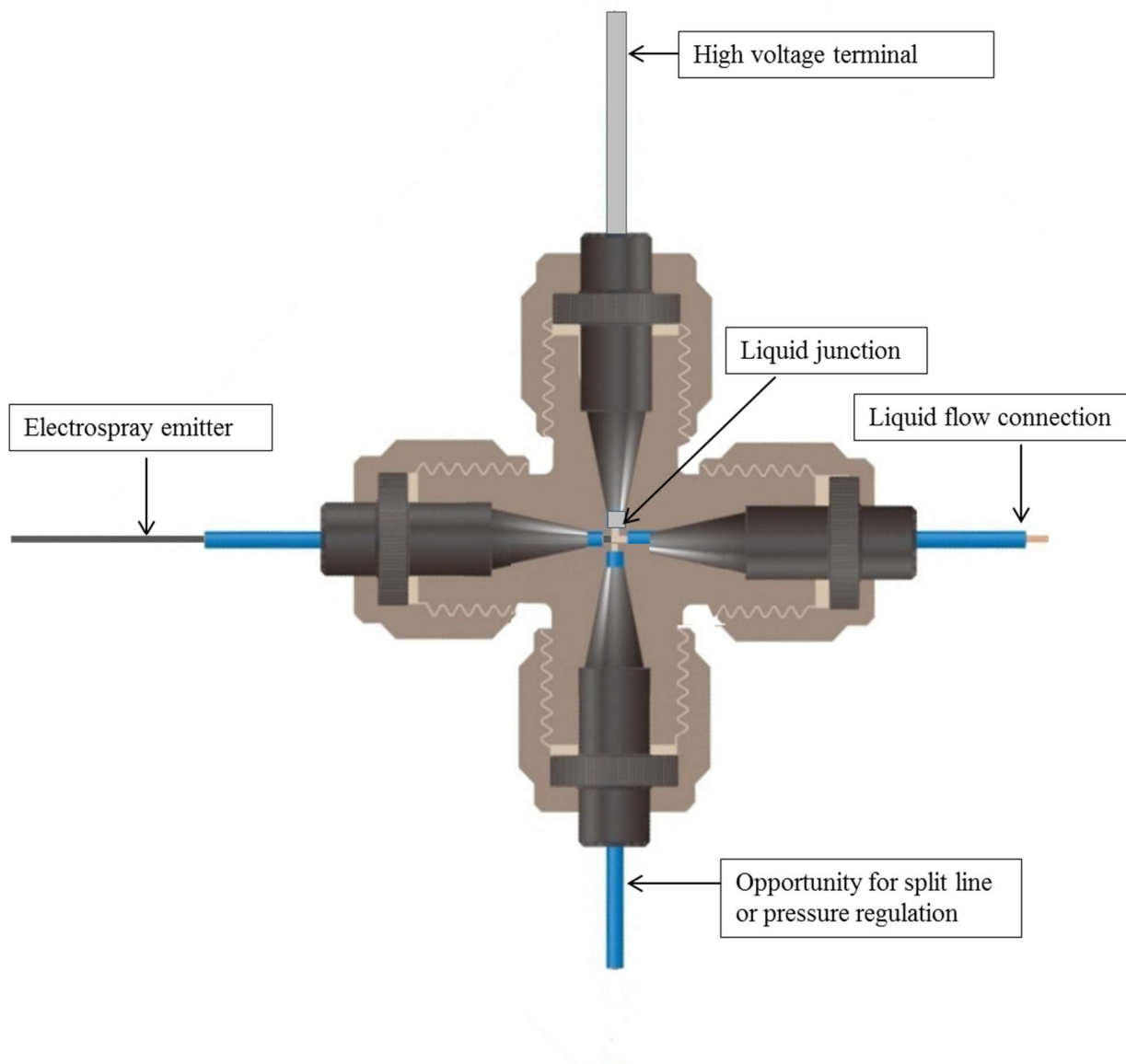

Figure 8 Schematic of the electrospray interface build up from an Upchurch scientific micro cross union (part. No. P-887). The inner bore diameter is 0.152 mm. The high voltage terminal is made from a titanium rod and is directly connected to the liquid inside the cross union.

A simple approach of an ESI-IMS setup is the positioning of the electrospray emitter in front of the IMS entrance (first ring electrode) in a close distance to the ion gate. The electrospray emitter tip potential and the IMS drift potential must be variable since stable spray generation strongly depends on the electric field strength between the electrospray emitter tip and its counter electrode. Hence, the electrospray voltage must always be several kV (e.g. 2-5 kV) higher or lower (positive or negative mode) than the IMS entrance potential.

3.3 *Drift tube design*

A homogeneous electric field inside a drift tube can be established by applying a voltage on a stacked tube of ring electrodes, separated by an insulation material. The ring shape has been investigated and optimized with computer based simulations by means of conducting material thickness and outer diameter[51]. The thickness of the insulation rings was also investigated by means of field homogeneity.[50b, 51] The final remarks of both authors, Liu and Eiceman was that the field definition throughout the drift tube is more important than the overall electric field strength in a stacked ring drift tube design. Especially the three regions of the ion source, the shutter field and the aperture grid to detector region need to be defined carefully by means of spacing and field definition. Non-homogeneous electric fields may arise from this regions or fields external to the drift tube. In general, a higher homogeneity is achieved with decreasing thickness of the drift ring electrodes. However, the electrical connection of resistors to thin electrodes is limited. The limitation can be overcome by the geometrical change of the inner ring shape. The ring can be designed with a sufficient thickness on the outer ring, while the wall thickness of the inner ring can be kept at a fixed value of 1 mm. Considering the geometry of the insulation ring, the inner and outer diameter was chosen to have the same diameters as the drift ring electrode (25 and 40 mm, respectively). The thickness of the insulation rings was chosen to be 8 mm. The width of 8 mm was shown to perform best in the drift region without significant changes before and after computer based simulated field optimization.[51] Additionally, the thickness 8 mm poses a sufficient width for the implementation of the ion shutter grid and aperture grid assembly, respectively. An interlocking geometry was chosen to align both, the drift ring electrodes and the insulation electrodes in a tubular arrangement.
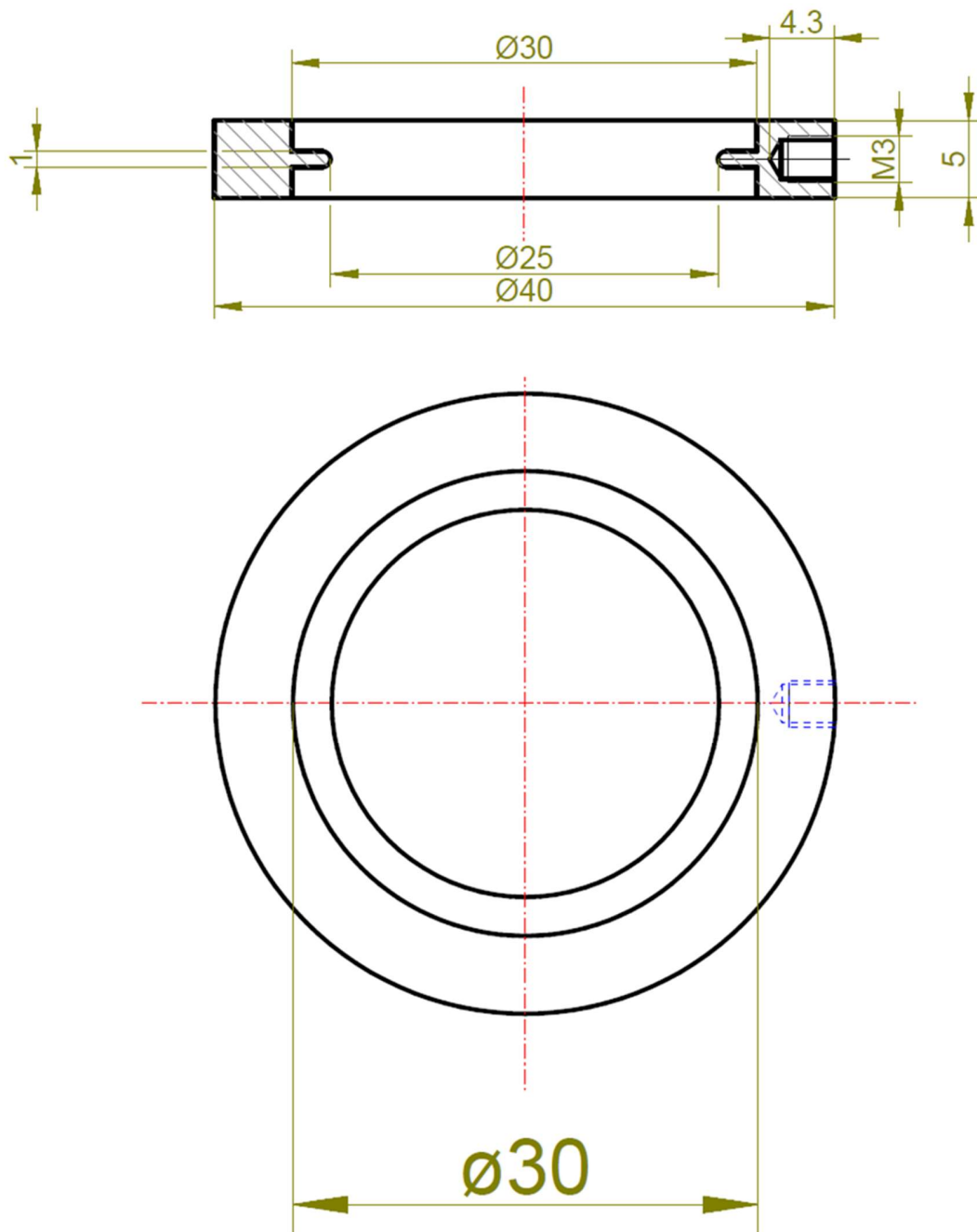
Figure 9 Drift ring electrode with an inner thickness of 1 mm and the outer thickness of 5 mm. The M3 thread is for the mechanical integration of voltage terminals. All dimensions in mm. Material: stainless steel
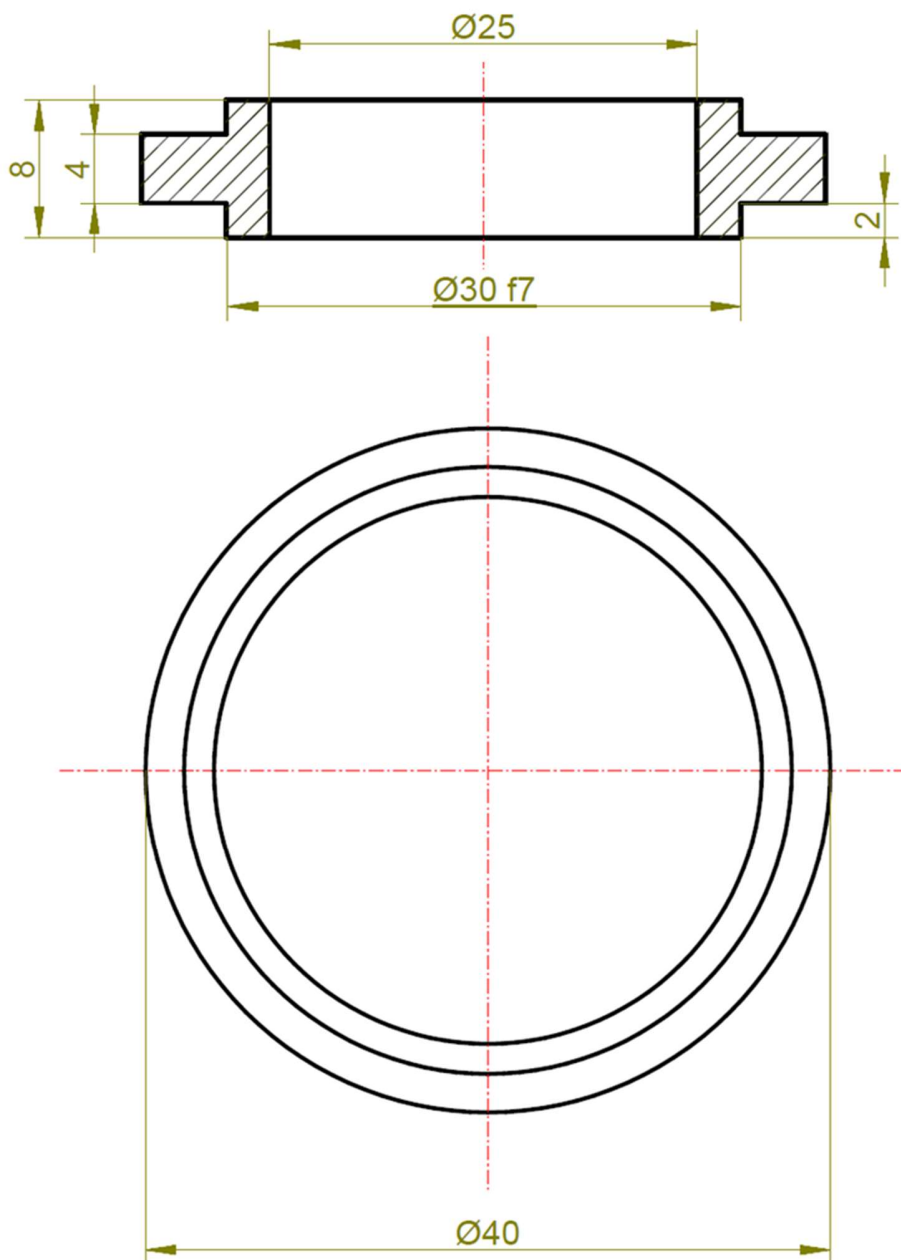
Figure 10 Technical drawing of the insulation ring. The diameter 30 mm f7 indicates a technical fit for the machinable ceramic material (Macor™) inside the drift ring electrode. The fit is approximately chosen so that material is not affected when the materials are expanding due to temperature increase. All dimensions in mm. Material: Macor™

The proposed shape of the rings for the construction of a drift tube has also been described in the literature.[52]

The creation of an orthogonal field to deflect or block ion passage into the drift region is accomplished by the biasing of two parallel wire sets located in one plane perpendicular to the flow of the molecular ion beam. Such an arrangement is called a Bradbury-Nielsen gate (BNG). The manufacturing of a BNG can be performed by etching[43c, 92] or weaving[93]. The weaving method is potentially able to produce a research grade BNG.[94] The principle of the weaving method consists of the wrapping of a defined wire around two screws located in parallel in a defined distance. The thread spacing of the screws determines the distance between the wires. After the wrapping, one side/layer of the wrapped wire (above or below the screws) is glued between two ceramic rings. Then separation (weaving) of two wire sets is performed manually. The mechanical integration of the two wire sets is achieved by twisting and fixation of the wires as electrodes. A research grade IMS requires temperature stability, electrical insulation and chemical inertness at the same time. Additionally, since the wire arrangement serves as electrodes, the wire material needs to be conductive (e.g. made from metal) and the wire holder has to be made from an insulator. The expansion of material with increasing temperatures complicates the technical layout of a BNG. In this instance, the dimension of the wires must be very stable at various temperatures. Invar was used as wire material of choice because of the low expansion property. Invar is an alloy with a coefficient of expansion of 1.3×10^{-6} K^{-1} in the range of 0-100 ° C, compared to stainless steel that is 1.3×10^{-5} K^{-1}.[95] The adhesive used for the wire fixation should have equal properties such as temperature stability and high electrical insulation. Ceramic cements are made from inorganic powders (e.g. SiO_2, ZrO_2) and some of them were intended to join ceramics and make electrical insulation coatings.

3.4 *Manufacturing ion gate according to Bradbury and Nielsen using the weaving method*

Two ceramic rings were designed to fit between two drift ring electrodes. The thickness of one ring is specified to be half the thickness of an insulation ring. The inner and outer diameters are identical to the insulation ring. For the housing of the wires after separation, a groove is inserted in a close distance to the wire plane.
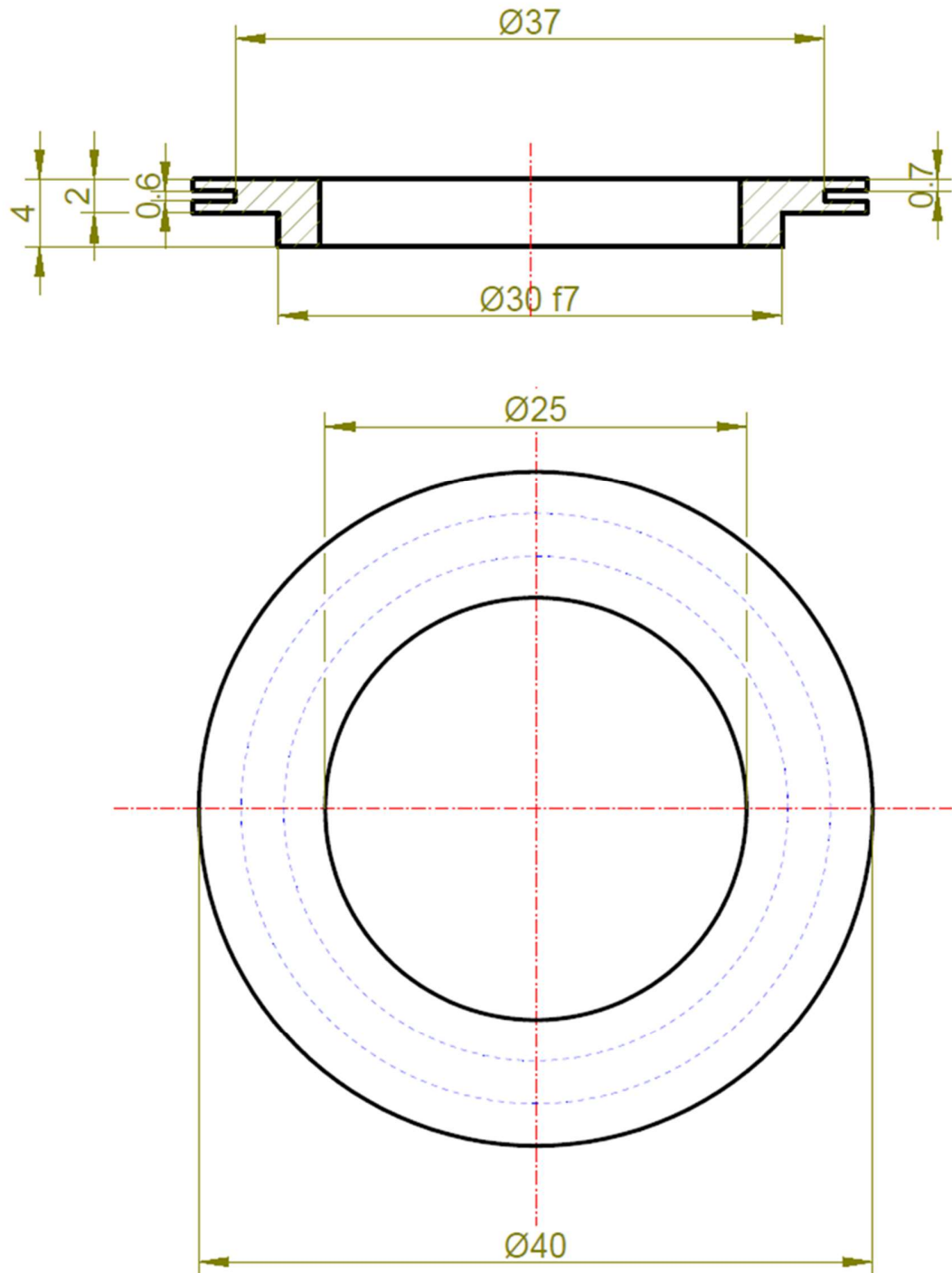
Figure 11 Technical drawing of the gate ring. All dimensions in mm

A winding tool consists of two brass screws mounted in a frame (Figure 12 (1)). The diameter of the screws is 40 mm. The screws have a thread spacing of 0.3 mm. Invar wire (0.008 mm diameter) was wrapped around the screws in every second thread, until a 26 mm wide area is wound. The gate half is put on a raised platform and the assembly of the screws mounted in the frame with the wound wire is slided over one gate ring (Figure 12 (2)). The cement (Polytec Resbond 940) is prepared according to the manufacturers application guide. In general, a thin layer between the gate rings is required and excessive adhesive should be removed. A dispenser tool such as disposable syringes was used for the application of the cement. The wires quickly mount after applying the ceramic adhesive, since it dries fast. The wires wound at the top should rest on the grooved side of the gate ring with a slight tension. The second gate ring is aligned quickly after the adhesive application with the grooved side facing down. With applied weight on top (Figure 12 (2)), the cement is cured at ambient conditions for 72 hours. After curing, insertion of a paper sheet in between the two layers of wires simplifies the visibility of the gate wires. Take a wooden stick and weave it between the wires so that the wires alternate between being above and below the stick (Figure 12 (3)). Repeat the procedure with a second stick and weave in the opposite direction. This procedure will result in the separation of four wire sets that are fixed on paper with the aid of adhesive tape (Figure 12 (4+5)). After removing the wooden sticks, two of the four wire sets are showing to the groove over which it lays when the wires are separated. The wires are pressed into the grooves and twisted with silver plated high voltage (HV) lead wire forming the two gate leads (Figure 12 (6+7)).
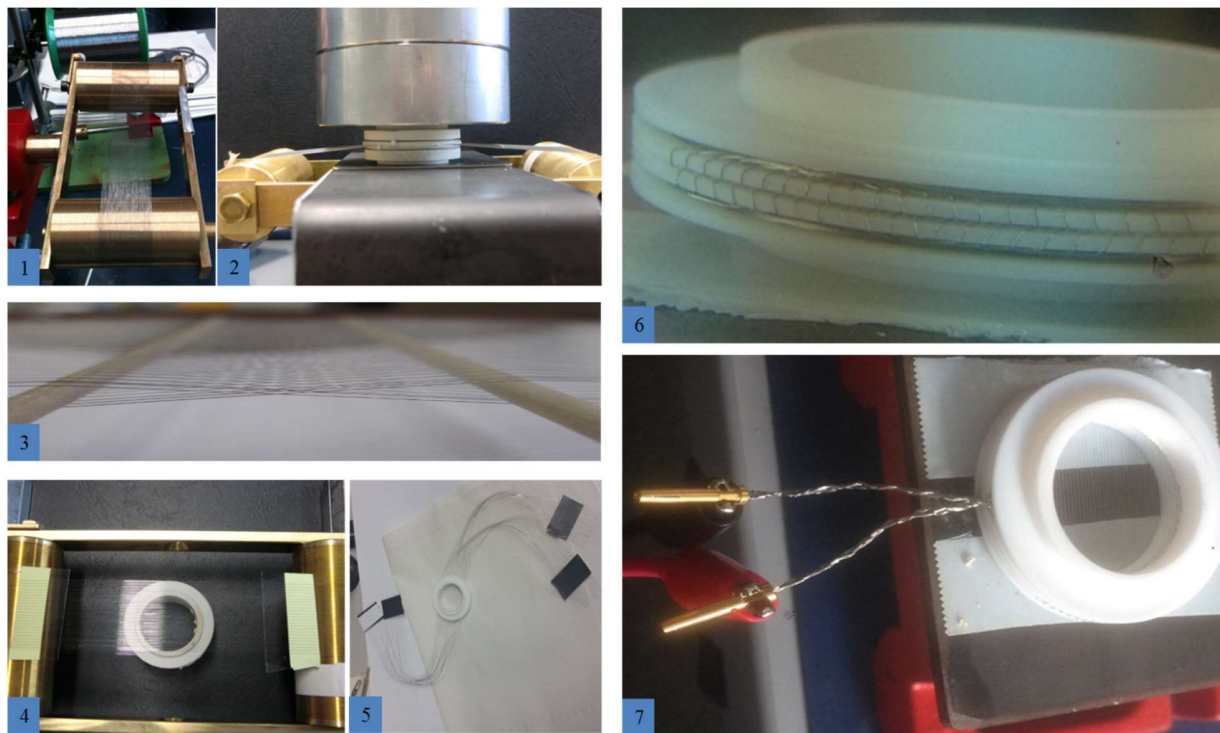
Figure 12 Procedure of making a Bradbury Nielsen Gate. (1) Winding of wire around screws. (2) Cementing the wires inbetween ion gate rings. (3) Weaving resulting in four wire sets. (4) Taping the wire sets on paper. (5) Gate assembly with four wire sets. (6) Wire sets pressed into the groove (7) Final assembly of the BNG.

The ion gate is also used as aperture grid when both wire sets are biased on the aperture grid potential. The drift ring, the insulation ring and the ion gate can be used for various drift tube lengths and designs (dual gate mode for example).

3.5 *Transimpedance amplifier and detector assemblies*

The detection of ions in an IMS is performed by transimpedance amplifiers. The used amplifier in this work is a Femto DLPCA-200. The device can perform in two modes. One in H-mode (high speed) with a gain up to 10^{11} V A^{-1} and second in L-mode (low noise) with a gain up to 10^9 V A^{-1}. The rise and fall times differ significantly in the two working modes. Since ion mobility injection times are in the range of several tens to a few hundreds of microseconds and the gain is usually set to a value in the range of 10^9-10^{12} V A^{-1} low noise mode performing at a gain of 10^9 V A^{-1} with a rise and fall time of 300 μs is rather inconvenient.
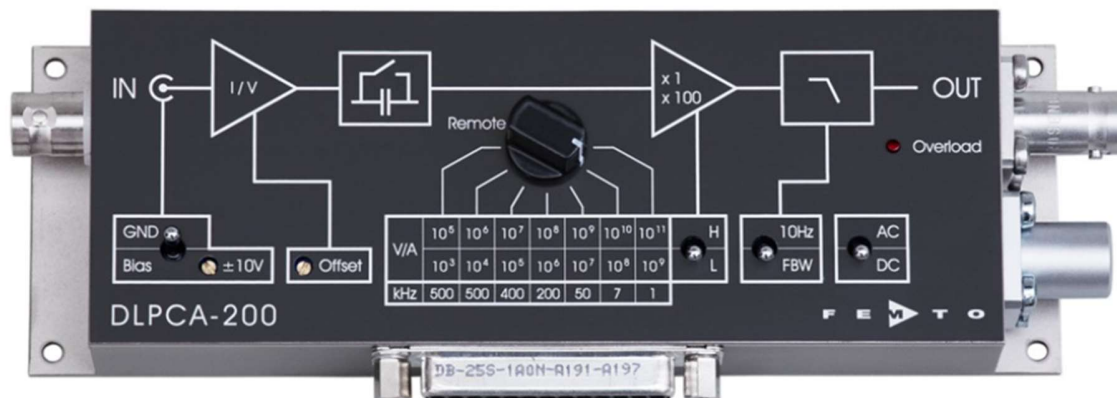
Figure 13 Variable gain low noise amplifier Femto DLPCA-200

The detector plate of an IMS is usually connected to the input of the transimpedance amplifier. Shielding of this lead is important and is simplified with the coaxial cable Bajonett Neill-Conc elman (BNC) connectors on the amplifier. The mechanical parts for the ion current detection is designed with regard to the BNC connection standard.

In this work, two design concepts are developed for the integration of an optical detection system in the detection region of a drift tube ion mobility spectrometer. One is an open stacked ring design with an open end for the integration of a fluorescence emission detection system. Second a closed unidirectional flow design is developed for the integration of both, photoionization and laser induced fluorescence detection. For the ionization of dye molecules such as Rhodamine 6G ESI is a favorable ion source, since the molecule is polar and ionic in solution. The open design setup was kept simple without temperature controlling and without gas flows. Fluorescence experiments require precision movements of excitation light source beams and that of the emission collection optics, respectively. That is why the open cell design was placed on an optical bench and the important features (electrospray emitter, excitation light source, emission collection optics) of the experimental setup were kept modular by means of spatial positioning (e.g. placed on x-y-z positioners).

The detector for the open cell design consists of a copper plate mounted in a modified BNC adapter and an aperture grid glued between two Macor support pieces. The aperture grid was manufactured by the winding method presented above. The adapter was modified, so that the aperture grid was

placed in a small distance (0.5-1 mm) to the detector plate. The copper plate can be designed in various diameters and lengths. A rather less mass used for the Faraday plate results in a reduced capacitance. The limits are in the thickness of the terminal and the thickness of the plate. The Figure 14 shows the detector assembly in four parts. The plate shown in (1) is mounted into the modified BNC connector Figure 14 (2). Invar wire (weaving method) is glued between two pieces of Macor (3) serving as mountable aperture grid for the miniaturized detector for open drift cells (4). The assembly of the detector for the open cell design is shown below.

Figure 14: Faraday plate detector assembly for the open drift cell design

Basic technical drawings of an research grade IMS detector can be found in the supplemental material of Eiceman et al.[18] This concept of stacked flanges provides diffusive gas flow for drift gas and a Faraday plate detector with wire feed through connection. Additionally the detector assembly is adapted to join the ion gate assembly.
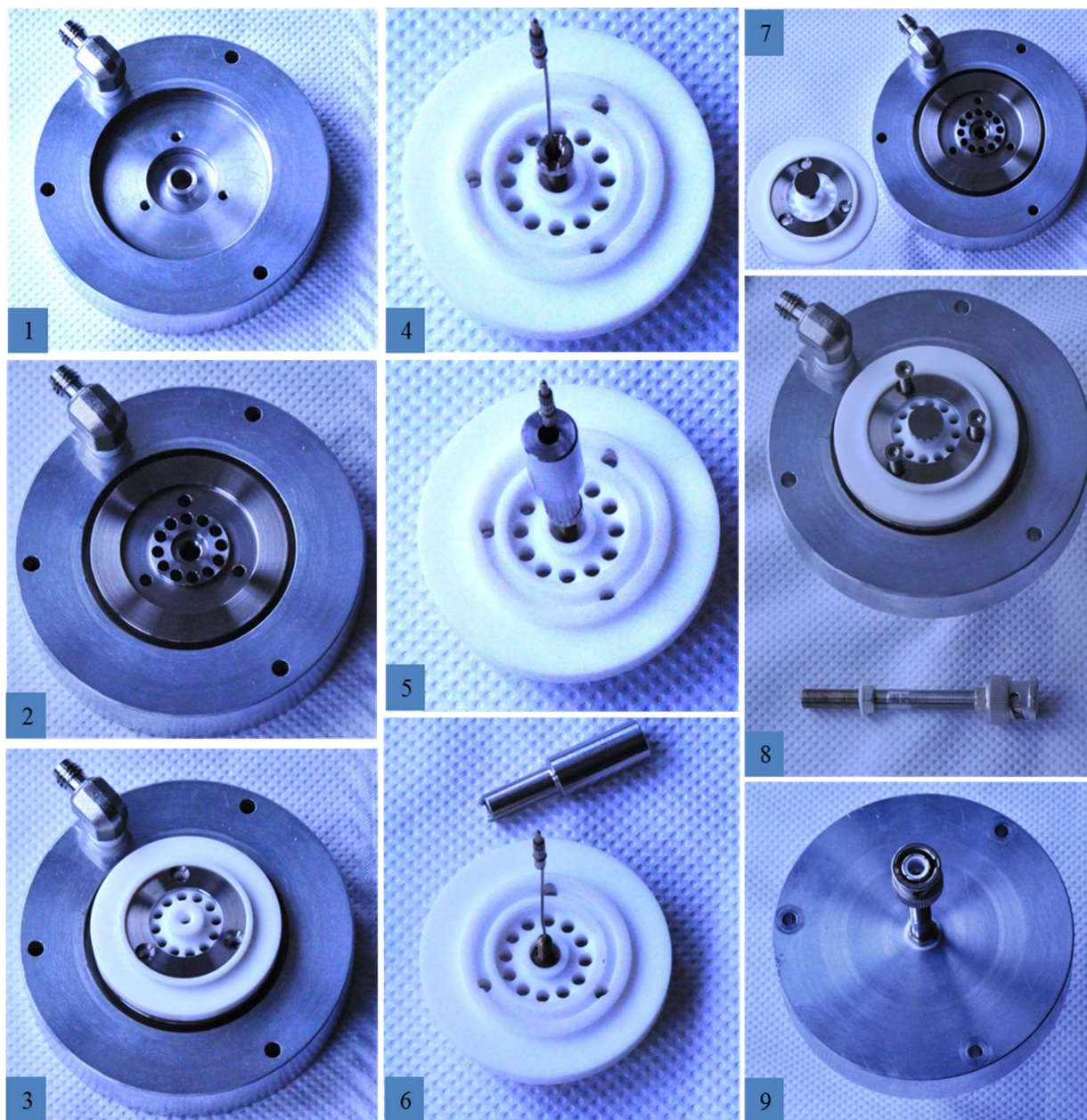
Explanation for the assembly of the IMS detector:

Figure 15 Stepwise detector assembly for closed drift tube arrangements. (1) basic flange with drift gas connector. (2) supporting electrode with diffusive drift gas outlet via 12 holes. (3) Last ring electrode mounted on isolation flange. (4) Detector plate mounted on isolation flange with special tool (5)+(6). (7)+(8) Plate detector with isolation flange assembly mounted on basic-flange. (9) Assembly of the plate detector terminal shielding.

3.6 *Electronic circuitry for IMS*

The general electronic circuitry for IMS electronics are described in the literature.[47] Unfortunately no generalization of drift tube designs exist, making every drift tube IMS a merge of unique technical assemblies that requires adapted electronics. However, the basic principles of the electronic circuits are highly similar in drift tube electronics. The electronics can be divided in four parts: The source electronics (when using other than ^{63}Ni), the voltage divider, the ion gate switch and the aperture grid voltage and current regulation, respectively. The following section proposes a circuit for the photoionization drift tube IMS. The number of drift electrodes is set to ten and can be varied if necessary. However, the voltage divider needs to be adapted in the same way. The capacitor C1 smooths the output signal of the transimpedance amplifier and has typical values of 100 nF. The capacitor C2 is added to the aperture grid to drain the induced current of the approaching ion cloud to ground potential. The capacitor values are in the range of several µF. In this work 5µF are used specified up to a voltage of 1 kV. The voltage difference between the lamp socket and the extraction electrode is discussed in the literature.[33, 85b, 87b] In general, a voltage drop between 500 and 1000 Volts is required to transport the ions towards the IMS drift cell. In this study, the value of the resistor between the PID lamp and the extraction electrode is set to 2.7 MΩ. A typical value of the aperture grid resistance against ground is 1/5th of the resistance between two neighboring drift ring electrodes (1MΩ). At a high voltage value of 2.5 and 5 kV applied to the circuit, the voltage drop between the PID lamp and the extraction electrode is 450 and 900 V, respectively.
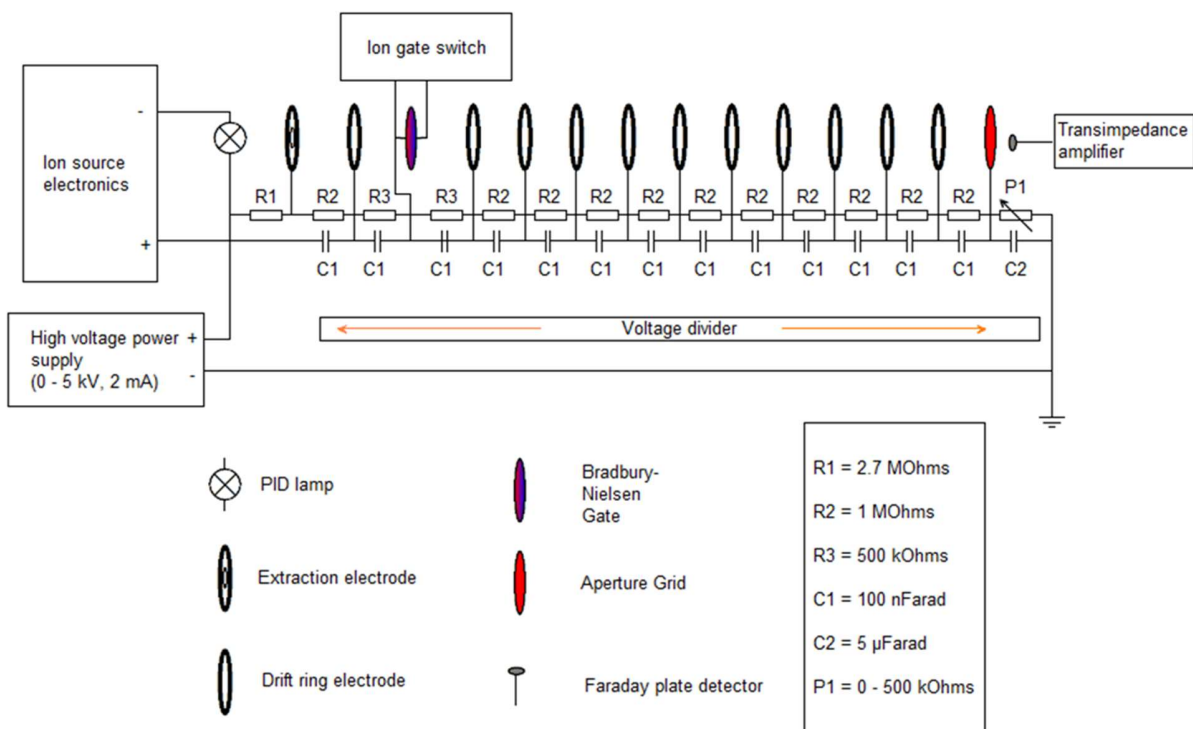
Figure 16 Overview of the overall electronic circuit for a drift tube ion mobility spectrometer with stacked ring design and Bradbury-Nielsen gate.

The essential components of this circuitry are the ion source electronics and the ion gate switch. The circuitry is described in the following paragraphs.

3.6.1 Ion source electronics - PID lamp power supply

The ion source electronics need to be located in the electric field in a close distance to the drift tube entrance to increase ion transmission. In the case of photoionization a separate high voltage is required to supply the PID lamp current. In this work the lamp socket of the PID lamp is used as first ring electrode (repeller) of the IMS. Therefore, galvanical isolation of the PID power supply from the IMS drift voltage power supply is required. This can be achieved by DC-DC converters. The PID lamp current can be monitored by the power supply, recommended from the PID lamp manufacturer. This feature was also implemented in the circuit for the PID lamp power supply. The LCD shows the PID lamp current in 4 digits (000.0) in the range of ~ 0.3-2 mA depending on the resistance adjusted by the Potentiometer (0-1 MΩ). The PID lamp socket can be connected to both,

the PID lamp power supply <u>and</u> the high voltage power supply that is necessary for the generation of the drift field. The circuit of the PID lamp power supply is shown below.
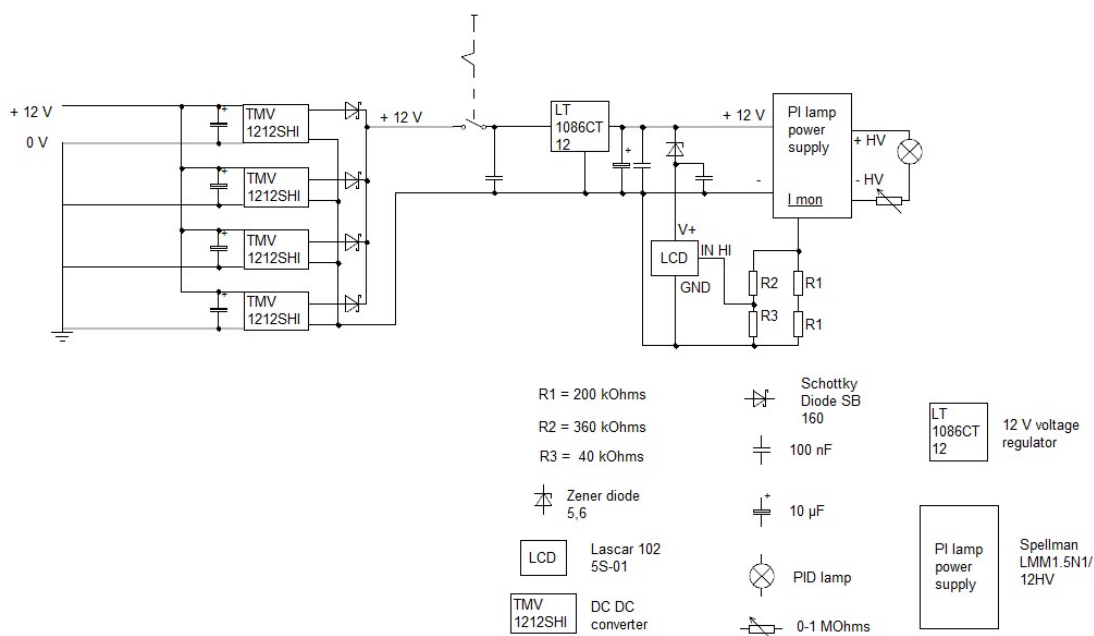

Figure 17 Electronic circuit of the PID lamp power supply for the integration of PID lamps in drift tube Ion mobility spectrometers

Since the high voltage power supply for the PID lamp is placed on a floating potential, the whole unit is placed into an isolating case made of plastic. Also the switch button to ignite the lamp is crafted from a rod, made of polyvinylchloride. The only piece of metal is the BNC socket providing the two electrical connections for the PID lamp. This socket is put on the highest electric potential when the PID lamp power supply unit is integrated into a drift tube PI-IMS. A photograph of the mounted circuit in a case is shown below.
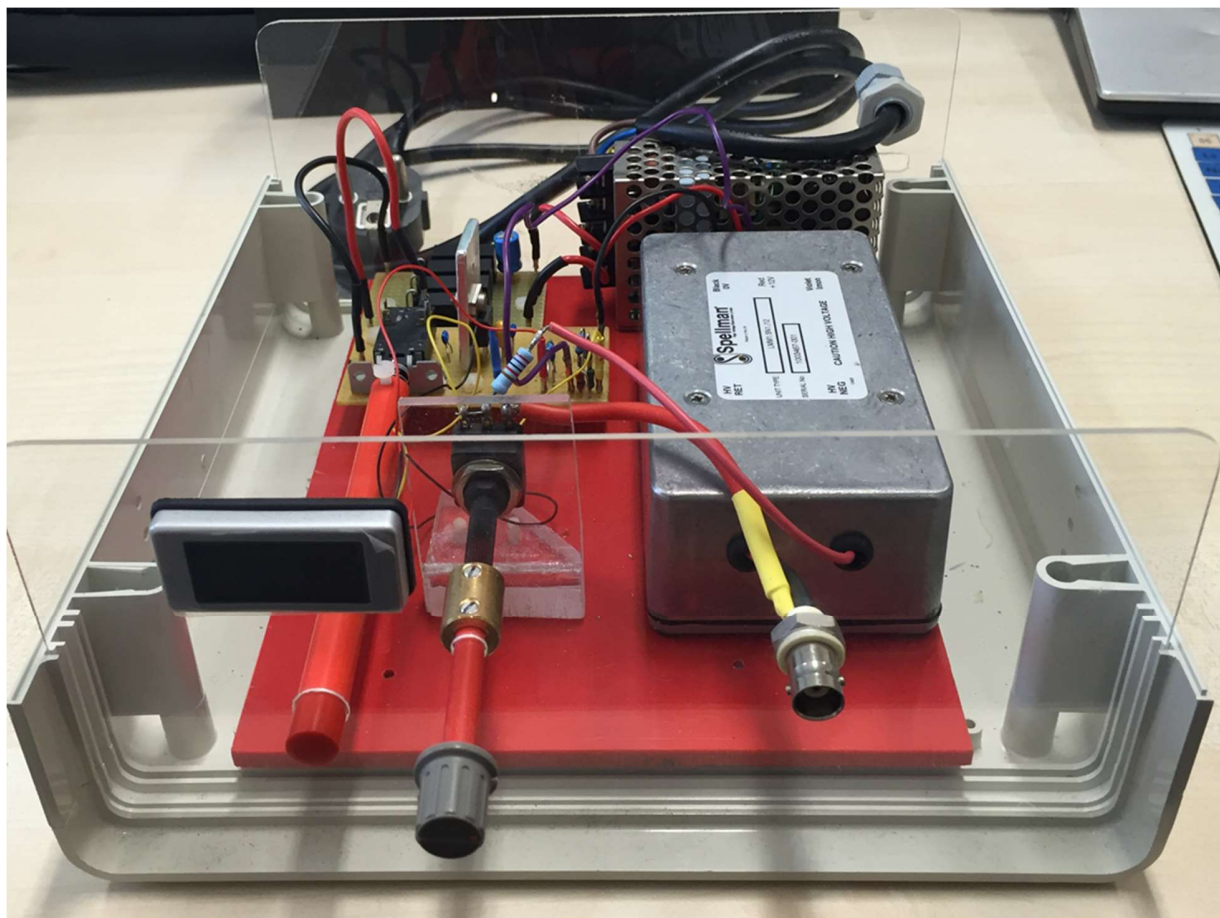
Figure 18 PID power supply unit with open lid

3.6.2 Electrospray-ionization electronics

In the case of electrospray ionization the high voltage connection at the liquid junction must be held at an appropriate potential over the highest drift tube potential to generate the electric field between the electrospray emitter and the IMS drift tube entrance. Example: The electrospray is generated when ±3-5 kV are applied to the electrospray emitter in a defined distance to a counter electrode. When the drift tube entrance ring is held at a potential of ±5 kV the electrospray voltage must be ±8-10 kV to generate the electrospray.

3.6.3 Ion gate shutter electronics

The description of the ion shutter electronics are not sufficiently described in the literature. The most simple description is the "on" - "off" operation of the ion gate in dependence on the potentials applied to the two wire sets required for a BNG.[47] "On" means, when the wires are at equal potential corresponding to the drift field potential at the location of the ion shutter. "Off" is the condition when the two wire sets are equally displaced above and below the drift field potential at the location of the ion shutter. The driver for the periodically operation of the "on" – "off", is a square pulse generator that needs to be decoupled from the high voltage circuitry with opto-isolation circuitry. No standardized electronics for ion gates exist to operate an IMS. The following section describes the circuitry required for the biasing of the ion gate wire sets relatively to the drift field potential.

The galvanical isolation of the bias potential from the high voltage potential is performed with transformers. The transformer (230 V, 20 VA, see Figure 19) provides AC voltage that is converted to a tunable DC voltage. This voltage needs to be placed on one wire set by means of the "on" - "off" operation, while the other wire set is always held at the potential at the location of the ion shutter. The voltage can be varied by the voltage regulator (TL 783). The isolation of the switching circuitry is performed with a second transformer providing the supply voltage of approximately 7.5 V AC (see Figure 19) that is converted into a fixed +5.25 V DC (LP 317, see Figure 20) required for the opto-isolation circuitry (the parts MAX 4429 and the HFBR 2528 require + 5V supply voltage). The HFBR 2528 is the receiver of light pulses that determine the pulsed "on"-"off" conditions for the ion gate. The light generation is performed via a second opto-isolated circuitry that generates a light pulse from a transistor-transistor logic (TTL) square pulse. (Figure 21)
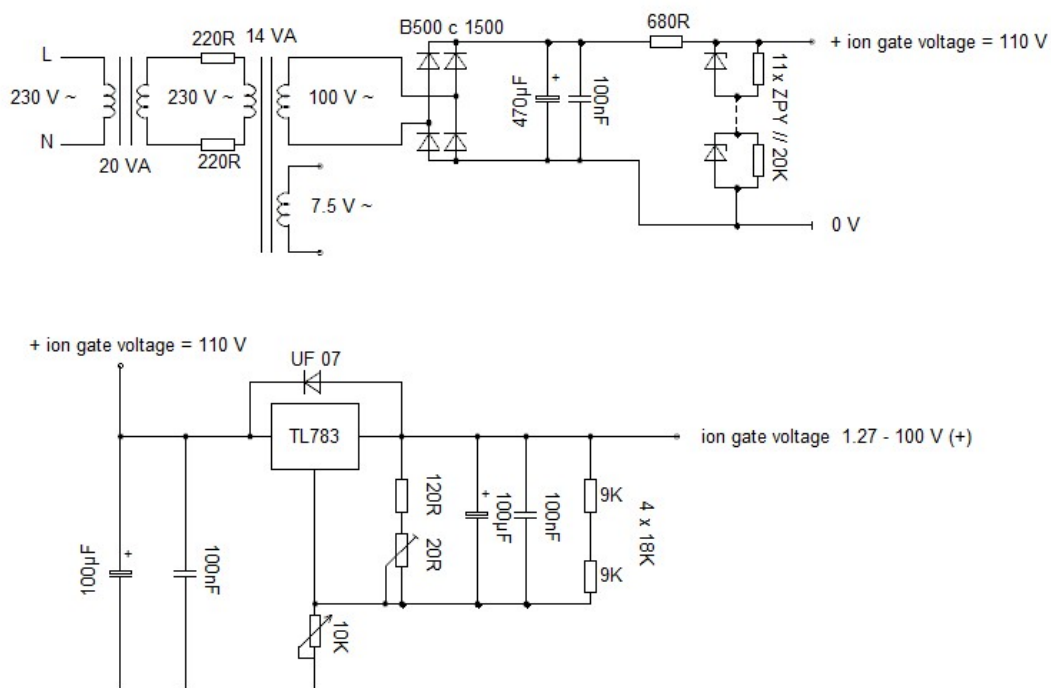
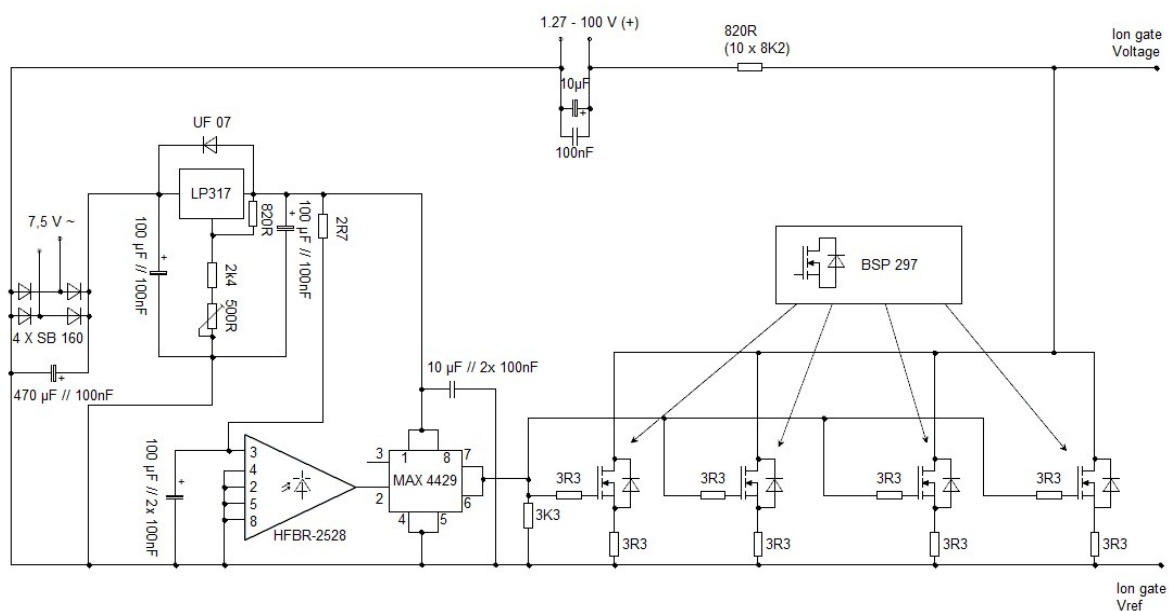Figure 19 Circuitry of the power supply unit for the ion gate bias voltage

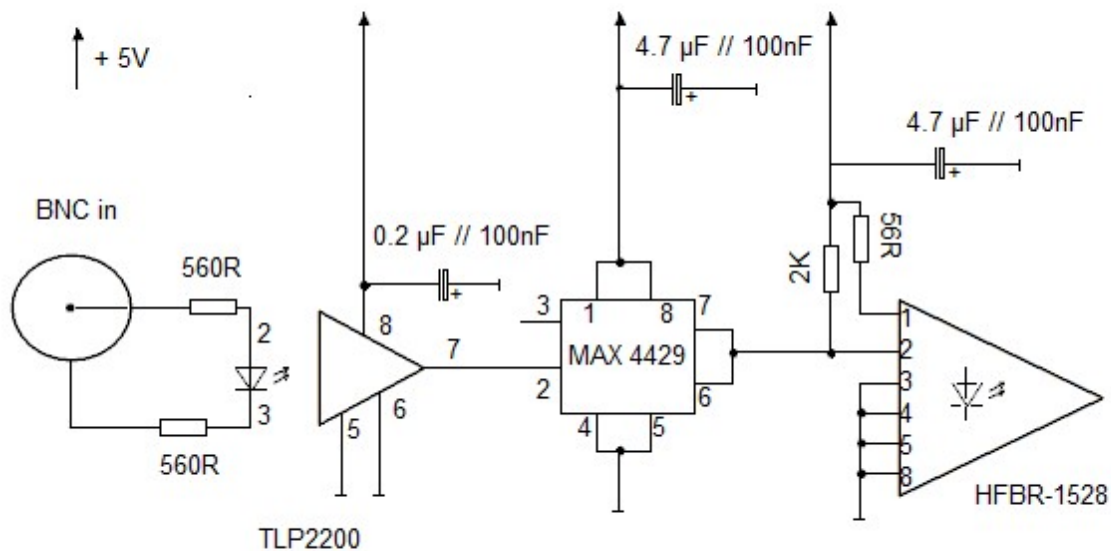Figure 20 Circuitry of the opto-isolated ion gate switching electronics

Figure 21 Circuitry of the light pulse sender generated from a TTL-square pulse going into the BNC input socket (BNC in)

The switching behavior of the opening (falling edge) and the closing (rising edge) were investigated. For this reason, the two wire sets were connected to the ion gate voltage terminal and the reference potential, respectively and the switching behavior was recorded with an passive probe connected to these wires and to an oscilloscope.
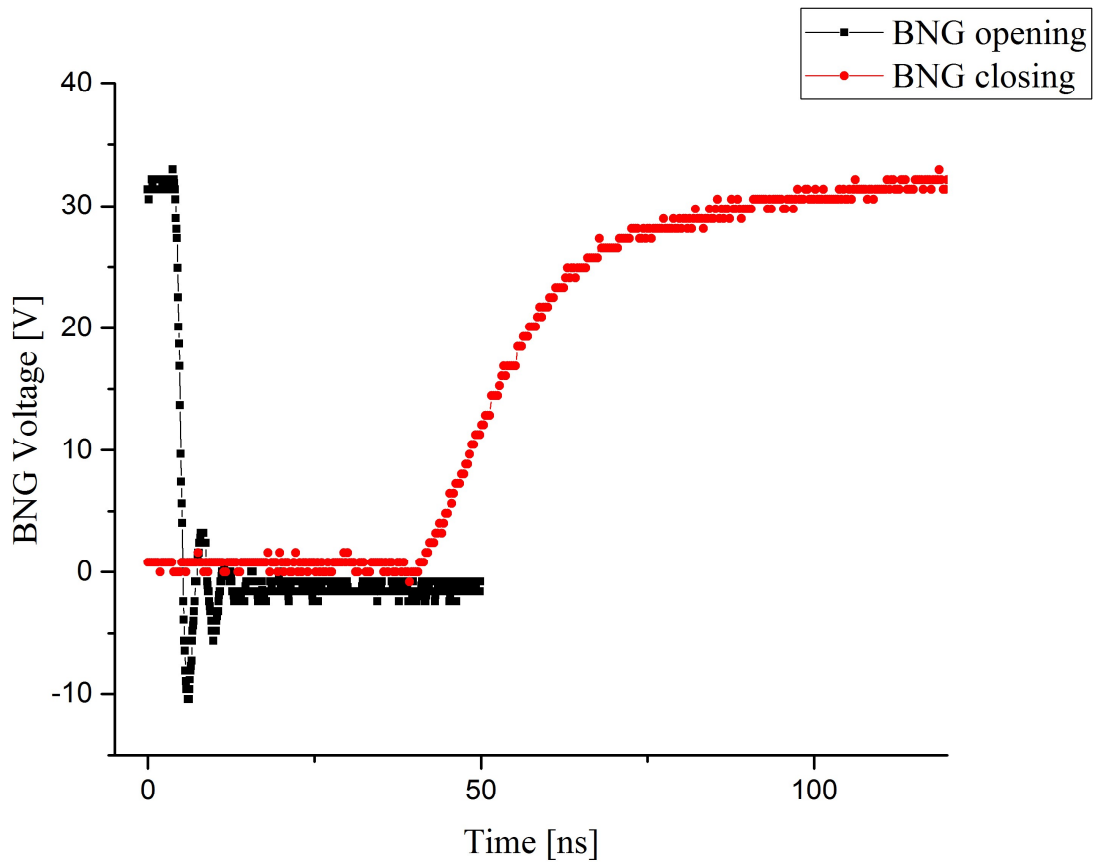
Figure 22: BNG opening (black points) and BNG closing (red points) times. The gate voltage was set to 30 V

The electronics are switching the BNG voltage in appropriate timing. Falling times of ~ 20 ns and rise times of ~ 125 ns, were determined respectively. Typical drift times are detected in the range of several milliseconds to tenths of milliseconds with peak widths in the range of several hundreds of μs to ms. Hence, the developed electronics will provide sufficient sharp injection pulses for ion mobility spectrometers. The shutter electronics for periodical ion injection can be implemented in any ion mobility spectrometer with electrically working injection grids.

3.7 *Implementation of excitation light sources into the drift region of an ion mobility spectrometer*

The open drift cell design consists of the electrospray source, four drift rings, the ion gate, and the miniaturized detector assembly. Between the last ring and the aperture grid, the excitation source is coupled into the center axis of the drift cell assembly. As a general consideration, the excitation of ions at atmospheric pressure requires monochromatic light with high intensity. A simple, low cost and robust monochromatic light source with high intensity can be made from commercial available high power laser diodes. Usually these diodes are available in standardized TO 56 housings. The number indicates the outer diameter of the housing of 5.6 mm. A small portion of the supplied electrical power is converted into light and the remaining power is converted into heat.
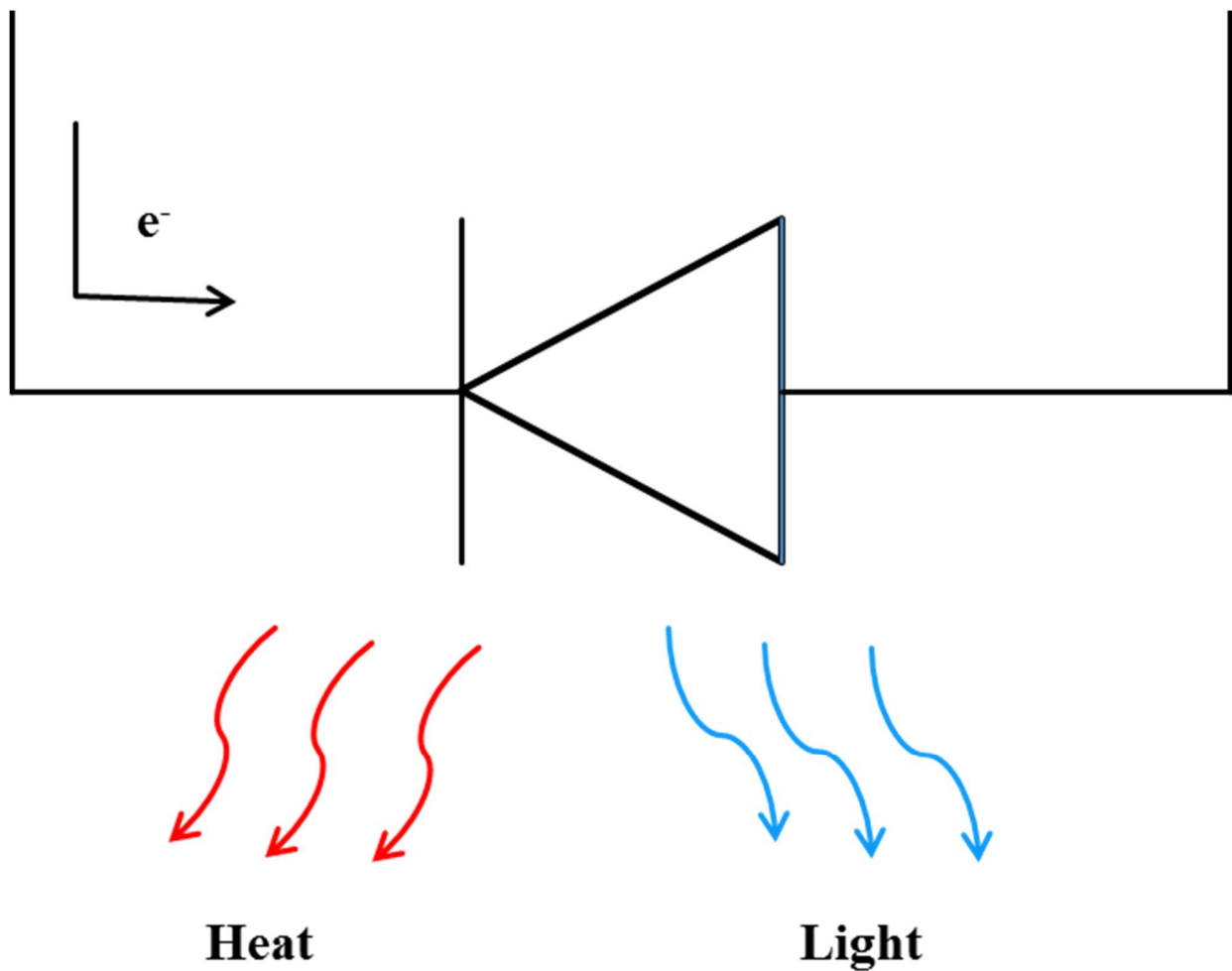
Figure 23 Laser diode principle

The ideal laser diode driver is a constant current source that is noiseless and delivers the exact current that the diode needs to operate.[96] The manufacturer often gives standard operating conditions for the operating current.

3.7.1 Continuous emitting excitation source for the analysis of fluorescent dye cations in the gas phase

Two diodes (PL TB450B, Osram, Regensburg, Germany), (NUBM07E, Nichia, Tokushima, Japan) have been used in the experimental work. These diodes emit the light with maxima at 447 nm and 462 nm and with optical output power of 1.6 W and 3 W, respectively. In the example of the PL TB450B laser diode, the diode is emitting 1.6 Watt of output power at an operating current of 1.2 A. Therefore a constant current source was designed operating at approximately 1.2 A. The voltage regulator LM 317 can be used as constant current source up to a maximum current of 1.5 A. When the wiring is correct, the circuit gives a constant current in dependence of the used adjustment resistor. The excessive current is converted into heat via the heat sink of the LM 317. The drop-out voltage of this integrated circuit is 1.25 V. Hence, for the required operating voltage (4.8 V) of the laser diode, a minimum voltage of 6.05 V is required for operation. The laser diode was mounted in a piece of aluminum to dissipate the excessive heat. This was facilitated with a fan, mounted to the aluminum holder. Due to practical reasons, the circuit with its additional heatsink is mounted on the cooled aluminum laser diode holder as well. Centered and in parallel positioning in front of the laser diode, a triplet collimator lens (focal length = 16 mm) was mounted to parallelize the emitted light. The complete assembly of laser diode is shown below.
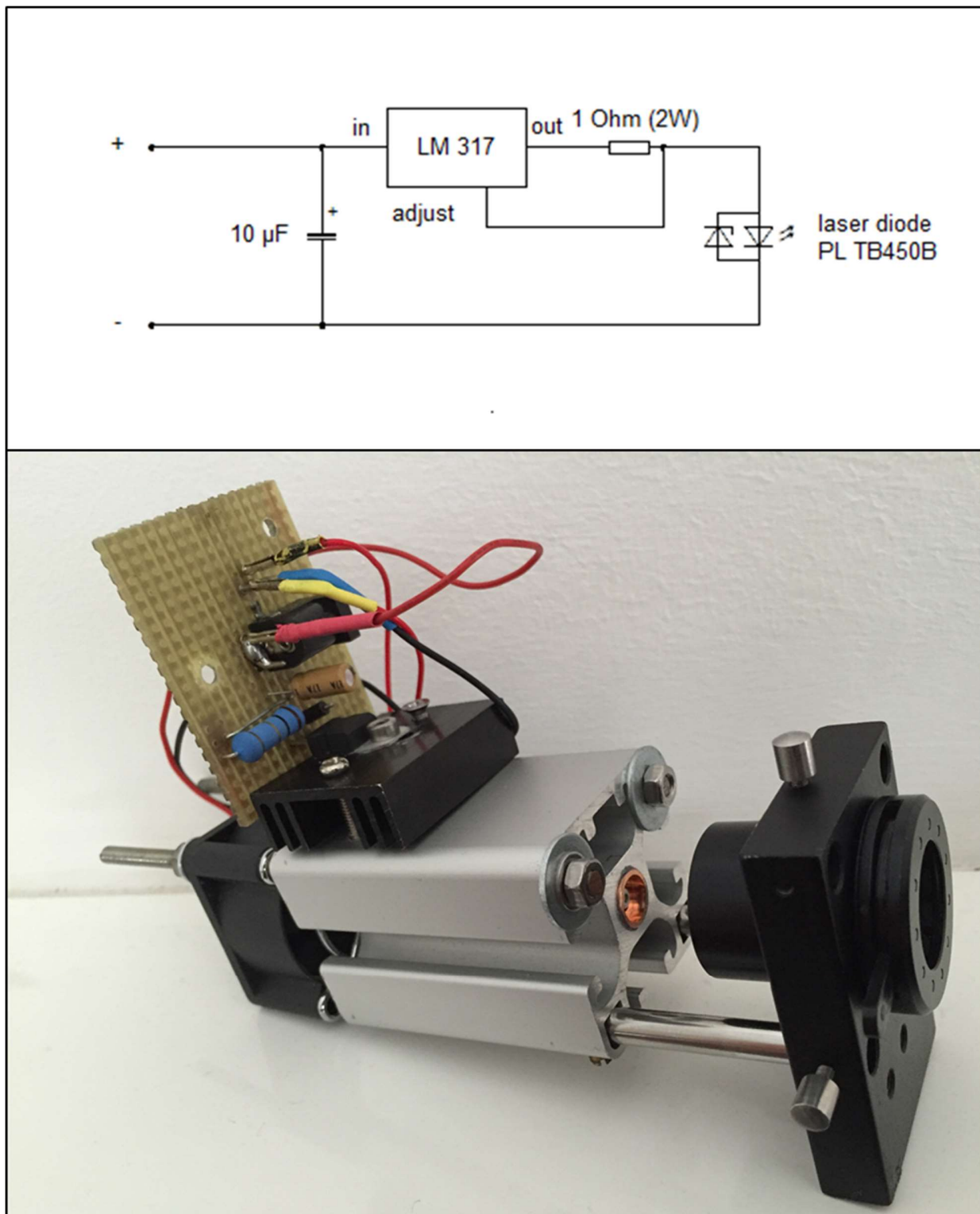
Figure 24 PL TB 450 B mounted in aluminum body. The constant current source is mounted with the heatsink on the diode assembly. The fan is mounted on the backside of the assembly. The lens system is mounted on rails to adjust the focusing point on the laser diode emitter.

The developed assembly allows the simple integration of monochromatic light into an IMS. The most important consideration is the dissipation of heat from the laser diode housing. With the Aluminum profile the heat can be drained away via the high surface at reduced material weight. The contact between the laser diode and the Aluminum housing is made with an adapted copper component and thermal compound paste. The additional fan supports the heat dissipation. The current flowing through the diode is constant. In the case of NUBM07E, a laboratory power supply is used with current limitation.

3.7.2 The coupling of IMS and LIF for the detection of PAHs

The determination of the fluorescence properties of polycyclic aromatic hydrocarbons in the gas phase has been studied by many groups. Whitaker and Bushaw studied the collisional quenching and quenching in the presence of oxygen of vapor phase pyrene.[97] A frequency quadrupled Nd:YAG laser was used in this study. Anthracene and fluoranthene were quantified in a mixture by laser induced fluorescence detection.[98] The fluorescence lifetimes of the two compounds were reported from the same authors.[99] A N_2-Laser emitting at 337 nm was used in these studies. The excitation and emission spectra as well as the fluorescence lifetimes of a broad range of particulate PAH were studied by Niessner.[100] A rather current study used a frequency quadrupled Nd:YAg Laser for the online detection of PAH mixtures (up to four different PAH with a the use of a reference mixture) in combustion gases. The 266 nm is a good compromise for the excitation of PAH since this is a region where most of the PAH strongly absorb. The available lasers have a short pulse width (in the range of 5-10 ns) that allows the study of fluorescence lifetimes.

3.7.3 Operating principle of a pulsed Nd:YAg laser

The photons for the stimulated emission of the laser medium are typically delivered from a xenon-flash tube lamp, also called pump source. The neodymium ions in the YAG (Yttrium-Aluminium-Garnet, $Y_3Al_5O_{12}$) crystal (laser medium) act as a laser gain medium. In case of the Nd:YAG the crystal is doped with ~0.7 % (weight) Nd^{3+} ions. The gain medium material has a major influence of the wavelength of operation. The stimulated emission of light is the first process of the laser mechanism. The return from an excited state into the ground state can be stimulated by the influence of a light wave that meet the Bohr conditions of frequency. In general, a photon hits an electron in the excited state that returns into a lower energetic state. Simultaneously a second

photon of the same frequency and phase is formed. Hence, the light is amplified. The light source must have a high radiation density and must emit in a suitable spectral range to excite the laser medium. The amplification of light and therefore laser action requires the inversion of population densities. In case of Nd:YAG lasers the used pumping sources consist of light sources (e.g. continuous emitting light sources and flash lamps). The stimulated emission processes must predominate to achieve laser emission. Hence, the factor of amplification (gain) must be high enough, or the (laser) photons must pass the laser medium several times.

The general setup of a laser is a characteristic arrangement of the active (laser) medium with optical elements such as mirrors, or prisms. A rod of the laser medium is placed in between two mirrors. One of the mirrors is semitransparent for the output coupling of the laser emission.

The duration of the laser emission can be reduced which is of high interest in many applications. With reducing of the emission duration the light power increases for a given pump energy. This formation of a light pulse with high power is performed by the quality switch (Q-switch). The standard pump pulse of a flash lamp in Nd:YAG lasers has duration of several 100 µs. The Q-switch is located between the laser rod and the reflecting mirror. The Q-switch opens the optical path of the resonator at the end of the pump pulse. This results in a high inversion and gives a short light pulse of high power. The lifetime of the Nd:YAG excited state must be higher than the pump pulse duration. The most frequently used Q-switches use Pockels-cells made from Pottasiumdihydrogenphosphate (KDP) that changes the polarization of the laser emission under the influence of an electric field. The 1064 nm laser line of the Nd:YAG is frequency doubled for two times to generate the 266 nm. The principle of this procedure lies in the formation of the non-linear component of the polarization processes in non-linear crystals. Many different non-linear crystals exist. The most common material is Pottassiumdihydrogenphosphate (KDP) which is transparent in the range of 200 – 1900 nm.[96] The laser used in this study (Polaris, New wave research, Fremont, CA, USA) has external triggering control and gives the user control over the timing of the laser pulse.

3.7.4 Spectrograph with Intensified charge coupled device camera (ICCD)

The detection of the fluorescence is performed with a spectrograph (Shamrock 303i, Belfast, North Ireland) equipped with a grating of 149 lines mm^{-1} and a blaze wavelength of 300 nm. This means the grating has the maximum degree of reflection at 300 nm. The optical path is according to Czerny and Turner. The detector consists of an intensified charge coupled device array (iStar DH734-18U-03, Belfast, North Ireland) of 1024x1024 pixels with an effective pixel size of 13 μm^2. The CCD can be cooled to reduce dark current. The integrated cooling system can reduce the dark current to ~0.5 e$^-$ pix^{-1} sec^{-1}, specifications are as follows. The CCD intensifier consists of a photo cathode (type W-AGT), an optical gate (min. optical gate width = 1.88 ns), a microchannel plate (a max. MCP gain of 255 corresponds to ~600 counts photoelectron^{-1} and a phosphor screen (Phosphor P43) located in front of the CCD array. The system is a wavelength resolving detector with high sensitivity (MCP gain) and low shutter opening times (optical gate) for the observation of fast light emission events (e.g. fluorescence lifetimes).

3.8 *The experimental setup ESI-IMS-LIF using open drift cell design and high power laser diode*

The assembly of four drift ring electrodes and the ion gate assembly is placed in an optical bench. The detector for the open drift cell design is aligned with the central axis of the drift cell and placed 10 mm behind the last ring electrode on a plate of polycarbonate. The blue laser diode assembly is mounted on a x,y,z-manipulator table and was coupled orthogonally into the drift cell center perpendicular 5 mm behind the last ring electrode. The drift lengths for the Faraday plate detection and the LIF detection are 35 and 28 mm respectively. The electric field is generated with a high voltage (ISEQ DPS 50205, Germany) applied to a series of 1 MΩ resistors connected in series between the ring electrodes (voltage divider). The voltage drop between the aperture grid is generated with 200 kΩ from the aperture grid to ground potential and the capacitor has 5 μF. The electrospray emitter of the ion source is placed in front of the first ring electrode and can be adjusted with another x,y,z-manipulator. The electrospray voltage is generated with a second high voltage power supply (ISEQ DPS 50205, Germany) with a potential 1-3 kV higher than the drift potential. A syringe pump (KD scientific) is used for the continuous infusion of Rhodamine 6G solution (500 μM in MeOH, 0.1% formic acid). Perpendicular to the drift cell and perpendicular to the laser

beam, the collection optics are mounted to a x,y-manipulator. The collection optics consist of a cylindrical lens (f= 40 mm) and a collimation lens (f= 75 mm F/6.8) in front of the collimation optic (LLZ010, f = 19mm, F/1.7) for the quartz fibres (72 fibres LUV100/110/125μ) with a numerical aperture of 0.12 going to a rectangular profile (0.125 x 9 mm) into the entrance slit of the spectrograph with ICCD detector. A detailed photograph of the drift cell is shown in Figure 25. The connection of the voltage divider is according to the schematic in Figure 16. The electronics for the Bradbury-Nielsen Gate are connected according to Figure 16, Figure 19, Figure 20, Figure 21.
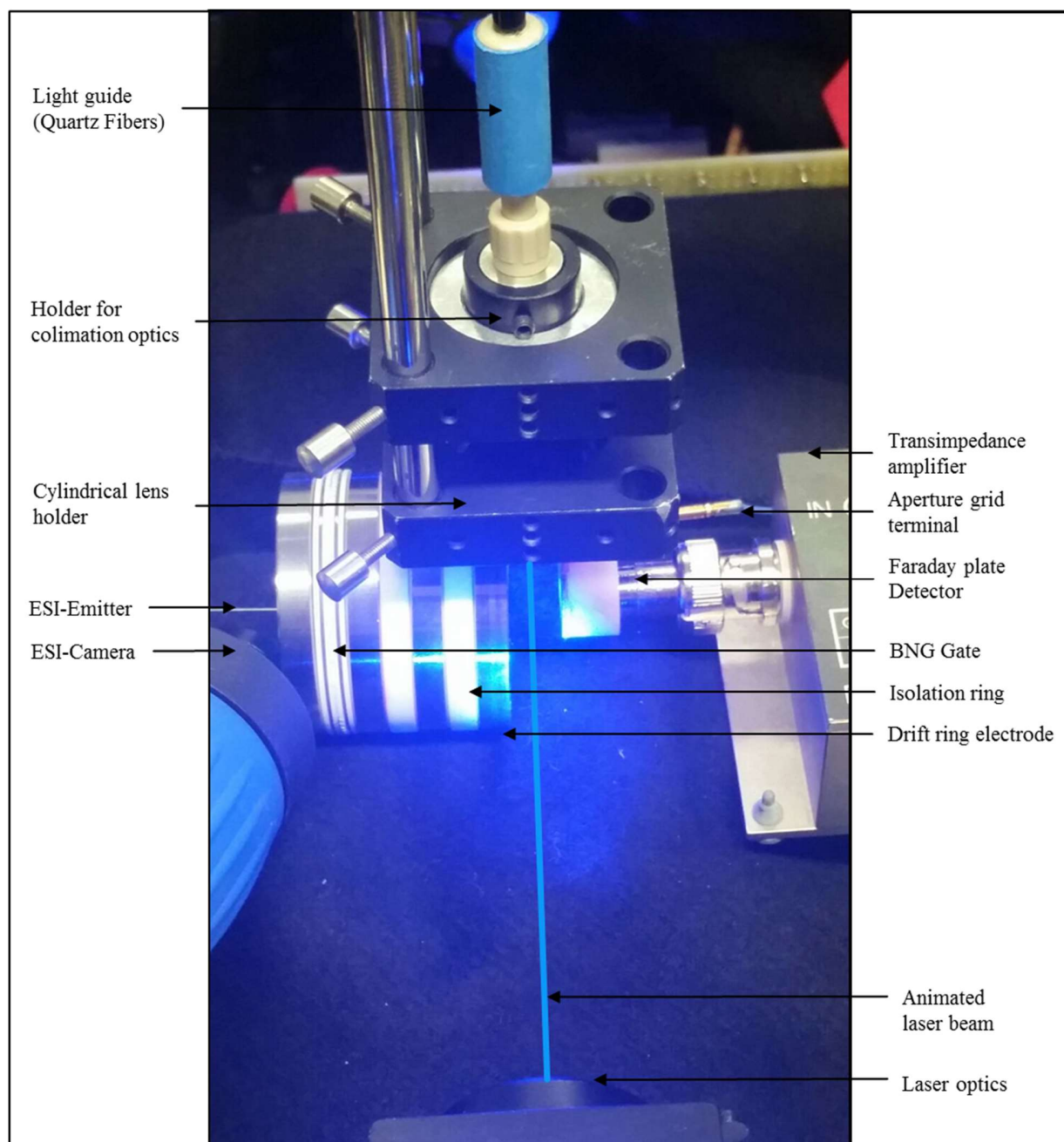
Figure 25 Experimental setup for ESI-IMS-LIF.

The experimental parameters affecting the laser induced fluorescence of a gaseous ionic dye is subject of section 0 in this work.

3.9 *The experimental setup PI-IMS-LIF using closed unidirectional flow drift cell with pulsed Nd:YAG laser*

The implementation of IMS and LIF is an alternative approach for the detection of polycyclic aromatic hydrocarbons (PAH) in waters. Sample introduction was performed with permeation tubes filled with pure substances of PAH. The principle of the setup for the instrumental coupling is shown in the schematic below.
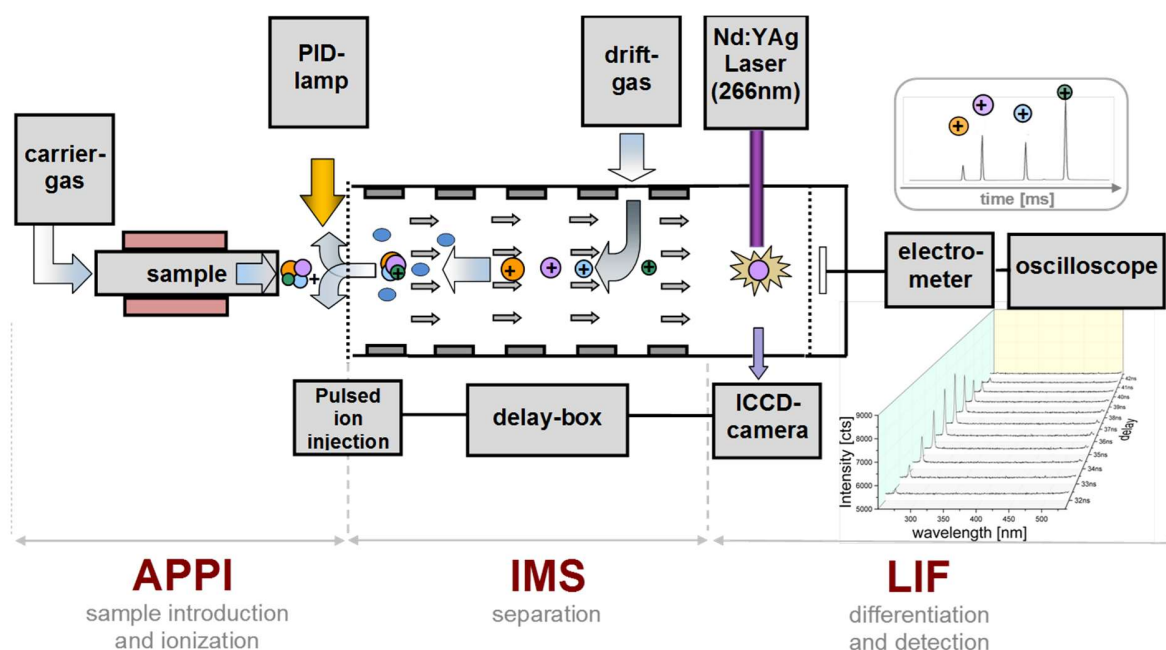
Figure 26 Scheme of the PI-IMS-LIF setup

The developed photoionization source was aligned with the extraction electrode and two drift ring electrodes (separated with an isolation electrode) in front of a BNG ion gate and connected to a drift tube made from a stack of drift ring electrodes (16 pieces) and insulation rings (15 pieces). The detector for the closed cell design was equipped with a flow cell made from α-Al_2O_3 placed between the detector plate and the last ring electrode. The overall drift length from the ion gate wire center of the gate to the detector plate is 16.33 mm ± 1 mm. The thickness flow cell made of aluminum oxide was 22.8 mm, with inner and outer diameter of 25 mm and 40 mm respectively. The flow cell was further equipped with three holes, located in 90° angle to each other. Two plane

quartz windows (λ/4, 10 mm in diameter, 0.5 mm in thickness) in 180° to each other were coated (anti-reflection coating in the range of 200-600 nm with Transmission > 97%). The third hole was modified for the insertion of the optical fibre (light guide) of the spectrograph. An aperture grid was implemented into this flow cell with the developed weaving method (see Figure 12). Two windows were for the coupling and decoupling of the laser beam. The third window served for the collection of the fluorescence. A photograph of the IMS-cuvette and the implementation with the detector and the whole IMS is shown below.
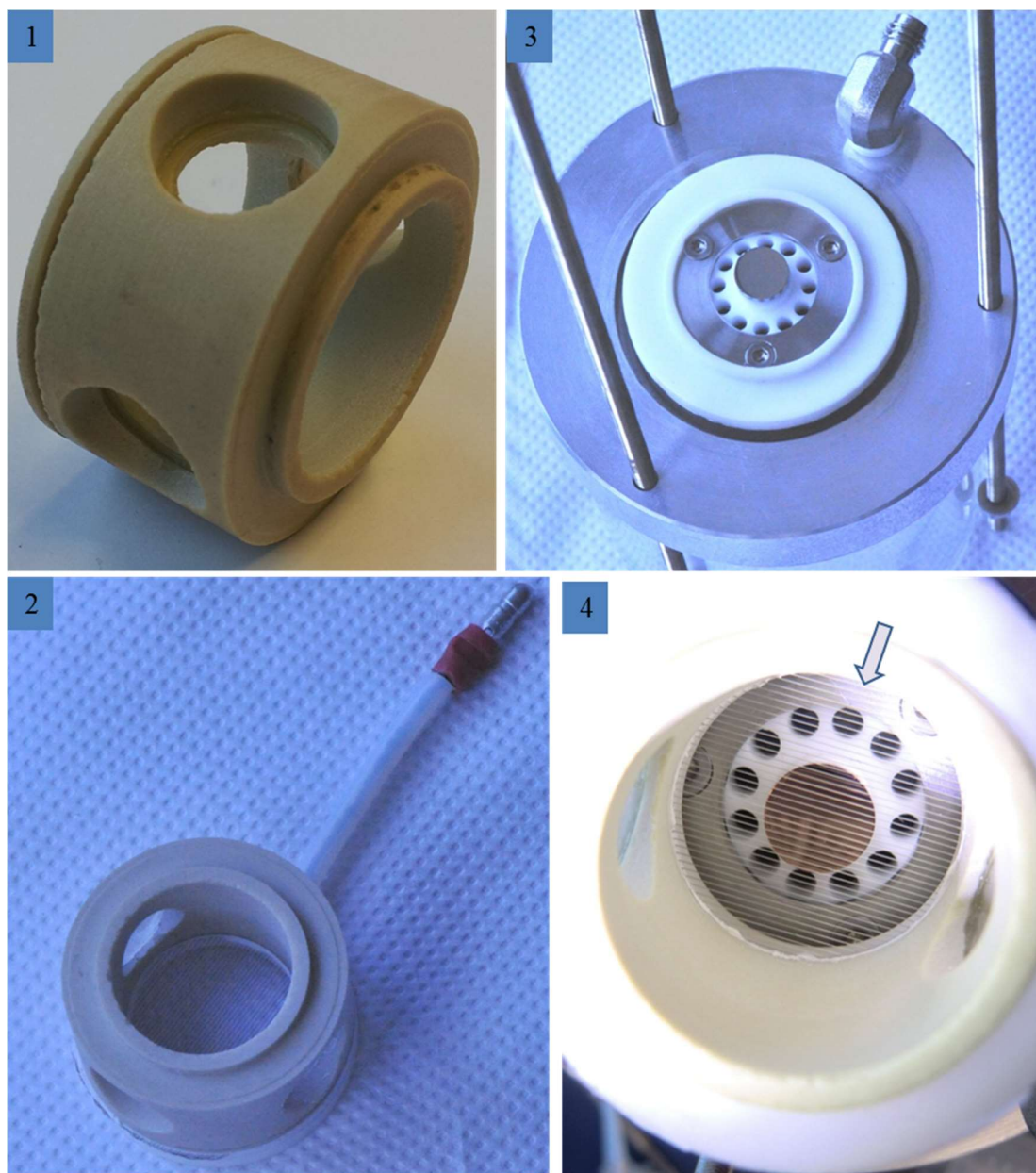
Figure 27 The LIF-detection assembly in the closed IMS. (1) LIF flow-through cuvette. (2) LIF-cuvette with aperture grid. (3) Assembled detector. (4) LIF-cuvette placed on the detector. The arrow marks the insertion direction of the optical fibre (light guide)

This design allows the analysis of the ion current by means of laser induced fluorescence spectroscopy in front of the Faraday plate detector. The implementation of the flow cell cuvette, the heated drift tube and heated photoionization source is described in seven steps in Figure 28.

The detector with the LIF cuvette (1) is aligned with the stacked drift tube (2). An isolation layer of Teflon (3) serves for electrical isolation of the heating mantle (3). The heating mantle encloses the drift tube including the ion gate region and reaction region. The reaction region is interfaced to the photoionization source via the extraction electrode seen in (4). (5) The Photoionization is mounted on the top of the drift tube. (6) The source heating and compression flange are mounted. This setup seals the drift tube with a drift gas leakage in the range of 1-10 %. The leakages were only located at the cemented joints of the ion gate and aperture grid. (7) shows the whole PI-IMS-LIF drift cell with mounted voltage divider.
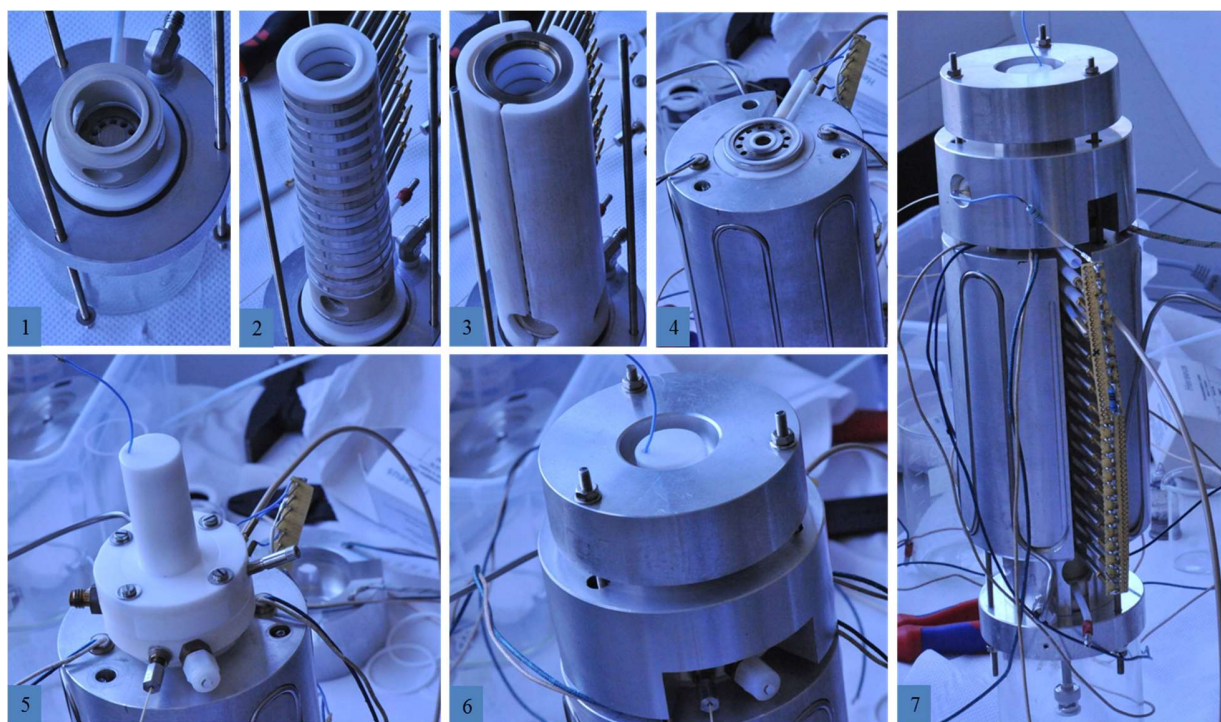

Figure 28 Assembly of the PI-IMS-LIF cell

The principle of the electric field gradient creation and the ion gate switching was shown in section (3.6). The voltage drop between the last ring electrode and the aperture grid was adjusted with a resistor value of ~ 2.84 MΩ. When the drift voltage of 5 kV is applied to the PID socket, the electric field should be homogeneous and corresponds to an electric field gradient of ~264 V cm^{-1}.

The assembly is placed into an optical bench for precise adjustment of the optical paths of the excitation and emission. A photograph of the drift cell with the excitation and emission optics implemented into the drift cell is shown below.
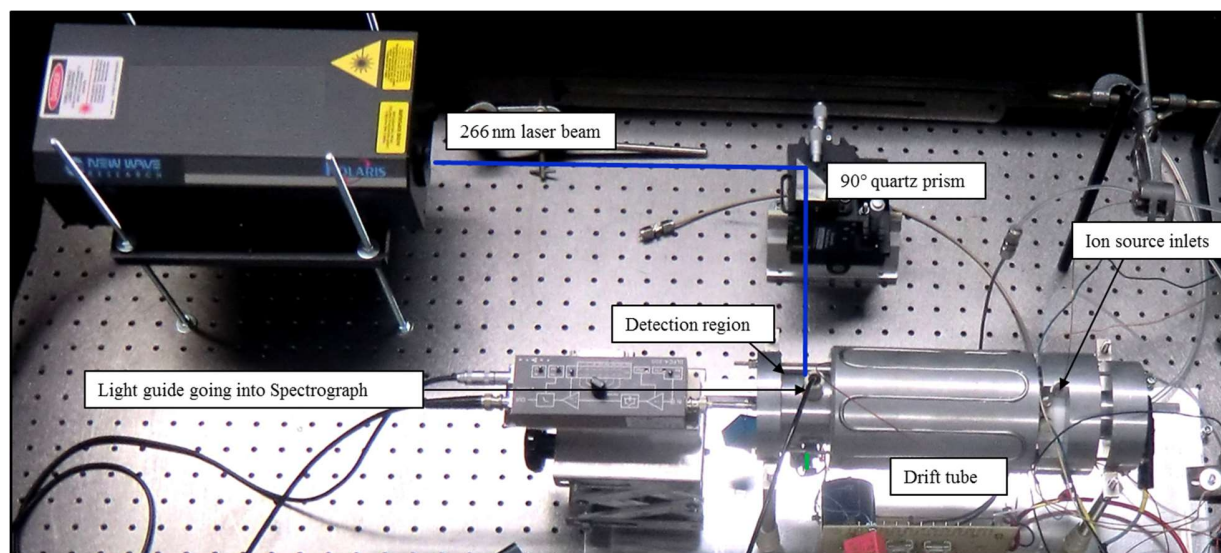

Figure 29 Experimental setup PI-IMS-LIF. The laser beam path is animated as a blue line

The sample introduction was realized with heated modified injectors. The injectors were used without liners as a closed vessel with gas inlet and outlet connections. The injectors were connected with fused silica capillary to the inlet of the photo ionization source. Therefore, the IMS was further equipped with gas flow connections to generate a unidirectional flow IMS. Nitrogen (99.999% purity) was used as drift gas, carrier gas and additional dopant gas carrier gas. The drift gas flow rate was in the range of $50 - 500$ mL min^{-1} and was adjusted by mass flow controllers (Aalborg GFC, Orangeburg, United States). The sample and carrier gas flow rates were also provided by mass flow controllers with a working range of 1-10 mL min^{-1}. Gaseous samples were provided into the ionization source by desorption of solids (in permeation tubes placed in heated ovens. Two sample introduction systems were connected to the ionization source. One was for the introduction of sample and the other was for introduction of dopants. A schematic of the flow scheme and a photograph of the injectors mounted to the photoionization source inlet is shown below.
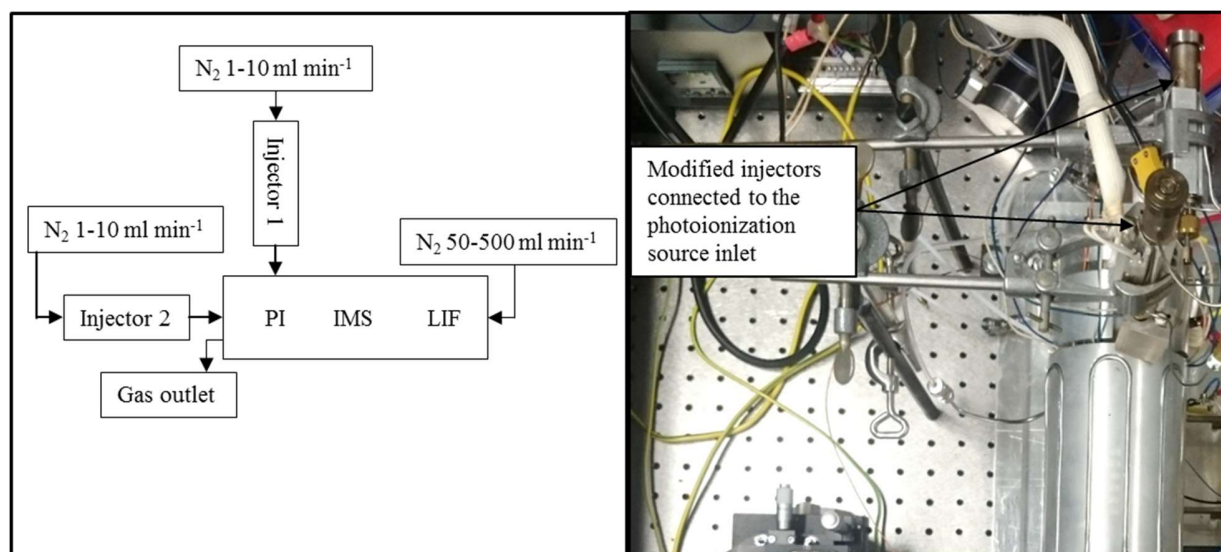
Figure 30 Schematic of the gas flow in the experimental setup (left). Photograph of the injectors (right)

The function of the ion mobility spectrometer was proven on the analysis of selected polycyclic aromatic hydrocarbons (PAH). A small portion of PAH in an open glass vial was placed into one of the injectors. The injector, the ion source and the drift tube was cleaned by heating (~180 ° C for two hours) before the next substance was put in the injector. The carrier gas was set to 10 mL min^{-1}. The drift gas was set to 500 mL min^{-1}. The injector temperature, the source temperature and the drift tube temperature were set to 80° C during the recording of drift time spectra. The electric field gradient was 264 V cm^{-1}. The BNG was set to a closing voltage of 30 V with a pulse width of 200 µs. The aperture grid was held at ~ 32 V above ground. The amplifier was set to a gain of 10^{11}. The trigger in the oscilloscope was set to the rising edge of the ion injection pulse. The resulting oscillogram (16 averages, DC mode) has been recorded with a digital storing oscilloscope (Agilent DSOX2022A, United States). The single drift time spectra of benzene (gas phase, AppliChem, 99+%), naphthalene, phenanthrene, pyrene (all from SigmaAldrich, 99%) are shown below.
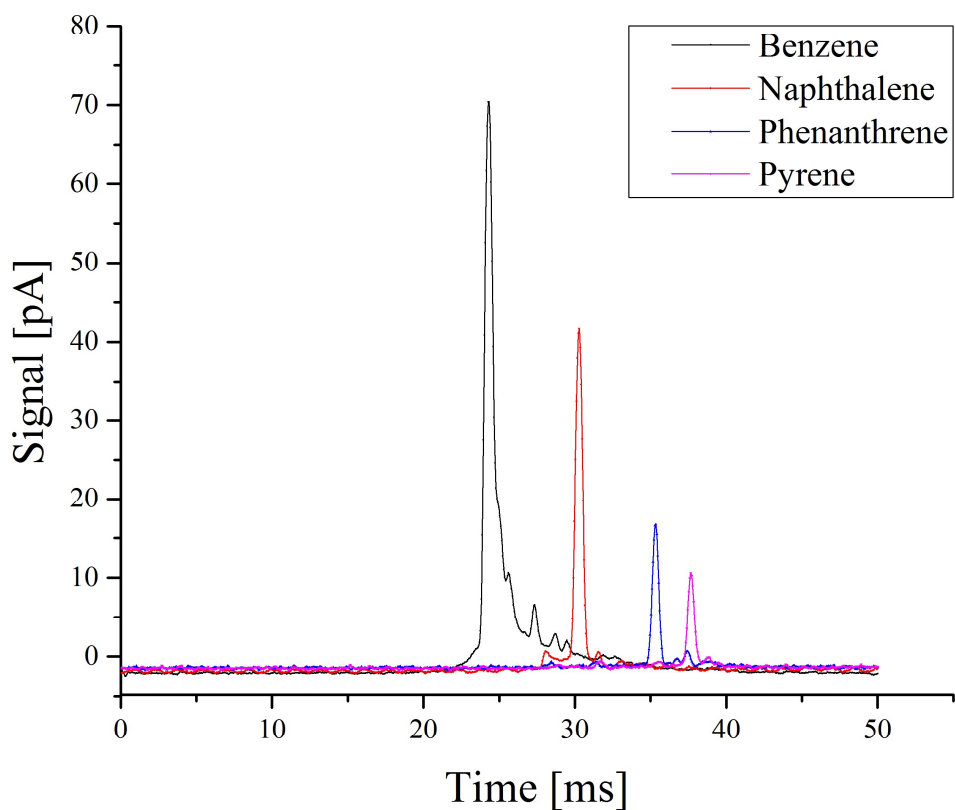
Figure 31 single drift time spectra of benzene and selected polycyclic hydrocarbons.

In Figure 31, the drift time spectra of the product ions from four aromatic compounds are shown. The PAH were put as solids into the injector and no changes of the peak properties were observed over time, as long as the analyte was present in the injector. With increasing number of condensed rings, the drift time increases. This can be explained by the reduced mobility of higher condensed polycyclic aromatic hydrocarbons. The reduced mobility is a result of the increase in collision cross section. The collision cross section is increased due to the changes of molecule geometry with increasing number of condensed rings. The advantage of the photoionization is the production of either the molecular ion or the MH^+. The problem of the occurrence of multiple peaks after chemical ionization is reduced. The trend of decreasing peak height with increased number of condensed rings can be explained by the vapor pressure of the pure solids.

The advantage of the experimental setup is, that the ion mobility based separation takes place <u>with</u> the presence of the implemented flow cell that enables the probing of the ion packet in front of the Faraday plate detection.

The investigation of the parameters affecting the laser induced fluorescence of PAH in this experimental setup is subject of section 5 in this work.

4 Drift time resolved fluorescence detection of gaseous ionic Rhodamine 6G

4.1 *Introduction*

Despite the fact that many investigations can be found about the different ionization and ion-injection techniques, rather less is known about alternative detection systems. Most of the existing IMS-analyzers use the principle of the Faraday plate with following signal amplification. However, the amplifiers are limited due to the high feedback resistance of the operational amplifier, resulting in a limited sampling rate over the drift time scale with a high electronic noise. The operation of the amplifier for drift tube IMS has been improved by introduction of suppression circuitry, however this method is physical limited.

The current work proposes laser induced fluorescence (LIF) as a complementary/alternative detection system that is potentially faster than a conventional electrometer and provides additional analytical information (e.g. fluorescence wavelength and lifetime).

In the present study, the feasibility of IMS with LIF detection was proven on example of the fluorescence detection of gaseous ions at atmospheric pressure in a simple drift tube ion mobility spectrometer.
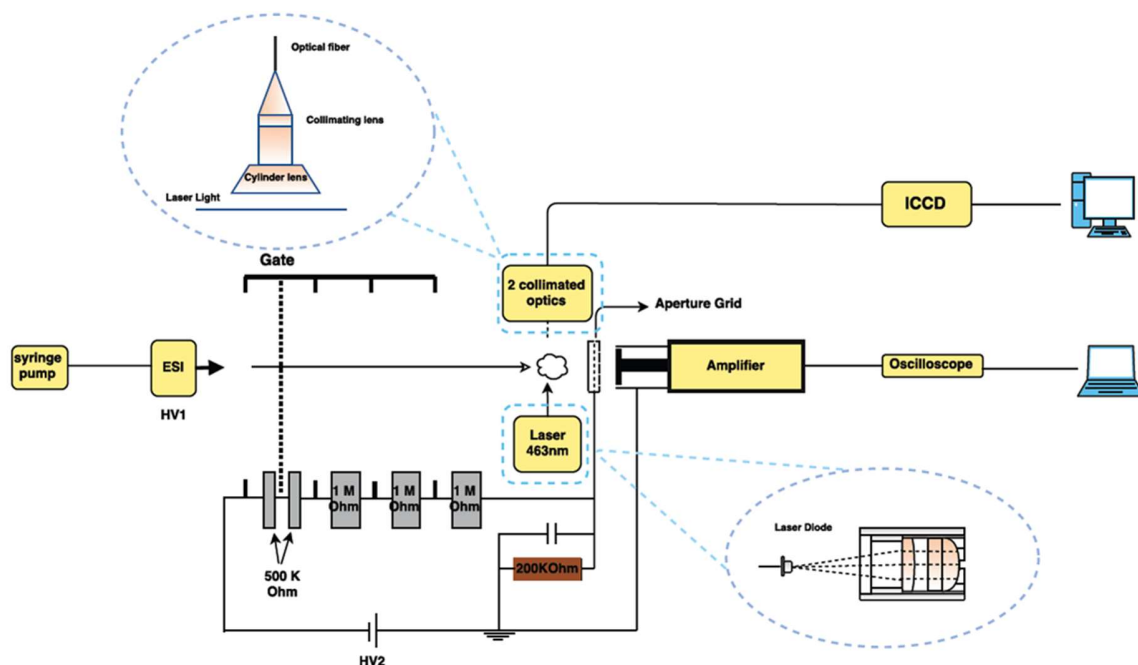
4.2 *Experimental*

Figure 32 Schematic of the IMS-LIF instrument. Light emitted from laser induced fluorescence is detected orthogonally to the ion drift direction

An ion mobility drift cell of open design was constructed in house. The drift tube consists of four cylindrical electrodes in a stack. The neighboring electrodes were insulated by interlocking glass ceramics (Macor) spacers of the same as electrodes diameter (8 mm thick). The drift electrodes were constructed according to Gormally and Philipps[52] with an inner diameter of 25 mm, an outer diameter of 40 mm, outer thickness 5 mm, inner thickness 1 mm. The whole drift region is 32 mm in length. An ion gate, constructed according to Bradbury and Nielsen, was placed between the first and the second ring electrodes. The ion gate was made of two sets of gold-plated parallel wires (Alloy 36 [1.3912], 80 μm diameter) located 600 μm from each other. The wires span a hole of 25 mm and are glued (Resbond 940, Polytec, Waldbronn, Germany) between two ceramic rings (O.D. 40 mm) of 4 mm thickness. The potential of the first set of wires corresponds to the potential of the ion shutter position in the drift tube. The other set of wires has the same potential when shutter is open (ions are transmitted) and higher potential when shutter is closed (ions are not transmitted). The shutter transmits no ions when a voltage difference between the sets of wires is higher than

69

+50 V. The electronic for the Bradbury Nielsen shutter was built in the electronics workshop of the physical chemistry department at the University of Duisburg-Essen. The key component of the Bradbury Neilson shutter electronic is a transformer providing a galvanic insulated AC voltage, which is converted into a switching DC voltage. This voltage can be superimposed on the DC high voltage potential corresponding to the Bradbury Neilson shutter position in the drift tube. The switching frequency is provided by a pulse generator (Digital Storage Oscilloscope DSO-X 2022A, Agilent Technologies, Santa Clara, CL, USA), determining the width and the length of the gate pulse. The drift voltage applied to the first ring was provided by a variable high voltage power supply (DPR 50 205 24 5 EPU, ISEQ, Germany) providing drift voltages up to 5 kV. An electric field gradient within the IMS drift region was realized by connection of each two neighboring cylindrical electrodes via 1 MΩ resistors. The detection for the ion current is a Faraday plate detector equipped with an aperture grid. The Faraday plate is made from a copper plate (4.6 mm diameter, 0.3 mm thickness) and connected to the input of a transimpedance amplifier (Femto DLPCA-200, Berlin, Germany). The amplifier is set to a gain of 10^9 V A^{-1} at 7 kHz bandwidth. An aperture grid, constructed in the same way as the Bradbury Nielsen shutter (wires of 5 mm diameter), was placed in front of the Faraday plate in a distance of approximately 1 mm. A ballast capacitor (5 µF, 1 kV) is added to the aperture grid circuit, as a ready source of electrons flowing into the aperture grid. The capacitor drains the induced current by the approaching ion packets to ground, which otherwise can disturb the ion-peak shape.[55] The aperture grid is held at an appropriate potential via a connection to ground potential over 200 kΩ resistor.

The electrospray ion source was based on a nano-ESI platform (nano ESI v 1.0, 2009, Thermo Scientific, Waltham, USA) consisting of a x,y,z-positioning system, and a liquid junction with electrical connection. Stainless steel (I.D. 30µm, O.D. = 150µm) and fused silica glass capillaries (I.D. = 50µm, O.D. = 150 µm) were used as electrospray emitters. 100 and 500 µM solutions of Rhodamine 6G (Thermo Fisher, Germany) were prepared in Methanol (Fisher scientific, Bishop, UK) with 0.1% formic acid (98%, Merck, Germany) and introduced into the ion source via a gas tight glass syringes (Hamilton, Switzerland) operated with a syringe pump (KDS Legato 210, kdScientific, Holliston, USA). The solution was delivered through a needle (22S, Hamilton, USA) connected to a PEEK capillary tubing (1/16" 300 µm, LC Packings, Netherlands) by a union (PEEK, 1/16", 300 µm). The peek capillary was connected to the liquid junction of the electrospray ion source platform. The voltage applied to the electrospray emitter was provided by a second high

voltage power supply (T1 DP 050 205 EPU, ISEQ Germany) and was set to potential of 1-2 kV above the first IMS ring electrode. When using electrospray emitter with an inner diameter of 30 μm, a stable spray was observed at a flow rate of 300 nL min^{-1} and an absolute potential of 3.33 kV.

Between the last electrode and the aperture grid (distance approximately 10 mm) (PL TB450B (Osram, Regensburg, Germany) or NUBM07E (Nichia, Tokushima, Japan) blue laser diode, was coupled. These diodes emit the light with maxima at 447 nm and 462 nm and with optical output power of 1.6 W and 3 W, respectively. The emitted light was directed orthogonally to the IMS drift axis into the drift region, over a three lens system. The emitted fluorescence was collected in an approximately 90° angle with a cylindrical lens (f = 40 mm) and a two lens collimation system guiding the light into a UV-grade quartz optical fiber (numerical aperture is 0.12). The fluorescence was analyzed by Shamrock spectrometer (SR-303i, Andor, Belfast, United Kingdom) with an optical path according to Czerny and Turner and has a slit set to 100 μm. The grating was 149 lines mm^{-1}. The light detector was a gated intensified charge coupled device (ICCD) (iStar, DH734-18U-03, Andor, Belfast, United Kingdom). The spectrograph was connected with an IMS over a quartz glass fibre equipped with a three lens collimation system. The fluorescence emission was filtered with a long pass filter (cut-on wavelength 470 nm when using the 450 nm laser diode and cut-on wavelength of 490 nm when using the 462 nm diode) to block the scattered laser light.

4.2.1 Fluorescence of Rhodamine 6G cation in the gas phase

100 μM solution of Rhodamine 6G in MeOH (0.1 % formic acid) was sprayed through a 60 μm (I.D.) stainless steel emitter at an ESI voltage of 3.8 kV and a flow rate of 2 μL min^{-1}. The laser (447 nm), mounted perpendicularly and centered to the electrospray axis was moved across the electrospray emitter axis within the distance of 6 – 40 mm. Both, the exposure time and the gate opening time of the ICCD were set to 0.1 s. The microchannel plate gain was set to a value of 50. One hundred accumulations were recorded with Andor Solis software.

4.2.2 Analysis of Rhodamine 6G cation in the gas phase by means of ion mobility spectrometry and laser induced fluorescence

500 µM solution of Rhodamine 6G in MeOH (0.1 % formic acid) was electrosprayed at a flow rate of 2 µL min^{-1} via a 30 µm stainless steel capillary. The ESI was mounted in front of the IMS entrance in a distance of about 10 millimeters. The electrospray voltage was set to 3.5 kV and the IMS voltage was set to 2.231 kV.

Laser induced fluorescence of R6G cations in the gas phase was analyzed behind the drift cell. In this experimets, the switching electronics of the ion gate were turned off, so that ions continuously pass the drift cell with a constant rate.

To investigate the influence of the shutter field on the Rhodamine 6G ion transmission, fluorescence emission spectra were recorded at different shutter voltages. Shutter voltages were varied within the range of 1.3 – 80 V. IMS spectra were recorded in pulsed ion injection mode and fluorescence spectra were recorded in continuous ion injection mode. Excitation was performed with a 447 nm continuous emitting laser diode with an operating current of 1.2 A. The LIF spectra were analyzed within a wavelength range of 418 to 703 nm. The spectrograph was equipped with a 470 nm cut-off transmission filter and with the 149.9 lines mm^{-1} grating (grating blaze of 300). The ICCD gate opening time was set to 100 ms and an exposure time to 118 ms. The gain level was set to a value of 100. The ICCD chip was held at -15 °C. Three replicates of one hundred accumulations were recorded with Andor Solis software.

Drift time dependent ion current signals have been recorded with the transimpedance amplifier operating in high speed mode with a gain of 10^{10} V A^{-1}. The trigger was set on the rising edge of the pulse for the Bradbury Nielsen gate electronics. The pulse generator was set to a pulse width of 200 µs at a frequency of 18 Hz. The ion gate voltage was set to 80 V. The resulting oscillogram (16 averages, DC mode) has been recorded with a digital storing oscilloscope. (Digital Storage Oszilloscope DSO-X 2022A, Agilent Technologies, Santa Clara, CL, USA).

4.2.3   Optimization of the experimental setup

Due to the decreased distance to the IMS entrance (0.5 – 5 mm) in the total ion current measurements, the electrospray voltage was reduced to 3.33 kV. The IMS drift voltage was set to 2.43 kV. 500 µM solutions of Rhodamine 6G were infused at 300 nL min^{-1} flow rate. The fused silica capillary with an inner diameter of 50 µm was used as electrospray emitter. Laser induced fluorescence of R6G cations in the gas phase has been analyzed behind the drift cell. In these experiments, the switching electronics of the ion gate were turned off, so that ions continuously pass the drift cell with constant rate. To investigate the influence of the shutter field on the Rhodamine 6G ion transmission, fluorescence emission spectra were recorded at different shutter voltages. Shutter voltages were varied within the range of 1.3 – 80 V. The electric field strength was varied by simultaneous increasing the ESI voltage and the IMS voltage. The voltage parameters are summarized in table 1.

Table 1 The experimental voltage parameters for the ion transmission fluorescence

ESI Voltage [kV]	IMS Voltage [kV]	Aperture Grid Voltage [V]	Electric field [V cm^{-1}]
2.33	1.43	68.10	340.48
2.53	1.63	77.62	388.10
2.73	1.83	87.14	435.71
2.93	2.03	96.67	483.33
3.13	2.23	106.19	530.95
3.33	2.43	115.71	578.57
3.53	2.63	125.24	626.19
3.73	2.83	134.76	673,81

Excitation of the approaching ions (total ion current) was performed with 462 nm continuous wave (cw) laser diode (Nichia NUBM07E) with an operating current of 1.35 A. The fluorescence was analyzed within the wavelength range of 472 to 756 nm. The spectrograph was equipped with a 490 nm cut-off transmission filter. The spectrograph was used with the 149.9 lines mm^{-1} grating (grating blaze of 300). The ICCD gate opening time was set to 100 ms and an exposure time to 118

ms. The gain level was set to a value of 100. The ICCD chip was set to -15 °C. Three replicates of one hundred accumulations were recorded with Andor Solis software.

4.2.4 Drift time dependent fluorescence detection at different ion gate pulse widths and different electric field strengths

The dependence of the ion current and fluorescence signals on electric field strength was analyzed within the electric field range of 340-674 and 510-638 V cm^{-1}, respectively. The shorter electric field range for the fluorescence measurements was chosen because of the much longer analysis time. The slight difference in the ESI-voltage is due to slight changes in the ESI emitter to IMS distance. The required stability of the spray was provided at a distance of 8-9 mm relatively to the first drift ring electrode of the IMS. The experimental parameters used in the ion current and fluorescence drift time measurements are listed in tables 2 and 3, respectively.

Table 2 The experimental parameters for the ion current detection. Applied voltages of the electrospray, the IMS and the aperture grid with corresponding electric field strengths

ESI Voltage [kV]	IMS Voltage [kV]	Aperture Grid Voltage [V]	Electric field [V cm^{-1}]
2.33	1.43	68.10	340.48
2.53	1.63	77.62	388.10
2.73	1.83	87.14	435.71
2.93	2.03	96.67	483.33
3.13	2.23	106.19	530.95
3.33	2.43	115.71	578.57
3.53	2.63	125.24	626.19
3.73	2.83	134.76	673,81

Table 3 The experimental voltage parameters for fluorescence drift time measurements Applied voltages of the electrospray, the IMS and the aperture grid with corresponding electric field strengths

ESI Voltage [kV]	IMS Voltage [kV]	Aperture Grid Voltage [V]	Electric field [V cm^{-1}]
4.133	2.142	102	510
4.233	2.251	107	536
4.333	2.356	112	561
4.433	2.465	117	587
4.533	2.570	122	612
4.633	2.658	128	638

The Bradbury Nielsen Gate closing voltage was set to 80 V with pulse width of 200 µs. Drift time to ion current spectra were recorded with a trans impedance amplifier (DLPCA-200, Femto; Berlin) in high speed mode with a gain of 10^{10} V A^{-1}.

The drift time resolved fluorescence of Rhodamine 6G cations was analyzed with a time delay to the Bradbury Nielsen shutter pulse. The experimental parameters were set as follows: electric drift field strength was set to 561 V cm^{-1} (IMS voltage of 2.356 kV), the ion gate pulse width was varied within the time range of 100-400 µs in 100 µs step, the electrospray voltage was set to 4.333 kV at an emitter to IMS distance of ~ 8-9 mm, and the Bradbury Nielsen Gate closing voltage was set to 80 V.

Fluorescence excitation of the approaching ions was performed with 462 nm cw laser diode (Nichia NUBM07E) with an operating current of 1.35 A. The ICCD camera was synchronized with the ion shutter pulse with a home build delay generator. The fluorescence was analyzed within the wavelength range of 472 to 756 nm. The spectrograph was equipped with a 490 nm cut-off transmission filter. The spectrograph was equiped with the 149.9 lines mm^{-1} grating with a grating blaze of 300. The drift time scan was performed with 100 µs step width in 20 steps. The measurements after six averages were recorded with Andor Solis software.

4.3 *Results and Discussion*

4.3.1 Fluorescence of Rhodamine 6G cation in the gas phase

A high number of gaseous ions can be produced by electrospray at ambient conditions. The analysis of laser induced fluorescence of Rhodamine 6G in the electrospray has been performed by excitation at 450 nm. The fluorescence emission was examined by excitation at different regions along the electrospray emitter axis. The dependence of fluorescence emission intensity on the distance to the electrode tip by excitation was examined within the distance range of 6 to 40 mm. At distances shorter than 6 mm insufficient desolvation of the Rhodamine 6G cation in the ESI plume was observed. Increase of the distance to the electrode tip resulted in the increase in the fluorescence intensity. The highest fluorescence emission intensity was observed when the distance to the electrode tip was 9 mm. The following increase in the distance to the electrode tip resulted in decrease in fluorescence intensity. The blank subtracted spectra recorded at different distances to the ESI tip are presented in Figure 33 and the dependence of fluorescence intensity on the distance to the electrode tip in Figure 34.
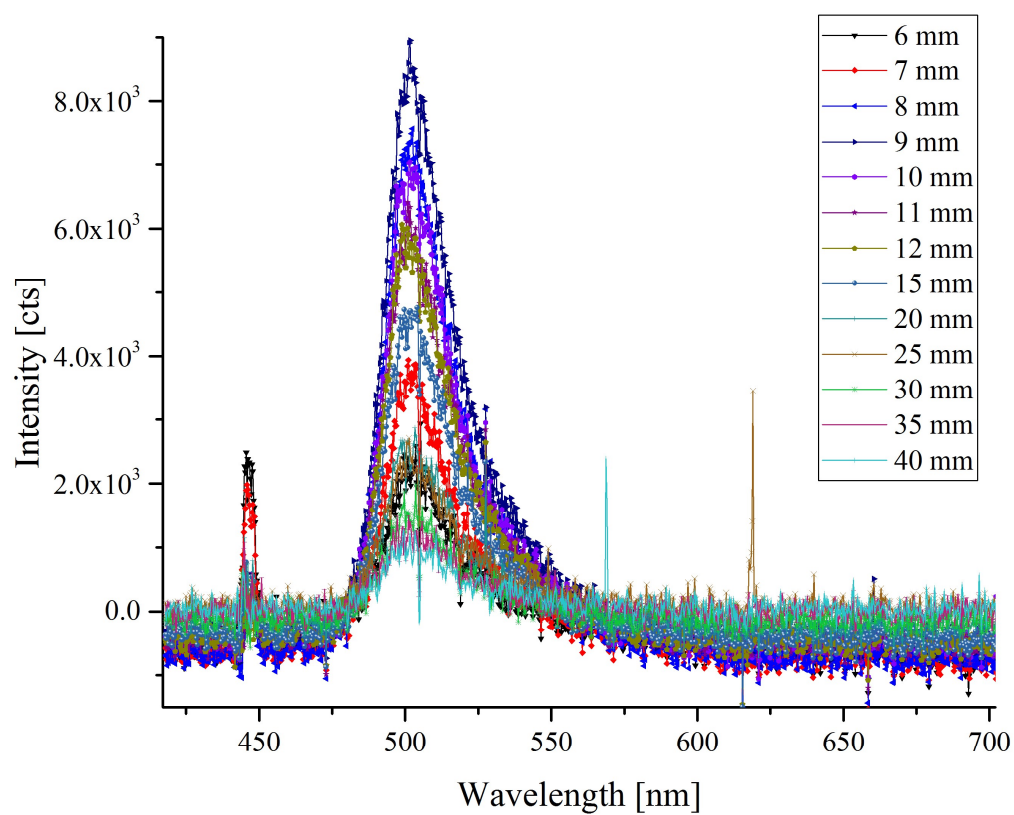
Figure 33. Fluorescence spectra recorded with excitation at different positions along the electrospray plume. The solution infused through the electrospray emitter contained 500 µM Rhodamine 6G dissolved in MeOH (0.1 % formic acid).
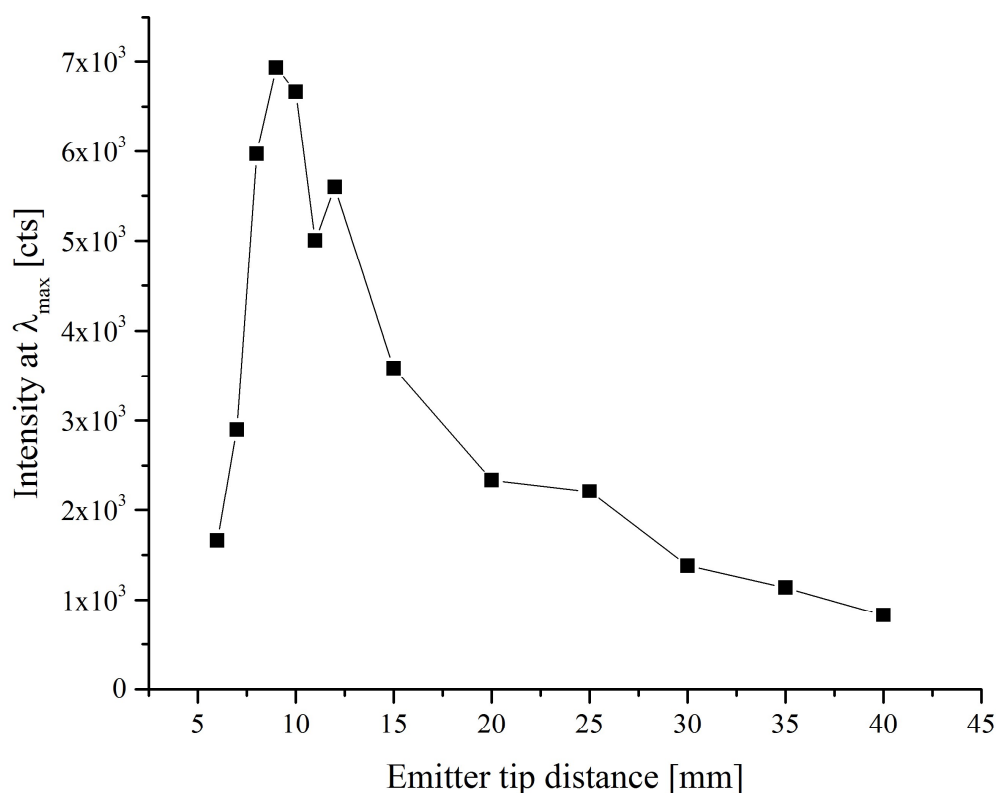
Figure 34. Relationship between the fluorescence emission intensity of Rhodamine 6G cations in the gas phase and the probed distance to the ESI tip. The flow rate of 500 μM R6G solution in MeOH (0.1% formic acid) was 2 μL min-1, the ESI voltage was set to 3.8 kV. The fluorescence emission intensity was analyzed at 505 nm.

In comparison to the fluorescence of Rhodamine 6G cation dissolved in methanol with emission maximum at 555 nm (not shown), Rhodamine 6G cation in the gas phase shows emission maxima at 505 nm. Therefore, based on the fluorescence maximum the desolation efficiency of Rhodamine 6G cations in ESI plume can be monitored. Small droplets, demonstrating high ability to desolvation, are generated when a conical tip is visible at the ESI tip.

The highest fluorescence intensity was observed at a distance of approximately 9 mm from the ESI tip. At approximately this distance the Taylor cone merges into the electrospray plume. This effect supports the evaporation model.

As it was discussed above no sufficient desolvation is achieved at the distances to the ESI tip lower than 6 mm. A possible explanation of increase in fluorescence intensity within the distance range of 6 to 9 mm is the more efficient evaporation of solvent molecules during the electrospray process in the plume. Riebe et al. explained this phenomenon by fluorescence quenching and determined the ion density in the electrospray plume.[101] In the current work, the effectiveness of the desolvation process can be determined by change of emission maxima from 505 nm (corresponds to Rhodamine 6G cation) to 555 nm (corresponds to solvated Rhodamine 6G cation). The same effect for the solvated and free ionic Rhodamine 6G was shown by Chingin et al. Laser induced fluorescence of Rhodamine 6G ions was recorded inside the ion trap of a Fourier-Transformation-Ion-Cyclotron-Resonance-Mass-Spectrometer. The spectral properties of cationic Xanthene dyes in the gas phase can be found in the literature. The gas phase excitation and emission spectra of cationic Rhodamine dyes in the gas phase have been investigated. In general, a blue shift is observed for the transition from solution into the gas phase for both the excitation and emission maxima.[79] The fluorescence emission maximum of Rhodamine 6G cation in the gas phase at approximately 504 ± 1 nm was demonstrated by Forbes et al.[79] This observations are in a good agreement with the data achieved in this study.

The current study demonstrates the drift time dependent laser induced fluorescence of ions in a gas phase in a constant homogeneous electric field under ambient conditions. Based on the possibility to detect ions at distances to the ESI tip up to 40 mm (see figures 4 and 5), it was assumed that the ions generated by electrospray can be analyzed in a drift region of comparable length and detected after separation at the exit of the drift region. The ions can be guided by electronic lenses connected to a voltage divider. A high voltage potential applied to the first electronic lens results in a voltage gradient dropping from several kilo volts over the drift distance to ground potential.

For the simultaneous detection of the ion current and the fluorescence emission, two detection systems are implemented at the end of the drift tube. A laser diode was assembled into the drift region between the last electrode and the aperture grid (distance approximately 10 mm) orthogonally to the IMS drift axis. A monochromatic continuous wave emission excites cationic Rhodamine 6G in the gas phase to induce fluorescence emission. The fluorescence was analyzed in a 90° angle. Because the fluorescence measurements take place within the drift field, the ions are further directed towards the detector plate. The invented module allows the IMS analysis with simultaneous detection of ion current and laser induced fluorescence.

4.3.2 Analysis of Rhodamine 6G cation in the gas phase by means of ion mobility spectrometry and laser induced fluorescence

In the previous section it was demonstrated, that the ion transmission can be detected over a relatively long distance. In the initial LIF experiments the ion gate was in the "open" mode to allow the continuous transmission of Rhodamine 6G ions. The ion transmission efficiency was monitored by the DC offset generated by the trans impedance amplifier. When the solution was infused continuously and the high voltage was switched on, the DC offset was monitored as a constant value of several volts. This corresponds to several tens of nano amperes. The fluorescence emission spectrum of the total ion current recorded at the exit of the 32 mm long drift cell is shown below.
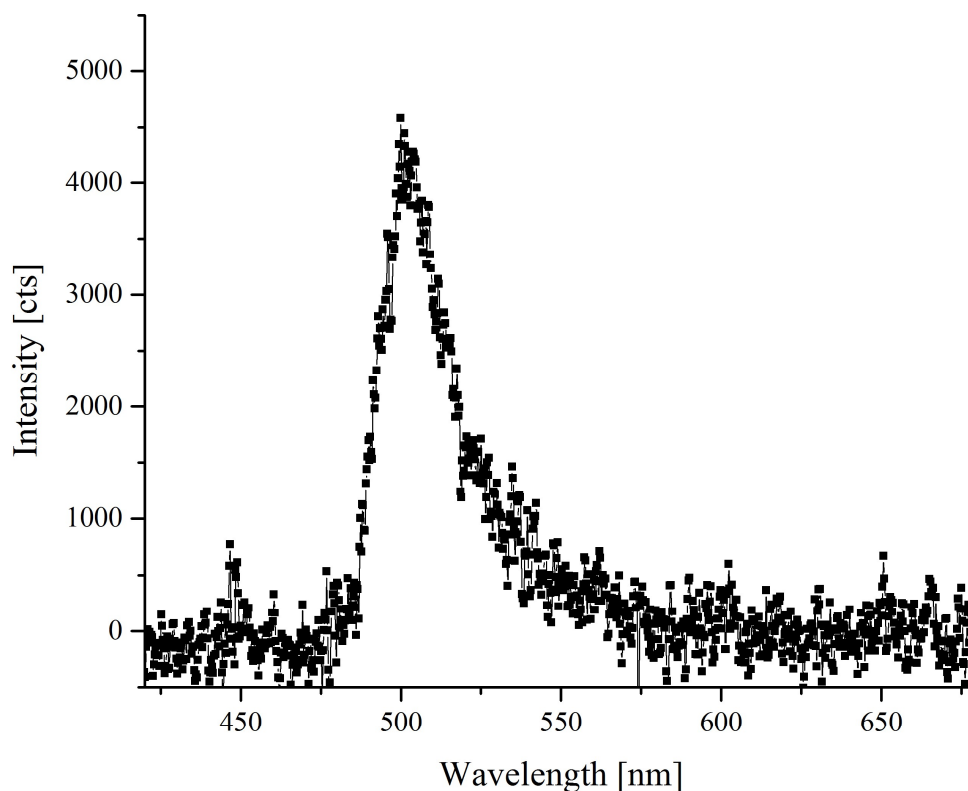
Figure 35 Fluorescence emission spectrum of Rhodamine 6G cation recorded at ESI voltage of +3.50 kV, IMS drift voltage of 2.231 kV (32 mm drift length), ESI flow rate of 2 µL min^{-1} with 500 µM solution of Rhodamine 6G in MeOH (0.1 % formic acid), excitation wavelength of 447 nm (cw) laser diode, 1.6 W output power), ICCD gate width was 100 ms, gain of 100, 100 accumulations, blank subtracted, average of n=3.

The fluorescence emission spectrum recorded at the exit of the drift cell is comparable to that recorded for Rhodamine 6G ion in the electrospray plume. This confirms the feasibility of IMS coupled with laser induced fluorescence detector.

4.3.3   Optimization of the experimental setup

In the following sections the optimization of experimental parameters for the drift cell (e.g. electric field strength, ion gate voltage and pulse duration) as well as for the LIF (e.g. excitation wavelengths) are described. Optimization of these parameters is essential to achieve the optimal transmission, separation, and detection of the ions.

4.3.3.1   Optimization of the ion gate voltage

To produce an ion mobility spectrum, the ions should be introduced into the drift region as narrow swarms. This function is realized by an iron gate (ion shutter). The shutter does not allow the ion transmission into the drift region when an electric field, perpendicular to the ions drift direction, is created between the shutter wires. Thus, the increase of the gate voltage should result in decrease in ion transmission. When the gate voltage is sufficiently high, no ion transmission should take place and the gate is "closed". Over the short period of time no electric field is created between the shutter wires and ions are transmitted into the drift region as a narrow ion swarms (shutter is "open"). To prove the influence of the gate voltage on the ion transmission the voltage deferens between wires was set to zero and then increased in 10 V steps. The decrease of the ion transmission can be observed by fluorescence emission of the ions of dye Rhodamine 6 G in dependence on the perpendicular ion gate field.

The fluorescence emission spectra at the different ion gate voltages are shown below.
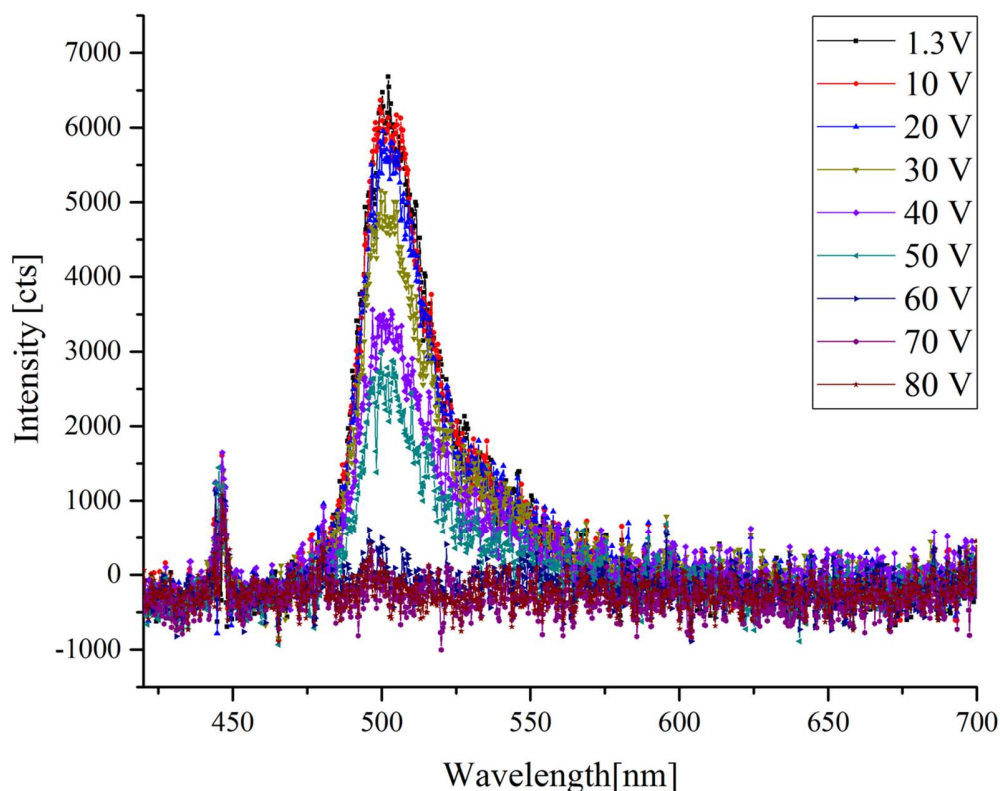
Figure 36 Fluorescence emission spectra recorded between the last ring electrode and the aperture grid at different ion gate voltages. Experimental conditions: ESI voltage =3.50 kV, IMS voltage = 2.231 kV, 2 µL min^{-1} flow rate of 500 µM Rhodamine 6G in MeOH (0.1 % formic acid), excitation with 447 nm continuous wave (cw) laser diode, 1.6 W output power, ICCD gate width 100 ms, gain 100, 100 accumulations, blank subtracted, average of n=3

The low electric field strength between the gate wires resulted in no or only minor effect on the transmission/deflection of the transported ions. This can be seen in only minor changes of fluorescence intensity when the ion gate bias value is in the range of 0 - 10 V. The high fluorescence emission intensity at lower gate voltages applied, indicates efficient penetration of ions through the ion gates wire arrangement. The increased gate voltage results in increase of a deflecting ion shutter field, generated between the gate wires. The gate field deflects the approaching ions, as they pass the wire arrangement. The deflection angle is strongly dependent on the electric field strength

between the two wire sets.[102] In general the ions get deflected to a larger extend at higher gate fields.

In the experiment with pulsing of the gate electronics, the ions that successfully pass the open drift cell arrangement can be additionally detected by the Faraday plate detector. The gate electronics pulse width was set to 200 µs at a frequency of 18 Hz. The electrometer (transimpedance amplifier) was set to a gain of 10^{10} V A^{-1}. The time-voltage signals in the oscilloscope were averaged 16 times. The dependence of the IMS signal on the gate voltage is shown in Figure 37.
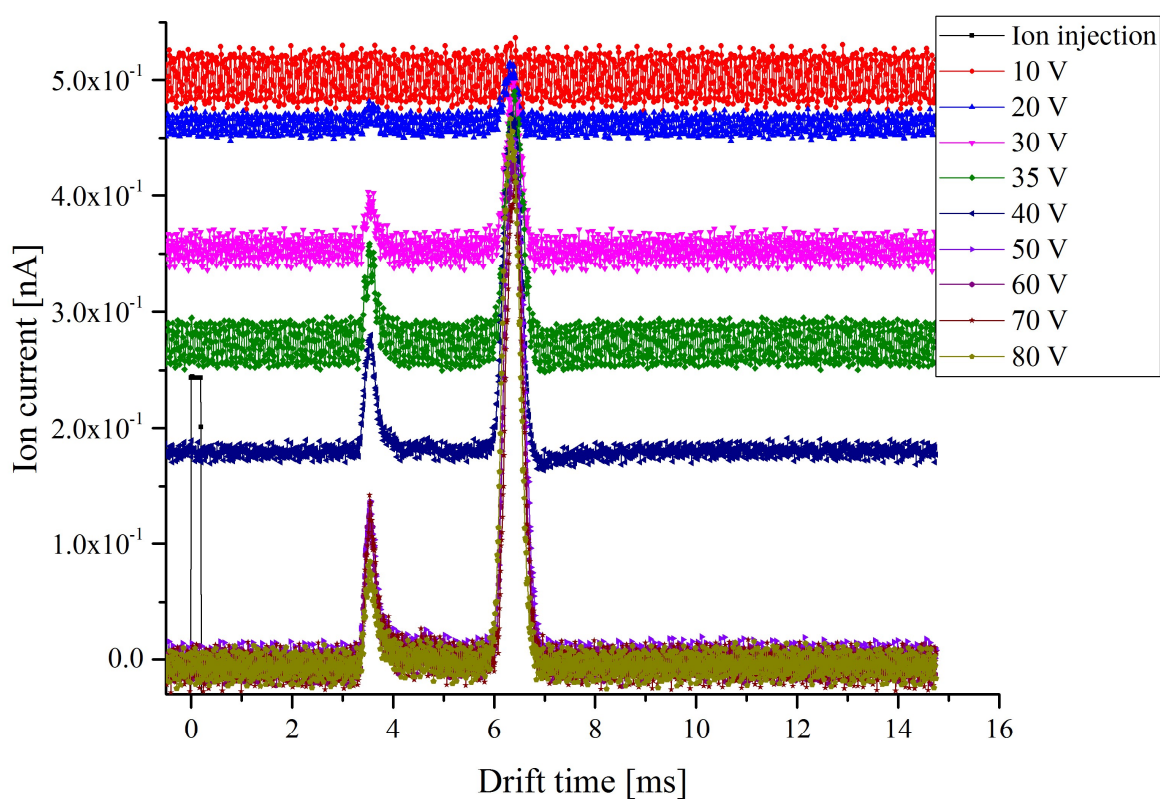
Figure 37. ESI-IMS drift time spectra of Rhodamine 6G solution (500µM, MeOH, 0.1 formic acis) at different gate voltages. The pulse width was set to 200 µs. Each spectrum represents the average of 16 measurements.

Similar to measurements with LIF phenomenon was observed, the low electric field strength between the gate wires has no or minor effect on the deflection of the transported ions. However, the strong dependence of DC offset which is often called "total ion current" (TIC) on the electric field strength between the gate wires was observed. The large DC offset (see Figure 37) indicates the penetration of ions through the ion gate at low ion gate voltages. The increased gate voltage results in an increase of ion shutter field, generated between the gate wires. The gate field deflects the approaching ions as they pass the wire arrangement. With the increase of the potential difference the absolute value of the peak maxima demonstrates only minor decrease (see Figure 37, peak at ~6.3 ms); the value of the baseline, however, strongly decreases. Thus, the peak intensity is increased with the increase of the gate voltage. This observation is in a good agreement with the described in the literature experiments.[45] The full width at half maximum (FWHM) of the main peak at ~6.3 ms (Figure 37), assigned to Rhodamine 6G ion, is calculated as 430 µs. The second peak with lower intensity cannot be assigned to a certain ionic species without further investigations (e.g. mass spectroscopic), but we believe that this signal corresponds to the solvent (Methanol with 0.1 % formic acid) or to fragments of Rhodamine 6 G.

Based on the both experiments discussed above, the ion gate voltage difference of 60-80 volts is required for the current experimental setup to avoid the undesired ion transmission (see Figure 36and Figure 37). Increase of the gate voltage to 60-80 volts increase the peak intensity (drift time resolved) and, hence, the sensitivity.

In conclusion, this experiment indicates the feasibility of mobility based detections with proposed experimental setup. Additionally, the results from the previous experiment support the possibility of orthogonal detection of the ions by means of laser induced fluorescence emission detection.

4.3.3.2   *Optimization of the electrospray emitter for the long-term measurements*

The time is the central parameter in drift tube based mobility measurements. A drift time spectrum is initiated with the pulsed injection of ions into a drift tube. Single spectra can show significant level of noise, so that an averaging of a number of spectra (e.g. 2-1000) is often required. Hence, the drift time spectra are recorded periodically. One period is the time between injection starting points (rising edge). The time window between the injections is the time available for the drift spectrum. When the drift time required for the analysis is 100 ms, the maximum frequency of 10 Hz can be used to generate drift time spectra.

Other important factors are a time required for the measurement of the single point on the drift spectrum and the sampling rate. In the previous section, all fluorescence emission spectra have been recorded with integration times for single point of 100 ms. Taking into account that with an injection pulse width of 200 µs the typical peak FWHM of the detected signals is ~ 400 µs the decrease of the integration time to at least 100 µs is required. This leads to the decrease of the signal intensities. This can be compensated by increased number of accumulations, resulting in improved signal to noise ratio, and/or increase of the signal intensities.

It is noteworthy to mention that a stable spray is necessary for reproducibility by the continuous drift time-dependent sampling. The IMS signal of the Rhodamine 6G show a drastically decreasing intensity and additional asymmetrical peaks after few hours of infusion. In worthiest case these peaks could be observed even after several minutes of infusion. No systematic dependence could be derived from the solution flow rate.

The formation of stable electrospray is strongly dependent on both, the flow rate and the electrospray voltage. The most disturbing effect however was found to be the stability of electrospray emitter. Microscopic investigation of the used stainless steel emitters was performed when the signal decay of drift time peak intensity and fluorescence emission intensity were observed. After a short period of working time (8-24 hours), the inner surface of emitter was covered by crystals of orange and brown color. The only way to remove these crystals was the washing with diluted H_2SO_4, whereas washing with methanol did not completely removed the crystals from inner surface of the steel emitter. In addition, corrosion at the stainless steel emitter tip was observed. These findings indicate the corrosive properties of Rhodamine 6G solution in methanol. The probable explanation for the corrosion can be a not sufficient quality of the steel used for the manufacturing of the electrospray emitter. Improvements of the ESI source were made to generate a stable spray of methanol solutions containing 500 µM Rhodamine 6G. To increase the corrosion resistivity of the electrospray emitter the stainless steel emitter with the inner diameter (I.D.) of 30 µm and outer diameter (O.D.) of 150 µm was replaced by fused silica capillary with I.D. of 50 µm and the same O.D. The high voltage was applied in the same way as with the stainless steel emitter via an in-line connector. Another part which has demonstrated a major influence on the stability of the spray is a syringe plunger of the gas tight syringes. Only new plungers were found to show the required stability over hours.

4.3.3.3   Optimization of the experimental setup – improvement of the excitation wavelength

In order to increase the signal intensity, the excitation wavelength was optimized. The possibility of this optimization was discussed by Forbes et al.[79].
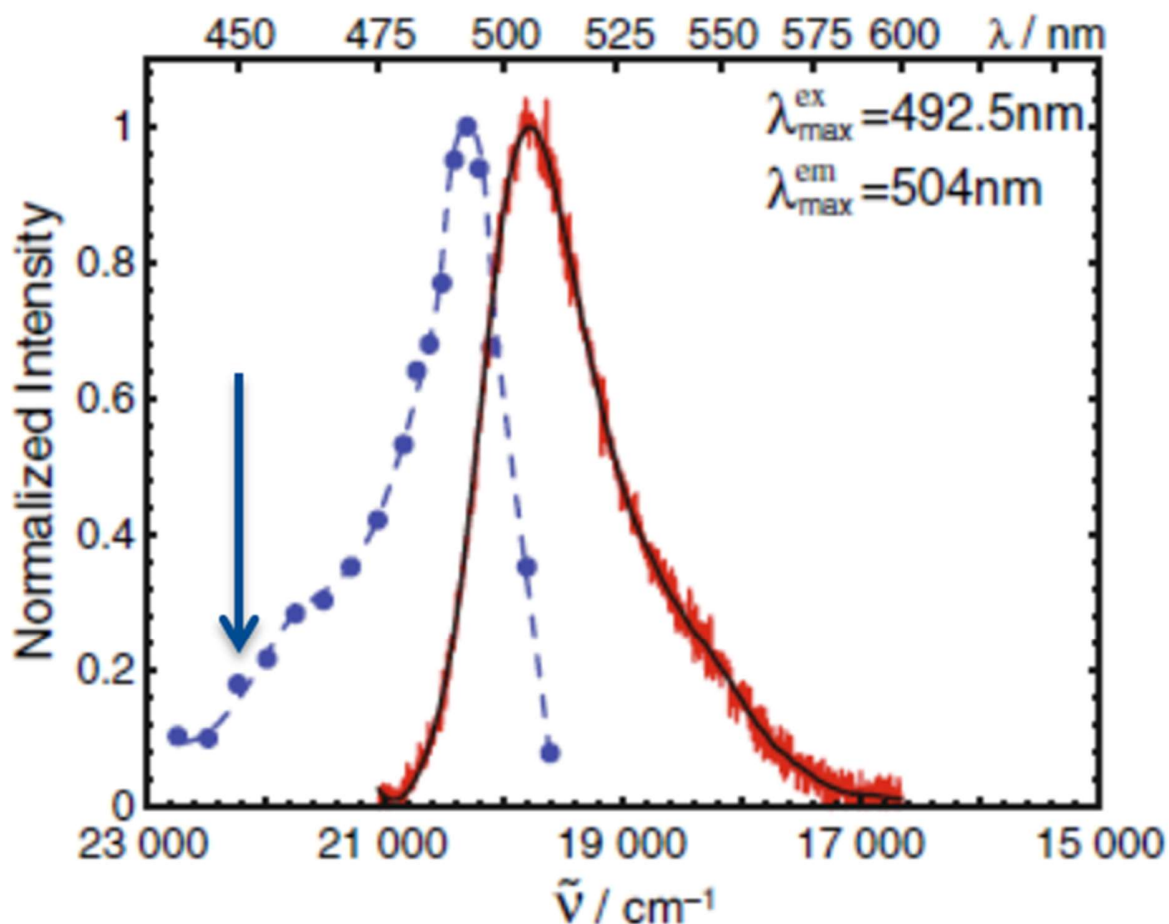
Figure 38 Excitation (dashed blue line) and Emission (red signal line) spectra of gaseous Rhodamine 6G.[79] The arrow marks the area of the excitation wavelength.

The excitation spectra of Rhodamine 6G cations in the gas phase demonstrate a maximum at 492.5 nm.[79] The closer the excitation wavelength to the excitation maxima of the analyte, the stronger the fluorescence emission is increased. However, the closer the excitation wavelength to the analyzed fluorescence signal, the stronger the analysis of this signal is disturbed by the laser light

scattering. This problem can be partially solved by utilization of appropriate light filter, e.g. dichroic or color filters. By this manner, the laser light scattering in the detection region can be efficiently filtered from the fluorescence emission. Another high power laser diode was employed in the previously described experimental setup. According to the data sheet of the manufacturer, this diode emits light with maxima at 465 nm. As compared to the emission wavelength of the previously used laser diode (447 nm), this laser diode has emission wavelength, that is approximately 15 nm closer to the excitation maximum of ionic Rhodamine 6G in the gas phase.Thus, the higher fluorescence intensity can be expected. A long pass filter with a cut-on wavelength of 490 nm was used to filter the laser scattering light in emission channel. Additionally, the adjustment of the collection optics was performed to improve the signal intensity.

The dependence of the ion transmission to the gate voltage, performed with optimized setup under the same conditions as in experiments demonstrated in Figure 36, is demonstrated in Figure 39.
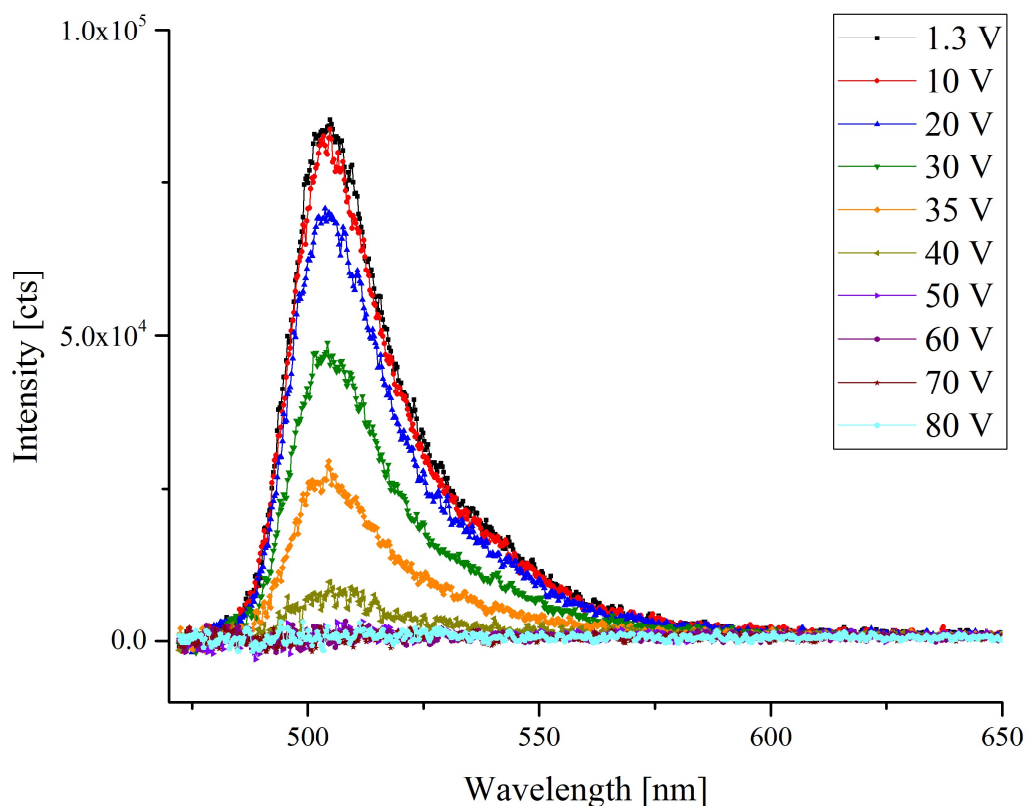
Figure 39 Fluorescence emission spectra of Rhodamine 6G at different ion gate voltages. Conditions: ESI voltage of 3.33 kV, IMS drift voltage of 2.43 kV, infusion flow rate of 300 nL min^{-1}.

The effectiveness of ions transmission under a constant electric drift field conditions and at variable ion gate voltage can be shown on example of the total ion current of R6G ion. These experiments were performed with continuously introduced Rhodamine 6G ions. To realize that the voltage on the ion gate was kept constant at desired ion gate voltage. With increase of the gate voltage the signal intensity decreases. This can be explained by the increase of the perpendicular electric field that is established in the drift tube and hinders ions to pass the wire arrangement of the ion gate. The signal intensity of the R6G ion transmission in dependence on the ion gate bias is shown in Figure 40.
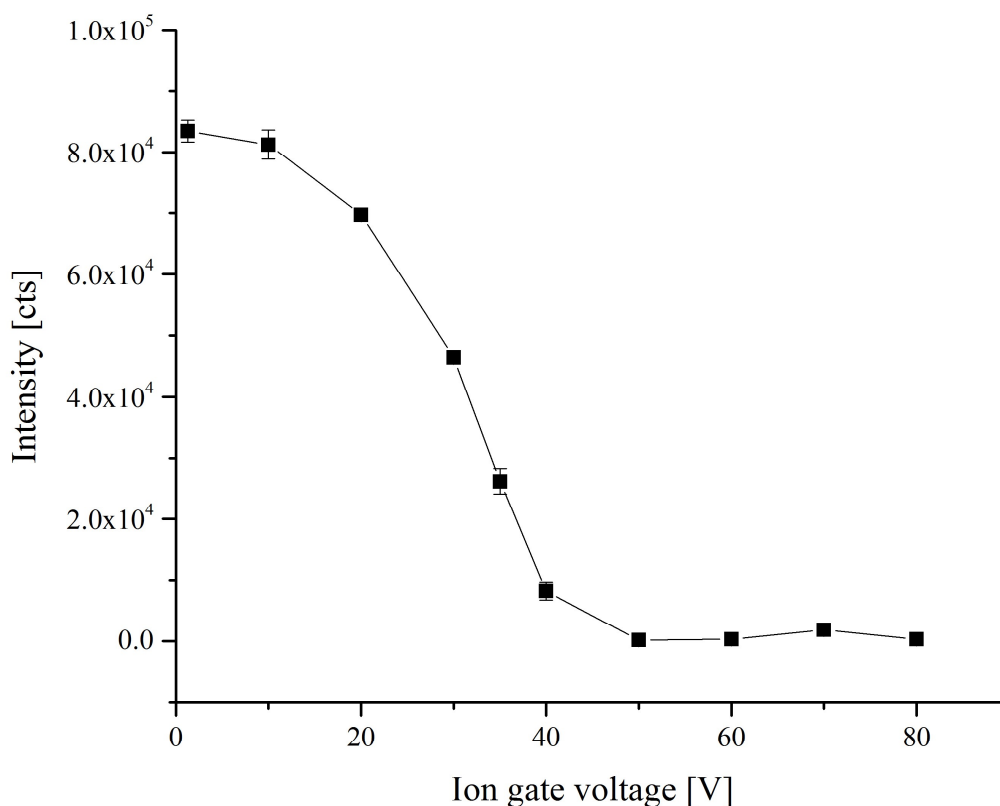
Figure 40 Dependence of the fluorescence intensity at emission maxima of gaseous Rhodamine 6G cations on the ion gate voltage

It was observed that, the ion gate voltage has a major influence on the ion transmission.

The improvements performed on the electrospray source and on the excitation source/wavelength resulted not only in increase of the fluorescence intensity, but also in an increase of long-term stability. Compared with the previous experiments (see Figure 36) signal intensities were improved by one order of magnitude. This is especially notable, because the ESI flow rate used in the previous experiments, and thus the amount of the infused Rhodamine 6G (solution concentration was equal), was 6.7 times higher as compared to experiments demonstrated in Figure 39 and Figure 40).

No ion transmission was observed at the gate voltage of 50 V and higher. However, in the experiments demonstrated in Figure 36 the ion transmission at the gate voltage of 50 V was reduced

only by 65 %. This difference is due to the much higher ESI flow rate used in the previous experiments.

The fluorescence intensity of ionic dye Rhodamine 6G strongly depends on the ion gate field. The increase of gate field decreases the ion transmission due to the perpendicular field, established inside the tube by the wire arrangement of the ion gate.

The dependence of the fluorescence intensity on the drift voltage is demonstrated in Figure 41. The ion gate was switched off in order to analyze the total ion current. In this case the camera integration time can be increased to values higher than 100 ms resulting in increased sensitivity. In these experiments, all parameters except of the high voltage applied to the electrospray emitter and the first drift electrode, respectively need to be held constant. To achieve the reproducible electrospray conditions, the voltage difference between the ESI emitter and the first drift electrode should be constant. Therefore, in each experiment the high voltage applied to the ESI emitter was adjusted to the high voltage on first drift electrode. At a constant gate voltage of 80 V and a pulse width of 200 µs, the electric field strength was varied between 340 and 674 V cm^{-1}. The effect of the electric field strength on the fluorescence emission spectra of the R6G total ion current at different electric fields is shown in Figure 41.
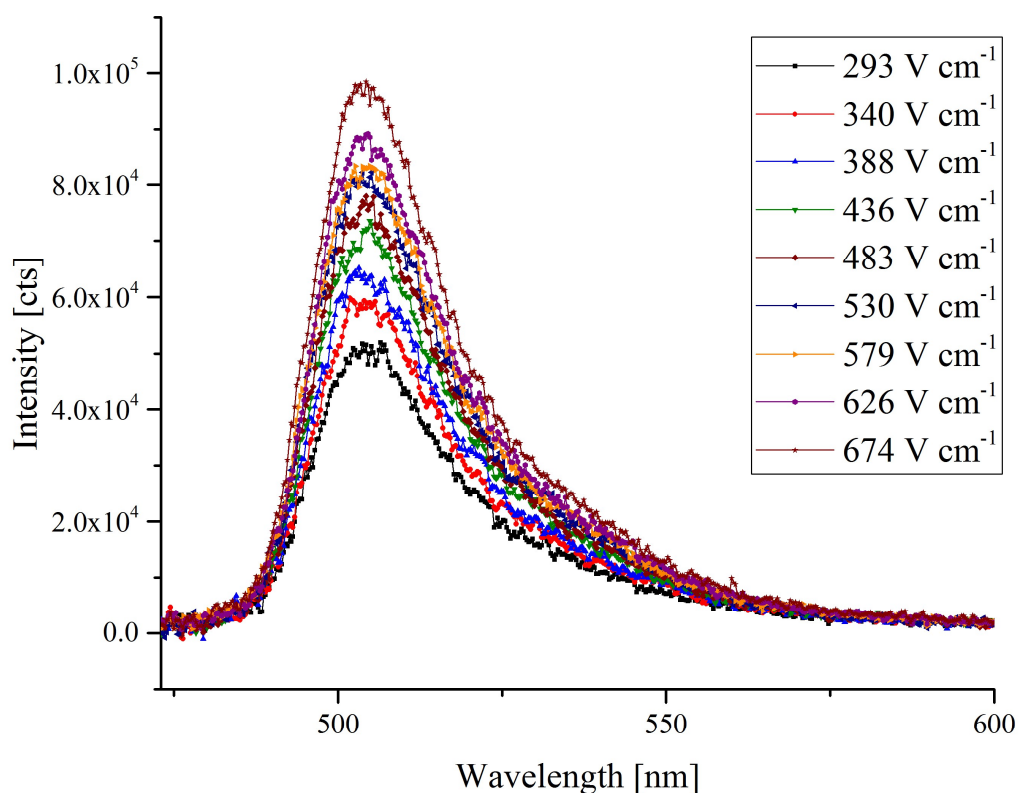
Figure 41 Blank subtracted spectra of R6G ions at different drift field strengths. Each spectrum represents the average of three accumulated (n=100) spectra, Settings of ICCD camera: gate of 100 ms, MCP gain of 100; The ESI and IMS voltages varied within the ranges of 2.13 – 3.73 kV and 1.23 – 1.83 kV, respectively. The Rhodamine solution was 500 µM in MeOH containing 0.1% of formic acid.

A linear relation, between the signal intensity of Rhodamine 6G and the drift field strength was observed Figure 42). Increase in the drift field strength resulted in proportional increase in the fluorescence intensity.

Equation	y = a + b*x		
Cor. R square			0.99326
		Value	Std. error
	intercept y-axis	18230.03411	1245.9524
	slope	111.24568	3.23803
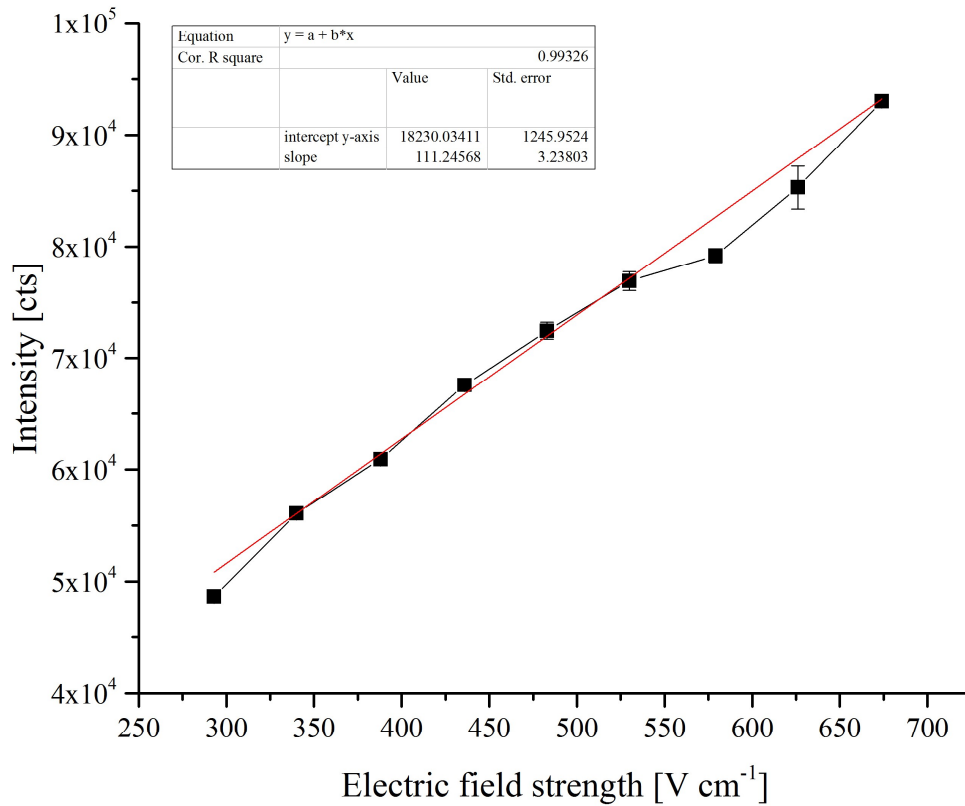
Figure 42 Fluorescence intensities of the R6G ion in dependence on the drift field strength. The intensity values were calculated as an average intensity within the range of 500 - 510 nm (n=3).

This effect can be explained as follows. The drift time is inversely proportional to the electric field in a drift tube.

$$t_d = \frac{L_d}{KE} \tag{7}$$

Where L_d is the length of the drift tube, K is the mobility constant and E the electric field strength.

During the drift the diffusion of the ions takes place.

The diffusion flux is time-dependent. Therefore, increase of the drift field strength leads to the reduced effect of diffusion. This results in reduced peak width (time scale) and increased intensity. Moreover, due to the reduced drift times the ions have less time for the undesirable reactions (e.g. charge transfer, recombination) which may lead to the reduced signal intensity.

In conclusion, the optimization of the experimental setup and conditions resulted in a significant increase of signal intensity. For further increase of the fluorescence intensity the higher values of drift voltage can be applied. However, the increase of the drift voltage by the constant ion gate times may result in the reduced IMS separation abilities. Due to these improvements, it should be possible to reduce the integration time in the LIF measurements to values of 100 µs or less required for the drift time dependent LIF analysis.

4.3.4 Drift time dependent laser induced fluorescence analysis at different ion-gate pulse widths and different electric field strengths

For the efficient excitation, the laser pulse time should be synchronized with the arrival time of the analyte ions swarm. Since the arrival time of the ions to the excitation area is unknown, it should be approximated from the distance between the excitation area and the faraday plate, the drift time and ion mobility measured by electrometer. The drift time spectrum recorded using the faraday plate detector with a pulse width of 200 µs was analyzed and the average of sixteen drift time spectra is shown in the Figure 43.
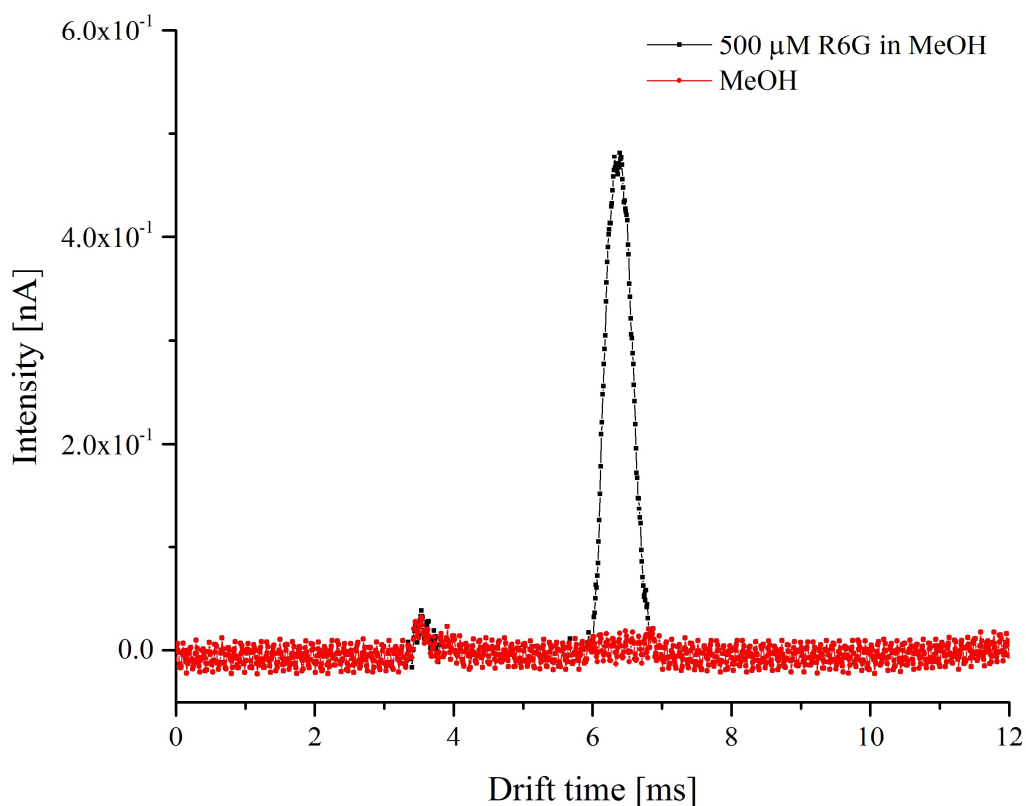
Figure 43 Drift time spectra of blank (MeOH) and R6G (500 μM in MeOH (0.1 % formic acid) ions. The ESI voltage was 3.33 kV, the IMS drift voltage was 2.431 kV, Ion gate voltage was 80 V, pulse width was 200 μs, demonstrated spectrum is a result of 16 averages.

Blank measurements of pure methanol showed only one peak of low intensity at 3.7 ms. However, in the analysis of the solution with R6G an additional peak of high intensity was observed. This indicates the assignment of the signal with the peak center at approximately 6.4 ms to the product ion of Rhodamine 6G ionized by ESI. The ion detection with LIF is performed *before* the arrival of the ions at the Faraday detector. Therefore, the approximated approaching of R6G ions to the LIF excitation area is expected to be between 4 and 6 ms. Frankevich et al. assigned mobility separated ions of Rhodamine 6G by FTICR MS. The mobility of Rhodamine 6G was determined to 0.96 cm Vs^{-1}.[81b] [1] The signal in Figure 43 has a peak center at 6.4 ms and the distance from the

---

[1] See Figure 4 and comments to Figure 6

injection grid to the detector palate is approximately 3.5 cm (the distance between the aperture grid and the detector plate is 0.5 – 1 mm). The velocity of an ion swarm traveling the distance of 3.5 cm in 6.4 ms is 5.47 m s^{-1}. The mobility normalized to 25° C and 760 torr is 0.94 cm Vs^{-1} can be compared with the value reported literature. The ion detection with LIF is performed *before* the arrival of the ions at the Faraday detector. The laser beam enters the drift cell 3 mm behind the last ring electrode. Hence, the distance between the injection grid and the laser beam is 2.8 cm. With a drift velocity of 5.47 m s^{-1} the ion swarm is expected to be detected by fluorescence detection at 5.1 ms. The time range between 4 and 6 ms is chosen for the detection of the ion swarm by means of drift time resolved laser induced fluorescence.

The optimization of electrospray materials and conditions has improved the long-term stability of the electrospray process. It was found that the fused silica emitter tip was not clogging in a few hours as the stainless steel emitter tip used in the previous experiments. One fused silica emitter tip could be used for at least one week of lab work. The voltage, the solution flow rate, and the quality of the syringe plunger were found to have an influence on the ion mobility spectrum. When the plungers of the syringe pump provided a sufficient sealing of the solution to the syringe body, the signal in the drift spectrum was constant and reproducible. Only minor changes of the peak position and intensity were observed over several hours of continuous operation.

4.3.4.1   *Correlation between fluorescence emission and the drift time spectra.*

A two dimensional fluorescence drift time spectrum of R6G demonstrated in Figure 44 was generated from 20 fluorescence spectra that were recorded after a certain time delay from the ion pulse injection. The 20 spectra include spectra containing no or weak signal of R6G (background/baseline at the lower and higher drift times), and spectra with significant fluorescence intensity of R6G ion. Each of 20 fluorescence drift time spectra was generated by 2000 accumulations. The time interval between the spectra was of 100 µs and the analyzed time range was 4-6 ms. The gate opening time of the ICCD was set to 100 µs and the exposure time of the ICCD chip was 2 ms. As compared to the LIF experiments described in previous sections, the required for the drift time resolved spectra reduction of both the gate integration time and the corresponding exposure time of the CCD chip resulted in a reduced signal intensity. To increase the signal intensity, in the measurements described in this section were performed with a micro channel plate (MCP) gain of 250 (ICCD camera) and with an increased number of accumulations.

It was found, that enabling the electron multiplying features (e.g. a gain value of 250) and the accumulation number of 2000 resulted in the acceptable quality of the spectra. The quality of the spectra (S/N ratio) can be further improved by the further increase of the accumulation number, however in cost of the increased measurements time. A drift time resolved fluorescence spectrum recorded within the time range of 4-6 milliseconds is shown in Figure 44.
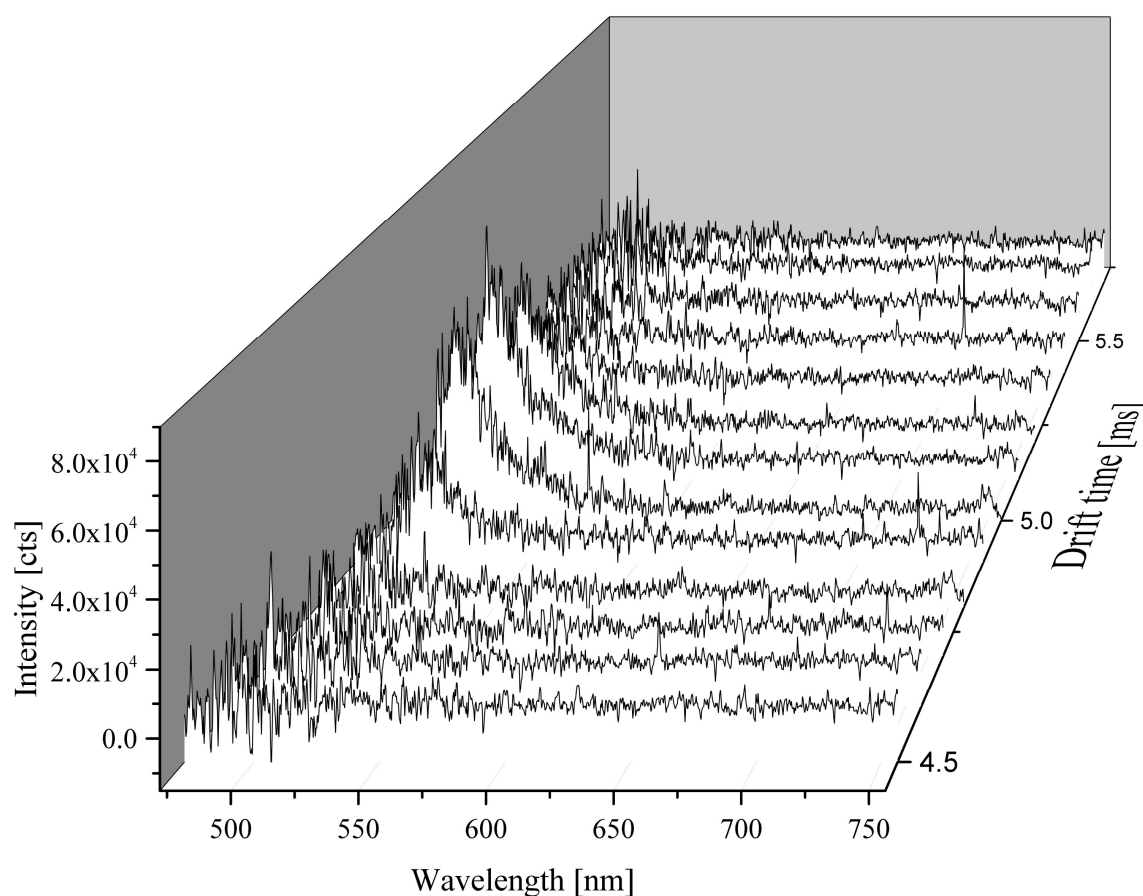
Figure 44 Fluorescence spectra of R6G (500 µM in MeOH (0.1 % formic acid, $\lambda_{Ex.}$= 462 nm)) ions generated by ESI at different gate delays (drift time axis). The ESI voltage was 3.33 kV, the IMS voltage was 2.43 kV. Ion gate voltage 80 V, pulse width 200 µs, each spectrum was recorded with 2000 accumulations. ICCD settings: gate opening time of 100 µs, MCP gain of 250, CCD exposure time of 2 ms

Thus, after all performed improvements it was possible to realize ESI-IMS-LIF coupling and analyze with this coupling R6G sample.

The drift time is a measure of ion mobility, which is dependent on many parameters including ion charge, mass, and shape. A fluorescence emission maximum depends on the configuration and population of molecular energy levels. Because the selectivity of these techniques is based on different parameters, these methods should be of high orthogonality. Thus, utilization of LIF detector should strongly improve the discrimination ability of ion mobility spectrometry.

To reduce the notices, the data were smoothed by the adjacent averaging method in Origin Pro 2015 with a window of 100 data points. No weighted averaging and no boundary conditions were selected. The smoothed data set is shown in Figure 45.
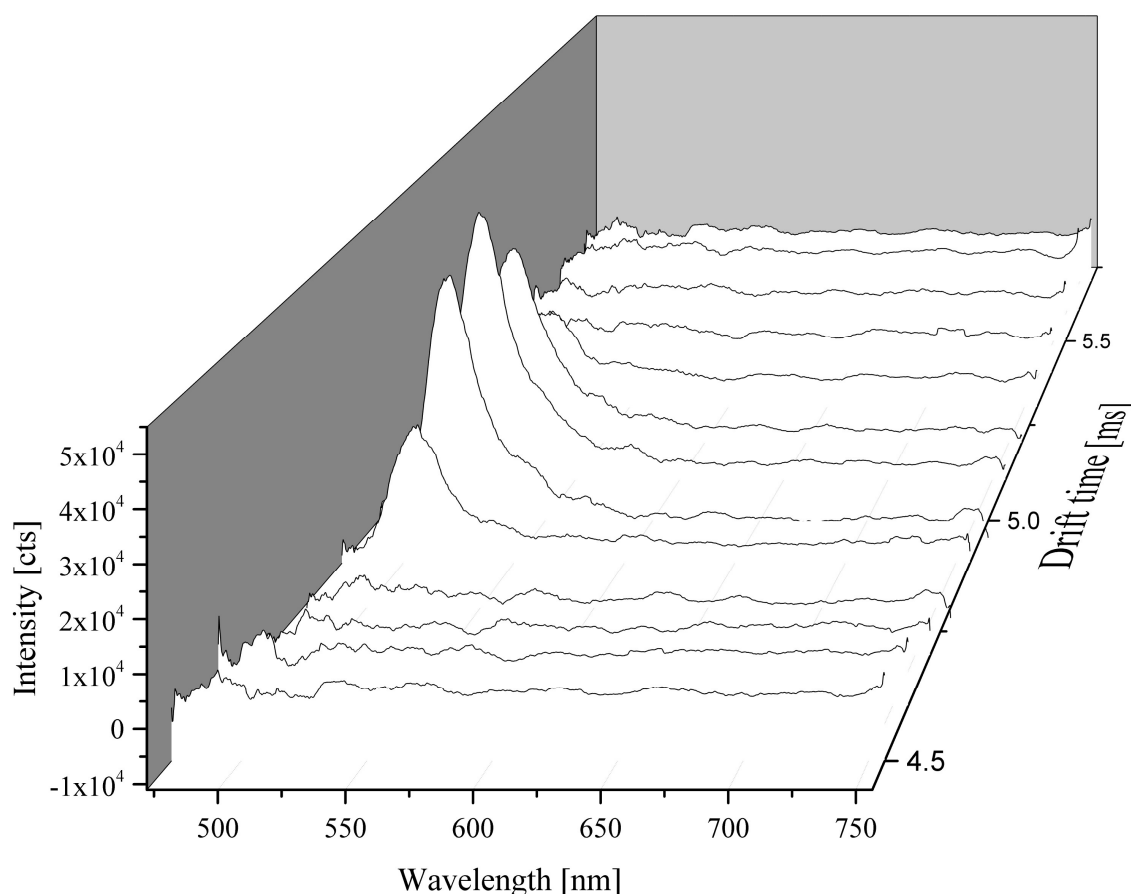
Figure 45 Smoothed fluorescence spectra (Origin Pro 2015, 100 points) of the data presented in Figure 44.

The maximal intensity of Rhodamine 6G peak was observed at the drift time of 5.1 ms (see Figure 46). To compare the recorded with LIF detector data with those recorded with electrometer, the values of fluorescence intensity at maxima (505 nm) were plotted as a function of drift time. This plot is the drift time spectrum of R6G cations in a constant electric field analyzed by LIF detector. The laser induced fluorescence emission intensity of Rhodamine 6G at 505 nm as a function of drift time is shown in Figure 46.
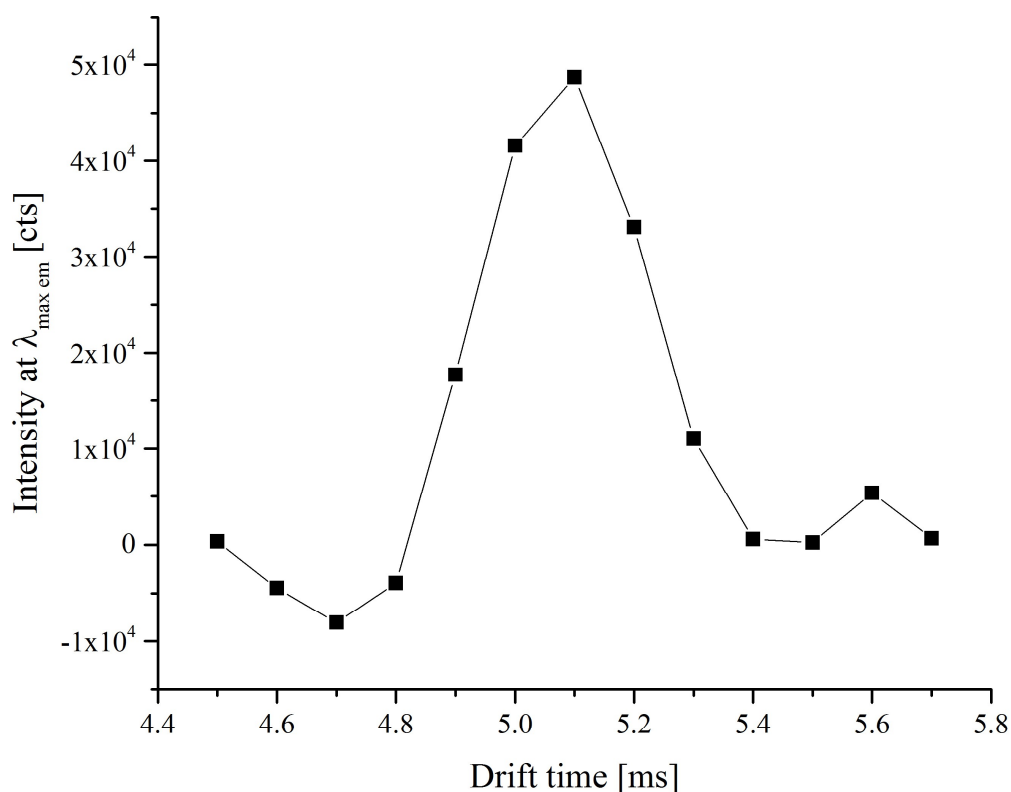
Figure 46 Fluorescence emission intensity of Rhodamine 6G at 505 nm as a function of the drift time. The settings were as follows: 100 µs steps, 200 µs ion gate pulse width, 2000 accumulations per point, blank subtracted, smoothed.

The Rhodamine 6G fluorescence intensity demonstrates a maximum value at a gate delay time of 5.1 ms. The variation of the baseline values (values shorter than 4.8 ms and longer than 5.4 ms) can be explained by reflections within the drift cell and the data processing, e.g. the subtraction of

blank measurements and data smoothing. However, slight deviations in the experimental conditions (e.g. electrospray stability) should be a main reason for the signal stability. The voltage applied to the electrospray emitter and the distance between the emitter tip and the IMS entrance (first drift ring electrode) are important, when stable electrospray performance is required. The electric field strength required for Taylor cone and plume formation is dependent on both the distance and the potential difference between the electrospray emitter and the first drift ring electrode. It was found that the efficiency of both the ion formation and the ion introduction into the IMS can be adjusted by variation of the distance between the electrospray emitter and the first drift ring electrode by 0.5-5 mm. This is especially important for the long experiments which requires the increased long-term stability of the product ion generation.

4.3.4.2   Dependence of the signal intensity and FWHM on the duration of the ion gate pulse

The ion gate pulse width has an impact on the fluorescence drift time spectra. In general, pulses of longer duration should show an increase in both the signal intensity and in the signal FWHM. These effects were demonstrated in experiments with drift tube ion mobility spectrometer equipped with conventional Faraday plate detector (see Figure 47). Theoretically, the ion gate pulse width should have equal influence on the peak properties (FWHM, intensity) detected by both the electrometer and the LIF detection systems. In the following experiments the ion gate pulse width was varied within the range of 100 to 400 μs. All other parameters were kept constant.

With increase of the pulse width the peak broadening and the increase in signal intensity were observed. The drift time spectra of product ions generated with ESI from 500 μM Rhodamine 6G solutions at field strength of 561 V cm^{-1} are shown in Figure 47.
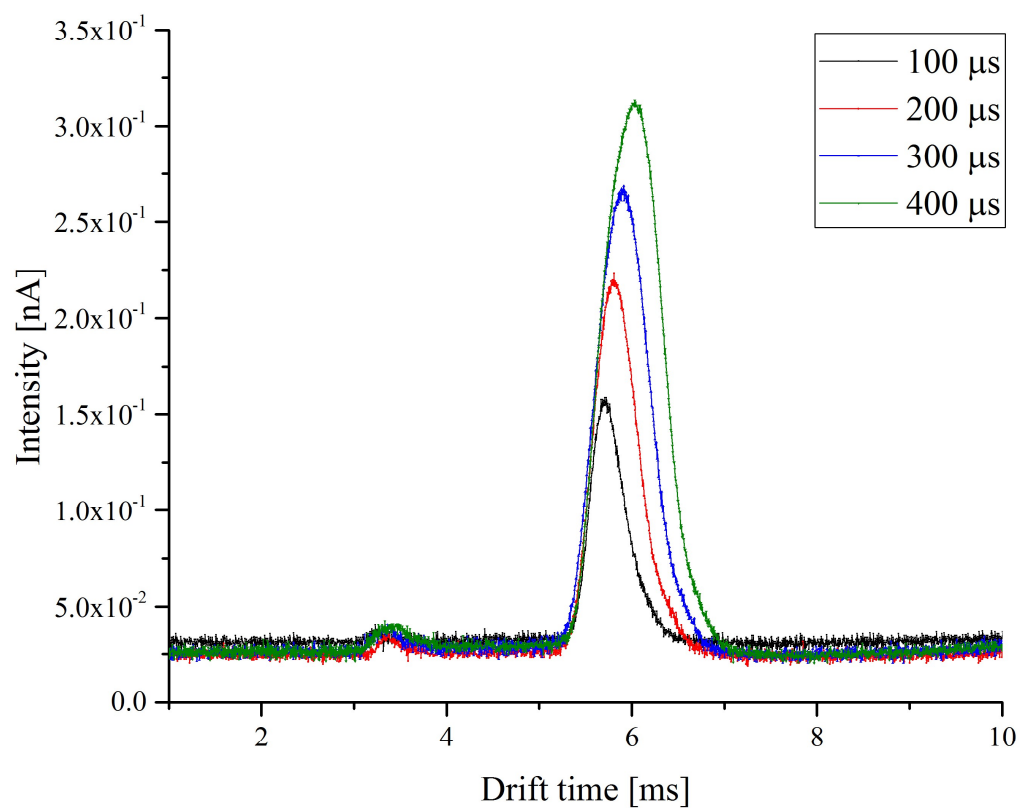
Figure 47 Drift time spectra of 500 µM R6G solution in MeOH at different ion gate pulse widths after 16 averages (electric field strength = 561 V cm^{-1}).
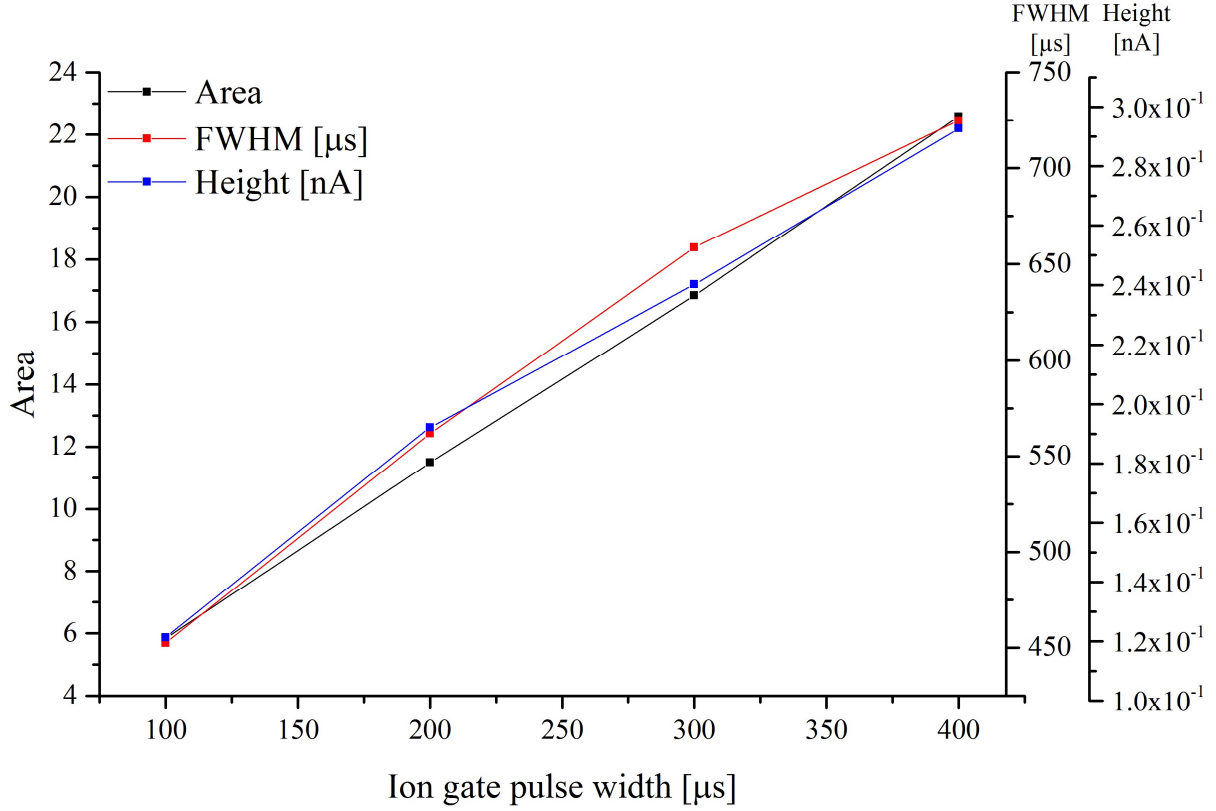
Figure 48 The R6G peak properties derived from the drift time spectra presented in Figure 47.

With decreasing pulse widths, the signal intensity decreases. Assuming that the coulombic repulsion / ion-molecule reactions are negligible and the initial pulse width has a Gaussian shape, the peak width (FWHM) can be described by the following equation:6

$$w^2 = t_g{}^2 + \left(\frac{16kT \; ln2}{Vez}\right) t_d{}^2 \tag{8}$$

Where k is the Boltzmann constant, T is the temperature of the drift gas, V is the drift voltage, e is the elementary charge, and z is the number of charges on the ion. The resolving power of IMS tube can be calculated as a ratio of the peak drift time to the peak FWHM:

$$R = \frac{t_d}{w} \tag{9}$$

Where td is the drift time and w is the FWHM of the ion peak. The influence of the pulse width on the IMS analysis was intensively studied on the example of chloride ions introduced in an IMS by Spangler et al..[103].

Besides the ion gate pulse width, other factors e.g. normal diffusion and ion-ion repulsion were found to have influence on the peak shape. The error functions were modeled and were shown to be clearly visible at injection pulse widths greater than 500 μs. However, the coulombic repulsions have been considered to be negligible in well-designed drift tube spectrometers. Under the real conditions, the drift of the ions is most likely affected by external factors such as temperature, pressure, and humidity. Drift time resolved fluorescence spectra recorded with different ion gate pulse widths are presented in Figure 49. To produce time resolved spectra for each investigated pulse width, six replicates were recorded, blank subtracted, and averaged.
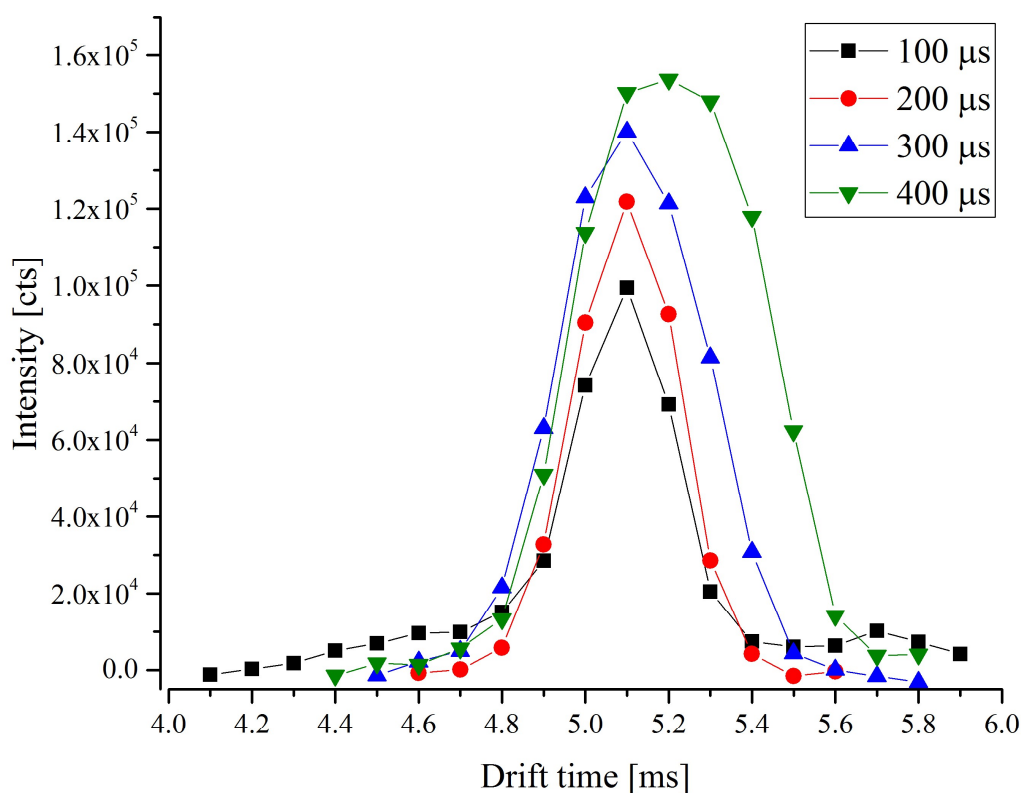
Figure 49 Drift time resolved fluorescence spectra recorded around drift time of Rhodamine 6G peak and at different ion gate pulse widths (average of n=6, 2000 accumulations per point, drift field strength was 561 V cm^{-1}

The drift time spectra produced with both, the Faraday plate detector and the laser induced fluorescence detector show the same trends as shown in Figure 47 and Figure 48. Besides the peak broadening, a shift of peak maxima towards bigger drift times with increase of the ion gate pulse width was observed. During the experiments with Faraday plate detector it was observed that the signal FWHM linearly increases with increase of ion gate pulse width (see Figure 48).

Therefore, the similar relationship between the FWHM values and the ion gate pulse width was expected for the measurements with LIF detection. The linear relationship between the FWHM values and the ion gate pulse width was observed at ion gate pulse width >= 200 μs. However, the

value of FWHM at the ion gate pulse width of 100 µs was somewhat higher as expected (see Figure 50).

It was observed that the signal FWHM increases with increasing ion gate pulse width. The additional peak broadening towards longer drift times can be explained by the increased injection time and, hence, shift of the ion package center towards longer drift times. Compared to the rise time limited electrometer, the fluorescence drift time has theoretically a temporal limit in the low ns (10^7-10^9 s) depending on the fluorescence lifetime of the product ion. The gas phase ion fluorescence emission lifetime of Rhodamine 6G has been determined to be 5.87 ±0.5 ns.[104] The effects of repulsion where investigated by conventional drift time detection in 10 µs intervals with the observation of differences in drift time (e.g. 10-40 µs).[105] The proposed method could be a relevant technique for the observation of small differences in drift time.

Thus, the ion gate pulse width has significant influence on the performance of an ion mobility spectrometer. The initial pulse width is the most contributing parameter that affects the IMS peak width.[94] That is why the influence of the pulse width on peak properties was intensively studied with the developed in this work experimental setup. The peak properties derived from the Gaussian fit are summarized in Figure 50.
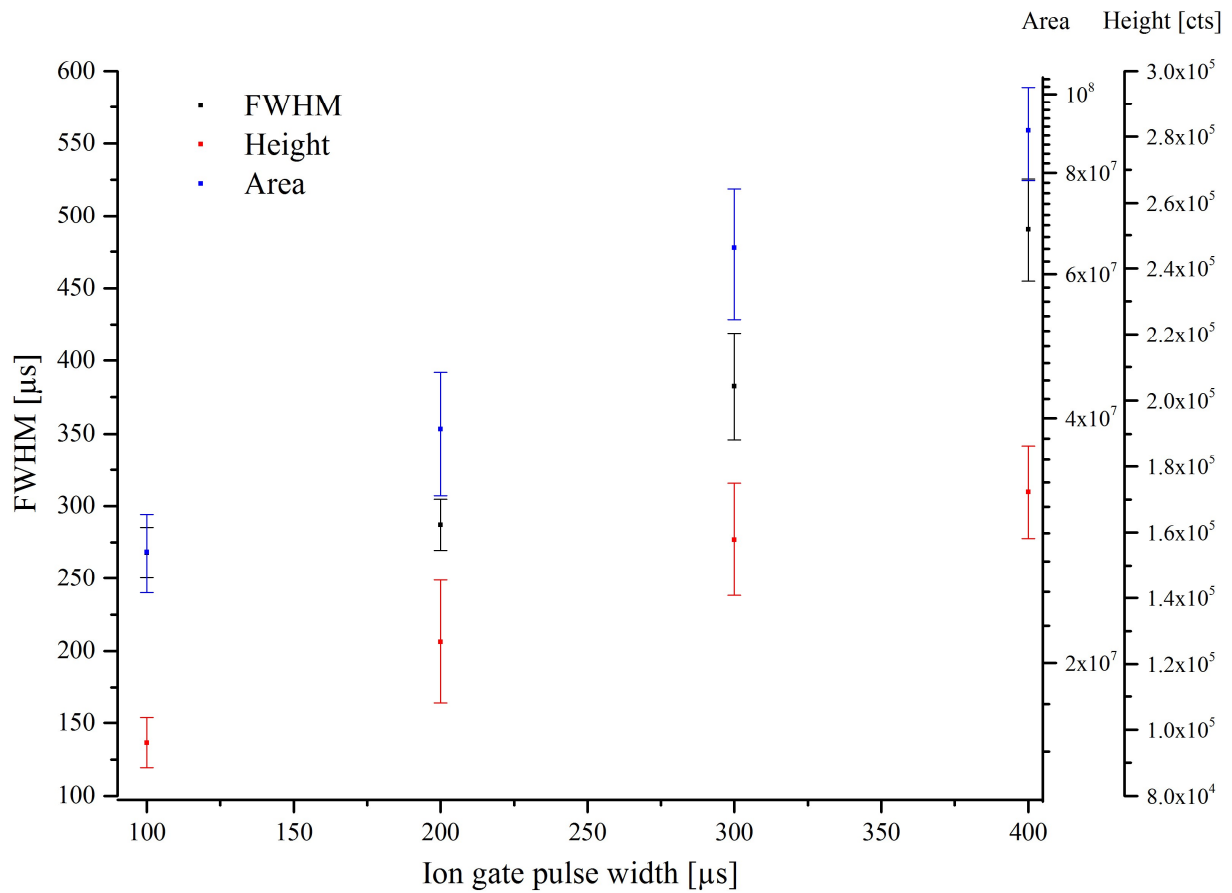
Figure 50 Relationship between the peak properties (FWHM, Height, Area) derived from the drift time spectra presented in Figure 49 and the ion gate pulse width.

The dependencies of the signal FWHM, recorded with LIF and Faraday plate detectors, on the ion gate pulse width are shown in Figure 51.
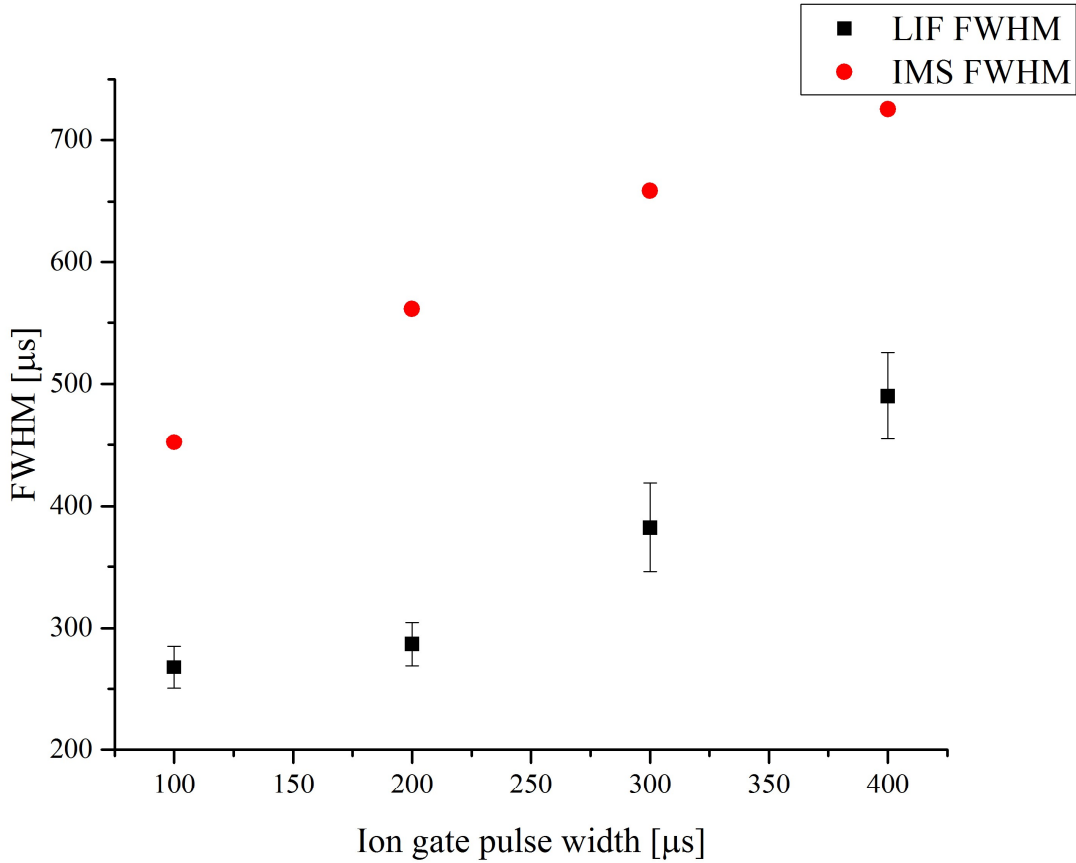
Figure 51 Comparison of the signal FWHM recorded with Faraday plate and LIF detectors.

The imprecision of time measurements may have been overlooked for the past 40 years of modern analytical IMS.[45] The time constants of the electrometer must be taken into consideration. An approximation for the minimal possible temporal width ω_{min} was defined as the square root of the sum of injection pulse width and the rise time of the transimpedance amplifier.[84]

$$\omega_{min} = \sqrt{\omega_{inj}^2 + \omega_{amp}^2} \qquad (10)$$

The simplified expression for the prediction of the ω_{amp} was also proposed.

$$\omega_{amp} = 0.9 \, t_{r \, (10-90)} \tag{11}$$

where $t_{r \, (10-90)}$ is the rise time from 10 to 90 % of the signal intensity. The rise time of the amplifier used in this study is specified to 50 μs at the gain of 10^{10} V/A. However, even at the higher electric field strengths (> 600 V cm^{-1}) the temporal width could not be compared with the minimal temporal width. This indicates a significant influence of the diffusion term which is not included into this equation and "mirror charges" of opposite polarity induced on the Faraday plate surface by the travelling in IMS ion packet. "Mirror charges" can be reduced but not completely eliminated by the aperture grid. The main focus of the current work lies on the implementation of fluorescence emission detection in IMS. The effect of "mirror charges" can be neglected for this detector type resulting in the decreased peak width.

The dependencies of the selected parameters on the electric field strength are demonstrated in Figure 52 and Figure 53.

At a constant gate voltage of 80 V and a pulse width of 200 μs, the drift field strength was varied within the range of 340 to 674 V cm^{-1}. For each analyzed drift field value, the high voltages applied to the electrospray emitter and the first drift ring electrodes were varied equally to keep the potential difference constant. The effect of the electric field strength on the drift time spectra is shown in Figure 52.
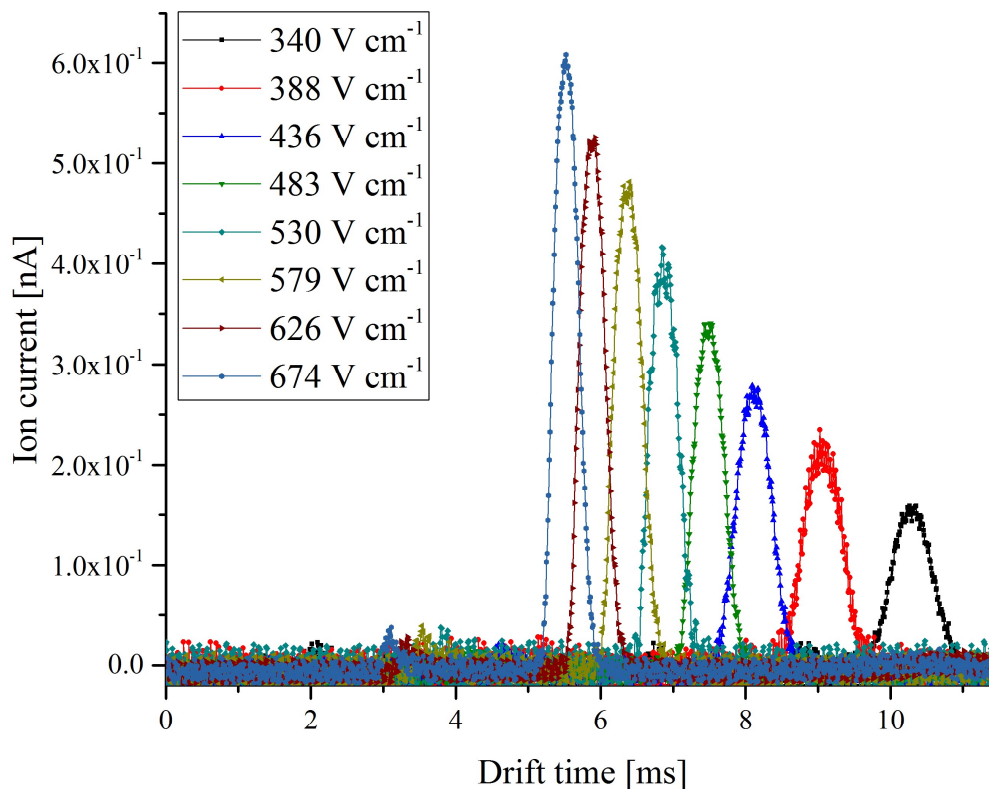
Figure 52 Drift time spectra of R6G ions (500 μM in MeOH (0.1 % formic acid) generated by ESI at different electric field strengths. The ion gate voltage and ion gate pulse width were 80 V and 200 μs, respectively. The amplifier was working in high mode at 10^{10} V A^{-1}. Each spectrum represents the average of 16 spectra.

With increase of the drift field strength the peak intensity increases, the FWHM decreases, and the peaks are detected at shorter drift time values (see Figure 52 and Figure 53). According to

$$t_d \ = \frac{L_d}{v_d} = \frac{L_d}{KE}$$

(12)

(where L_d is drift length, v_d is drift velocity, K is ion mobility constant, and E is drift field strength) the drift time decreases with increasing field strength. The peak parameters, recorded with faraday plate detector, in dependence of drift field strength are summarized in in Figure 53.
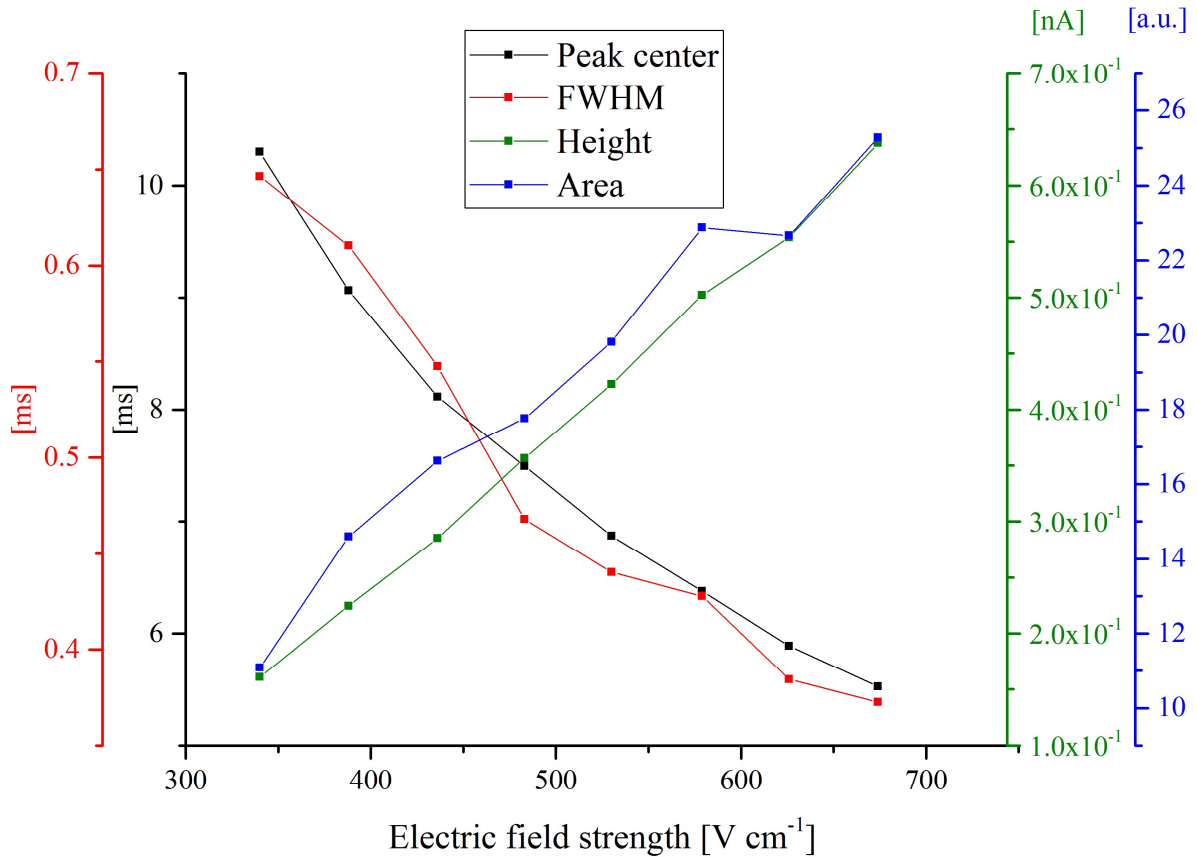
Figure 53 Dependence of the R6G peak properties for the drift spectra shown in Figure 52 on the drift field strength.

The peak intensity and the peak area increases with increase of electric field strength. During the drift the ions are dispersed by diffusion within the drift cell. This results in the increase of the FWHM. However, the influence of the dispersion/diffusion is dependent on the time and, thus, on the electric field strength applied to the drift tube. This can be seen by the decrease of both the FWHM and the drift time with the increase of the drift field strength (see Figure 53). The increase of electric field strength increases the velocity of ions. Therefore the ions reach the detector at shorter drift times and have less time for the diffusion. Thus, the axial diffusion is reduced and this

results in a decrease of the FWHM. The reduced influence of diffusion (axial and radial) is an important reason for increase of both the signal intensity and the peak area. The diameter of the Faraday plate detector used in this work is 4.6 mm and corresponds to ~ 1/5 of the cross-section of the drift cell. Increase of electric field strength increases the radial focusing of the ions towards the central axis of the drift tube. Therefore, the radial diffusion is decreased resulting in increased fraction of ions that can be detected with the mounted in central axis of the drift tube Faraday plate detector.

The relation between the diffusion coefficient (D) and the ion mobility coefficient (K) is known as the Einstein equation.

$$K = \frac{eD}{kT} \tag{13}$$

Where e is the ion charge, k is the Boltzmann constant and T is the gas temperature. This dependence is limited to the low field conditions ($<<$ 10 kV cm^{-1}) because under the high field conditions the mobility coefficient becomes to be not constant and dependent on the E/N ratio. The degree of dispersion can be estimated from the difference between the full width at half maximum of the time-voltage signal and the initial pulse width of the ion gate.

The same experiment has been performed with the fluorescence emission detector. The drift time resolved spectra at various electric field strengths are presented in Figure 54. These spectra represent the dependence of the R6G fluorescence intensity at 505 nm on the drift time.
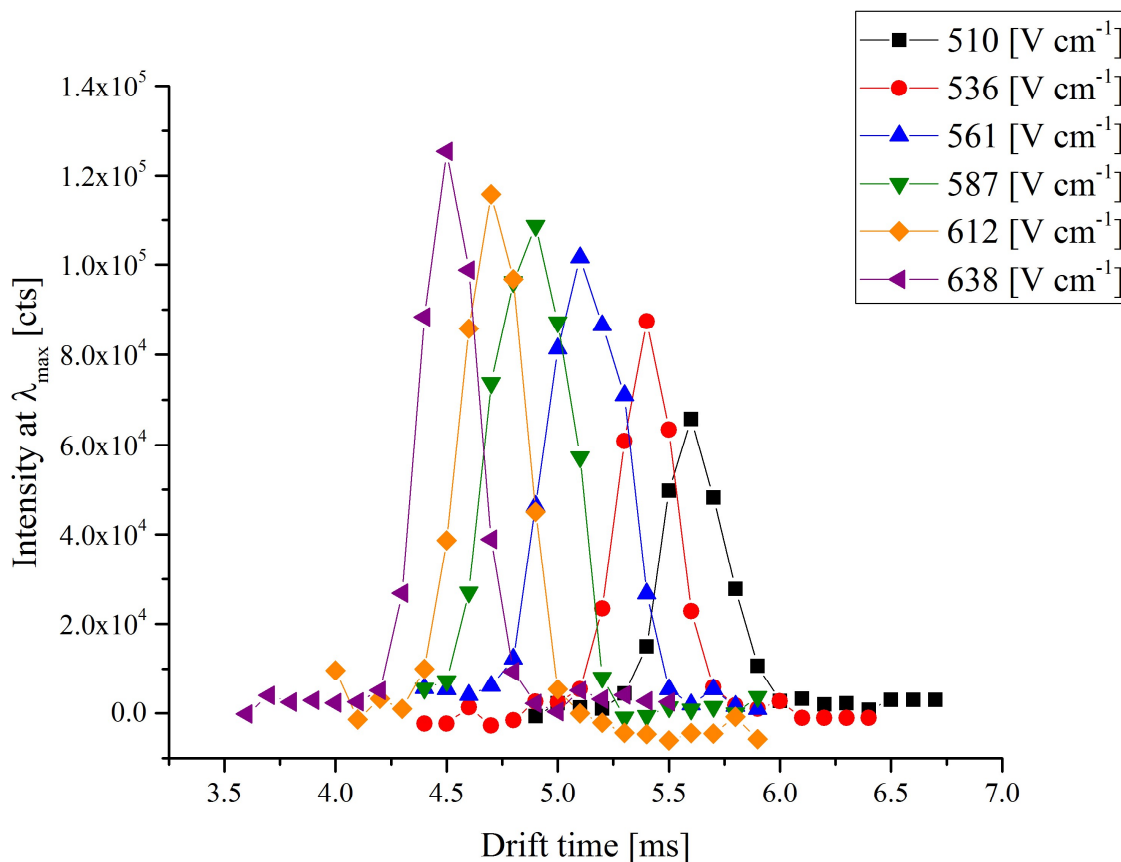
Figure 54 Drift time resolved fluorescence spectra of R6G derived from fluorescence emission intensity maxima at different ion gate delay times. The experiments were conducted at various electric field strengths. Each curve represents the average of n=6. R6G (500 µM in MeOH) ions were generated by ESI at different electric field strengths. The ion gate voltage and pulse width were 80 V and 200 µs, respectively.

It was observed that with increase of electric field strength the peak positions shift towards smaller drift time values. This trend is comparable to that observed in the drift time spectra recorded with the Faraday plate detector. Due to the spatial arrangement of the detection systems, the fluorescence emission is detected prior to the ion current detection. The LIF detection and the ion current detection take place sequentially downstream the drift tube. Therefore, the drift times recorded with LIF detector are shorter as compared to the corresponding drift times recorded with the Faraday plate detector. To calculate the peak parameters (e.g. FWHM, Height, Peak center) the peaks from

Figure 54, were fitted with a Gauss function using the Levenberg Marquardt iteration algorithm. The dependencies of peak parameters (FWHM, Height, Peak center) are presented in Figure 55.
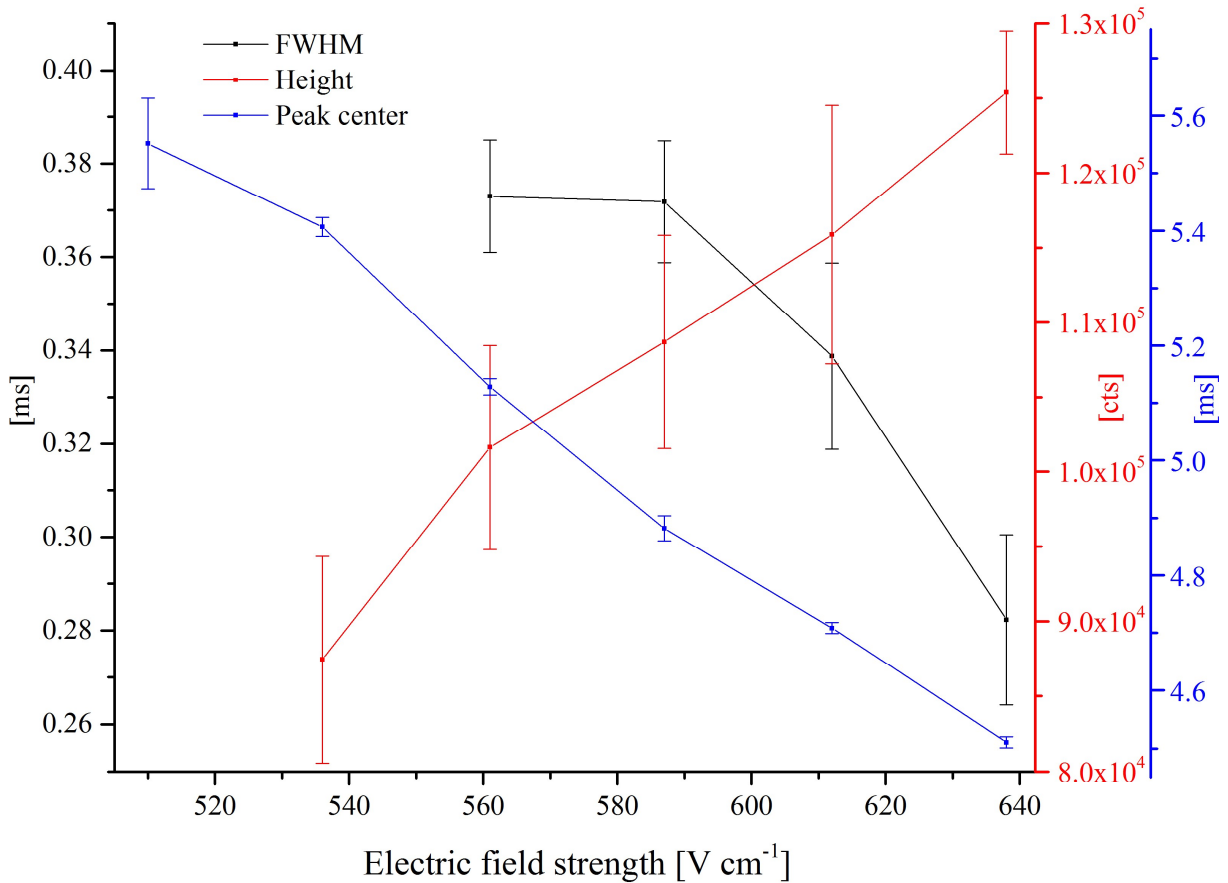
Figure 55 The peak parameters for the spectra presented in Figure 54. Full width at half maximum (FWHM), height, and center of peaks are presented in dependence on the electric field strength

The drift time decreases with increasing electric field strength. This is consistent with the effect of electric fields on ion motion. The increase of peak height and the decrease of FWHM with the increase of the drift field strength are consistent with described relationships between the diffusion, ion velocity, and field strength. The standard deviation of the peak center values indicates a good agreement with the previously discussed effect of the electric field strength on ion motion. The high standard deviation values for the peak height and the FWHM can be explained by following factors. Firstly, the sampling rate used by LIF detection is limited by the gate opening time of the ICCD (100 µs). Theoretically, this time can be reduced to a 2 ns (minimum value for the utilized

ICCD camera), however, in cost of sensitivity. Additional deviation results from the data fit. Variations of the FWHM values result in the variations of the signal intensity and vice versa. Additionally, some external disturbances may have an influence on the peak intensity and the peak width. In the current experimental setup, the electrospray ion source and the drift cell arrangement were constructed in open design and were operated in the ambient air of the laboratory. Therefore, minor changes in temperature, pressure, and humidity may result in significant alterations in the electrospray performance and in mobility of ions. Dependencies of the drift time and the peak height values of Rhodamine 6G on the drift field strength recorded with both the LIF and Faraday plate detectors are shown in Figure 56.
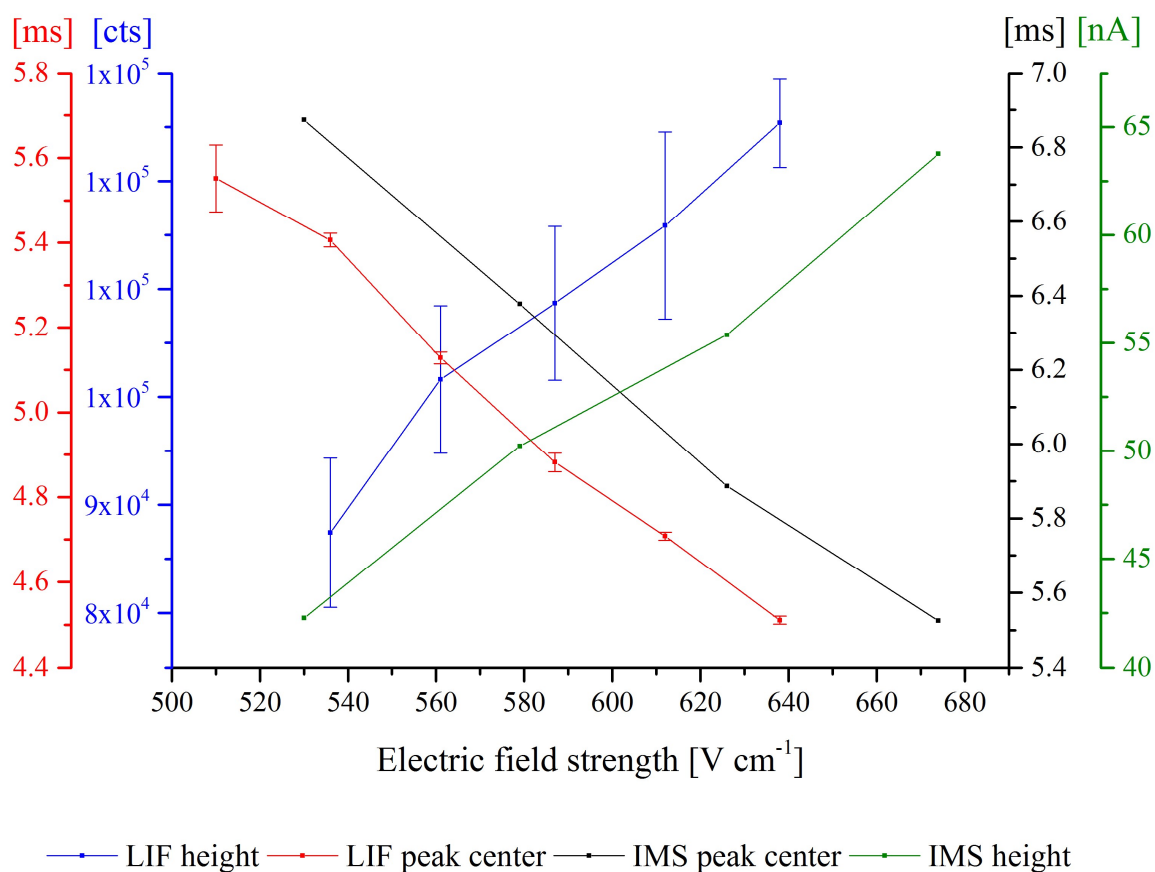
Figure 56 Dependencies of the drift time and the peak height values of Rhodamine 6G on the drift field strength recorded with both the LIF and Faraday plate detectors.

The comparison of the peak height and the peak center values indicates similarities between both detection systems. With increase of electric field strength the drift time decreases and the signal intensity increases. Interestingly, a difference between the FWHM values calculated from drift time resolved spectra with both LIF and Faraday plate detectors was observed (see Figure 57).
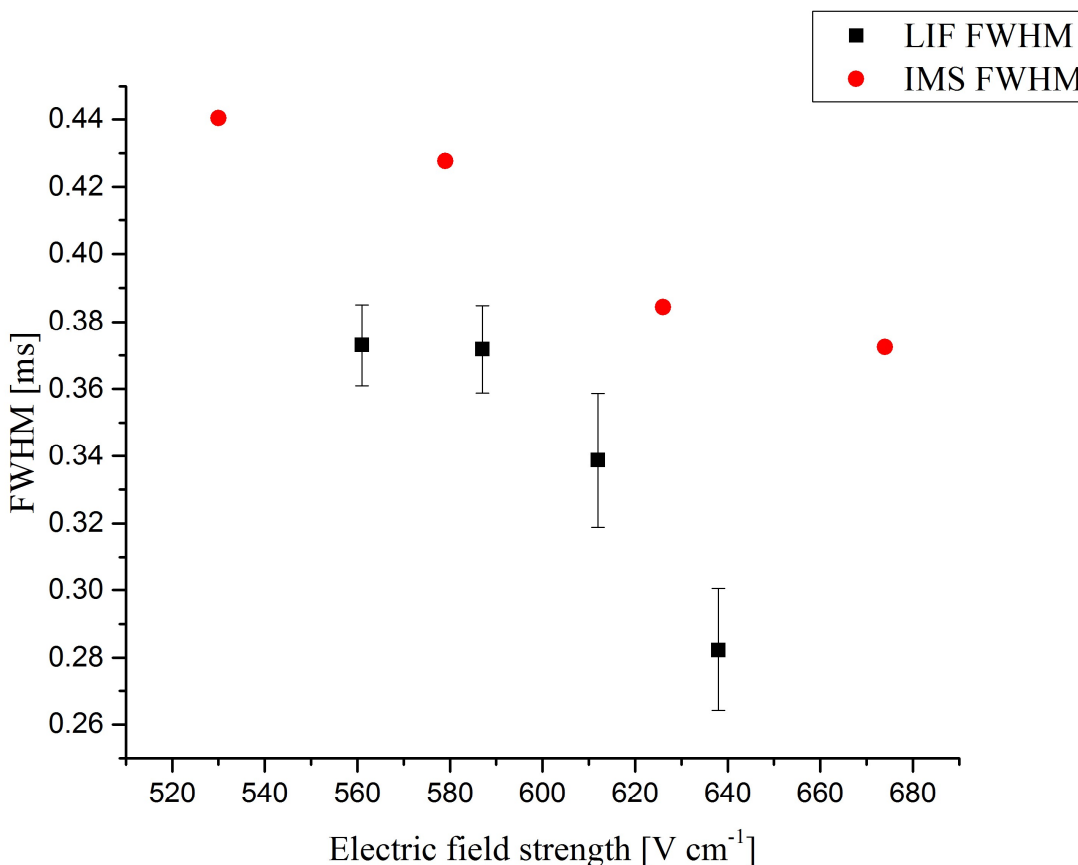
Figure 57 FWHM values calculated from R6G drift time resolved spectra with both LIF and Faraday plate detectors.

It can be concluded that in spectra recorded with both detection systems the FWHM decreases with the increase of the drift field strength. However, this trend is strongly limited by two factors, namely the ion gate injection pulse width and the rise time of the electrometer. Additional sources have been located in the Faraday plate detection system. Firstly, construction of the cell and the geometry (parallelism) of the aperture grid wire arrangement. Secondly, the uniformity of the electric field and the electric field distribution within the cell.[55]

It was found that, within the analyzed drift field strength range, the FWHM values calculated from drift spectra with LIF detector are smaller than those calculated from drift spectra with Faraday plate detector. These results are in a good agreement with the results presented in Figure 51. The main reason for higher FWHM values achieved with Faraday plate detector is probably the additional peak broadening caused by amplifier (see comments to Figure 51). Additionally, the induction of the current by the approaching ion clouds in the region between the aperture grid and the detector can be a reason of the peak broadening.[55] Increase of the drift field strength results in increase of ion velocity and thus in decrease of drift time. Rokushika et al. have found that at a pulse width of 0.2 ms, an electric field of 120 V cm^{-1} would provide the best resolution in a conventional IMS.[106]

At high electric field strengths (> 600 V cm^{-1}) the diffusion should play a minor role, however, it will be problematic to resolve the signal with decreased FWHM for the currently utilized transimpedance amplifier. Contrary, at low electric field strengths (~ 500 V cm^{-1}), the peak broadening is controlled mainly by diffusion and the sampling rate of the electrometer is sufficient to resolve the ion mobility spectrum.

4.4 *Conclusion and Outlook*

In this part, the feasibility of IMS-LIF coupling is demonstrated on the example of R6G dye ionized by ESI. The fluorescence of the ionized dye in the gas phase has been investigated in a simplified IMS drift cell of open design. The influence of most important parameters on the IMS-LIF was analyzed. This influence was analyzed for both, the drift time resolved spectra recorded with classical Faraday plate detector and the drift time resolved spectra recorded with LIF detector. It was found that the FWHM is dependent on the initial ion gate pulse width. However, the detection of low ion currents, in the pA – nA region, by classical Faraday plate with transimpedance amplifier is limited by the required amplification gain and consequently by the bandwidth of the transimpedance amplifier. This increases the amplifier rise time and thus, the FWHM. The optical-electronic detection is known to be fast (up to femtoseconds). Therefore, the FWHM achieved with the presented and only partially optimized LIF setup were significantly smaller as compared to that

achieved by the Faraday plate with the transimpedance amplifier. Further improvements of the stability of product ion generation may significantly increase the performance of IMS-LIF.

Furthermore, the proposed detection method (LIF) provides additional to usual for IMS drift time information, namely wavelength of fluorescence maxima and fluorescence lifetime. Therefore, the better selectivity/distinguishing can be expected.

Practically, IMS-LIF spectra are currently generated in 24 minutes (see Figure 44). However, the recording time required for the analysis of the full drift time range (e.g. 0-20 ms) will be significantly increased. Therefore, only the IMS-LIF analysis of the selected ranges (peaks) is reasonable with the current setup.

The increase of the electric field results in a decrease of both the drift time and FWHM. Additionally, at high electric field strengths the diffusion plays a minor role. The FWHM can be further decreased under the high field conditions (>10 kV cm^{-1}). However, at these conditions the ion velocity is no longer proportional to the electric field strength.

The proposed method could be a relevant technique for the observation of small differences in drift time.

5 The coupling of IMS with LIF on the example of PAH

5.1 *Introduction*

The monitoring of hydrophobic contaminants is of great importance.[107] Polycyclic aromatic hydrocarbons are the biggest group of environmental contaminants introduced by humans due to the continuing increasing use of fossil fuels. PAH are of major concern, because they pose a potential risk for humans, with the potential ability, being cancerogenic and mutagenic.[108] Powerful laboratory methods exist, with the ability to determine low concentrations of PAH in aqueous solutions and sediments[109], however, a loss of concentration is expected during sampling, transport and sample preparation. Moreover, laboratory based methods for the determination of PAH are tedious due to the time-consuming procedures of sample preparation and transport. The interest of miniaturized onsite/on-line analytical systems has grown in recent years. Sampling, preparation, separation and a subsequent identification with a high certainty in one single device, is desired. In this work, the instrumentation for the drift tube ion mobility spectrometry (DT-IMS) laser induced fluorescence (LIF) coupling for the fast detection/identification of polycyclic aromatic hydrocarbons (PAH) is presented. The detection of ions in ion mobility spectrometers is performed with the Faraday plate detector, providing ion currents as a function of drift time. Sampling and identification of the approaching ion swarm in an IMS is provided by mass analyzers, interfaced with the Faraday plate detector. These so-called mass-identified mobility spectra are generated with a tremendous instrumental effort, making on-site/online identification almost impossible.[21] The coupling of IMS and LIF is a multidimensional detection system for ion pulses in an IMS and provides sufficient detection parameters for on-site identification of PAH. The resolution of an IMS is comparably poor with chromatographic techniques. With the fast LIF detection of analytes (containing fluorophores) the coupling of IMS and LIF promises both, analyte specific information from the fluorescence spectrum an enhanced resolving power of the IMS, respectively. Analysis of fluorescence signals in general allows the identification of compounds since the fluorescence of a compound is connected with electronic and vibronic transitions in the molecule of interest, and hence gives additional information keeping the facts: known analyte, differences in drift time, differences in emission spectra - in mind.

For the fast on-site detection of organic substances, the ability of drift tube ion mobility spectrometry that is separating ions in the gas phase (at atmospheric pressure) - the coupling of IMS and LIF is a promising hyphenation for the on-site identification of selected environmental contaminants. Due to the absence of pump sets the DT-IMS has proven to be a field deployable device for the sensitive detection of hazardous chemicals in the anthropogenic atmosphere.

Photoionization increased the selectivity for organic compounds. The absence of reactant ions in the ion mobility spectrum is a side effect of the photoionization. Thus, the entire spectrum can be used for the monitoring of ions. However, dopant assisted ionization is of major importance to increase selectivity and sensitivity in atmospheric pressure gas phase separation systems. For the ionization of PAH, the continuous development of photoionization and dopant-assisted photoionization gets "more and more" attention in the literature. In fact, photoionization by means of direct current glow discharge found its first application in the photoionization ion mobility spectrometry (PI-IMS) next to the photoionization detector (PID) in Gas Chromatography.

LIF detection has been widely studied to understand intramolecular processes, mostly in liquid solution. Rather less is known about the fluorescence of ions at atmospheric pressure. New methods exist, using MS and LIF to analyze fluorescence dyes and proteins in the gas phase.[77-78, 110] The present work demonstrated the feasibility of IMS with LIF detection on the example of gaseous ionic Rhodamine 6G. These findings should be used for the application of PAH analysis. The fluorescence spectroscopy has been proven suitable for the environmental monitoring of PAH.[111] Many PAH give emission in the same region. Fluorescence techniques are very sensitive to the micro-environment of the sample matrix and photo-physical processes (e.g. quenching, excited-state complex formation, etc.) The direct analysis of PAH mixtures is therefore a challenging procedure. The rapid gas phase separation could overcome the problem of interfering fluorescence from other present PAH. The drift time resolved fluorescence is a promising approach to couple rapid separation of PAH with analyte-specific detection in form of fluorescence spectra.

5.2 *Experimental*

The instrument was built in the University of Duisburg-Essen. The scheme/description of the experimental setup can be found in section 3.9. The components of the unidirectional flow IMS consists of an (1) photoionization discharge (PID) ion source, a (2) drift region and the (3) detector system. The PID ion source consists of a vacuum ultraviolet Kr photoionization discharge lamp (PKS 106, Heraeus, Hanau, Germany). The PID lamp is sealed concentrically onto the ionization chamber with a conical shell of 0.13 mL volume. The sample is introduced with a carrier gas of 10 mL min^{-1} and exits the ionization chamber at the tip of the conical shell through a ~1 mm opening. The ion source is interfaced to the drift region with an extraction electrode similar to the on-axis arrangement of the Krypton DC-glow ion source of Tabrizchi et al[85b] and an ion gate according to Bradbury and Neilson[42]. An additional cylindrical electrode (25 mm I.D., and 40 mm O.D.) was placed between the extraction electrode and the ion gate. The electrode consists of a shape according to Gormally and Philipps[52] with an inner diameter of 25 mm and an outer diameter of 40 mm. The ion gate was made of two sets of 1.3912 parallel wires (80 μm) located 600 μm from each other. The wires span a hole of 25 mm and are glued between two ceramic rings (O.D. 40 mm) of 4 mm thickness. The drift tube consists of 17 cylindrical electrodes (geometry mentioned above) in a stack and neighboring electrodes were insulated with interlocking PTFE spacers with the same diameters. The drift length from the Bradbury Nielsen ion gate to the detector was 16.8 cm. A high voltage power supply (DPR 50 205 24 5 EPU, ISEQ, Germany) was used as a voltage source for generating the electric field. The highest potential of 5 kV was applied to the Socket of the PID lamp. The principle of the Bradbury Nielsen gate electronics is a transformer providing a galvanically isolated AC voltage, which is converted into a switching DC voltage that can be superimposed onto the DC high voltage potential of the Bradbury Nielsen gates position in the drift tube. For blocking of the ion transmission, a closing potential is applied to one wire set while the other wire set is held at the reference potential. The switching frequency is provided by a pulse generator, determining the gate pulse width and the length of the ion mobility spectrum to be recorded. The gate closes with a voltage difference of +5-25 V superimposed on the potential of the ion gates position in the drift tube. Opening of the gate is achieved, when all wires are set to the potential equivalent to the position of the ion gate. The voltage drop and the distance between the PID socket and the extraction electrode was ~ 570 V and 6 mm, respectively. The voltage drop over the neighboring cylindrical electrodes was realized by 1 MΩ resistors connected in series

providing a homogeneous electrical field of 264 V cm^{-1}. The detection of the ion current is carried out with a Faraday plate detector adapted from the supplementary material of Eiceman and Karpas[18]. The electrometer was a transimpedance amplifier (DLPCA-200, Femto, Berlin, Germany). The aperture grid was placed approximately 1 mm in front of the detector and was manufactured similarly to the ion gate. The potential applied on the aperture grid was approximately 30 V. The drift gas was set to 50 mL min^{-1} with a mass flow controller (Aalborg GFC, United States). Ion currents were converted with a transimpedance amplifier (Femto DLPCA-200, Germany) with a gain of 10^{10} V/A. The insulation ring between the last ring electrode and the aperture grid was replaced by a 22,8 mm thick flow through cuvette made of aluminum oxide with three inserted windows in a 90° angle to each other. The windows for the entrance and output of the laser beam were made of quartz (Q1) and coated with an anti-reflection coating. The third hole was for the insertion of the glass fibre. The inner and outer diameter of the cuvette is 25 mm and 40 mm respectively. The electric field gradient through the cuvette was adjusted to the electrical drift field gradient to 263 V cm^{-1}. The IMS was held at 60° Celsius. For the excitation of the approaching ion swarm a frequency-quadrupled Neodymium:Yttrium-Aluminum garnet Laser (Polaris, New Wave Research, United Kingdom) was used irradiating at 266 nm with a pulse width of ~7 ns FWHM and a maximum pulse energy of ~20mJ/pulse. The Nd:YAG laser flash lamp was set to maximum intensity. The attenuator was set to a value of 400. The emitted fluorescence was collected in 90° angle with the light guide inserted into the flow-through cuvette. The collected light was guided into a spectrograph with an optical path according to Czerny and Turner. The grating was 150 lines mm^{-1}. The light detector was a gated intensified charge coupled device (Andor, United Kingdom). The emitted light was temporarily recorded after the laser pulse because of the spectral distortions generated by the laser. Thus, the fluorescence decay needed to be determined. The provided pulse for ion gating was synchronized with the laser xenon flash lamp and the Q-switch of the laser was synchronized with the ICCD camera with a delay generator (TGP 110, Thurbly Thandar instruments, Huntingdon, England). The spectrograph was set to a scan range from 280 to 565 nm. The spectrograph was used with the 149.9 lines mm^{-1} grating with a grating blaze of 300. The ICCD camera gate opening trigger was set to 6 ns after the light pulse with a gate width of 100 ns. The gain was set to a value of 200. Each spectrum was generated by 1000 accumulated spectra. Three replicates were recorded and stored with Andor Solis software.

A continuous introduction of the analyte was provided by a permeation tube. A permeation tube, filled with the analyte (Naphthalene and Pyrene from Sigma-Aldrich 99%) was placed in a thermostatic oven that was connected between the carrier gas mass flow controller (Aalborg GFC series) and the photoionization source inlet with a fused silica capillary (I.D. ~720 μm). The Naphthalene permeation temperature was 75° C, otherwise noted.

5.2.1 The effect of the photoionization lamp discharge current on the fluorescence of naphthalene

The IMS source and tube temperature were held at 60° C. The carrier gas was connected to the injector and the gaseous analyte was directed in the photoionization source inlet with a nitrogen flow rate of 10 mL min^{-1}. The data was blank subtracted and smoothed with the Savitzky-Golay method in Origin Pro 2015. Second Polynomial order with no boundary conditions was selected. A data window of 60 points was selected. The total ion current was probed by means of LIF inside the flow through cuvette located between the last ring electrode and the aperture grid.

5.2.2 The effect of the ion gate voltage on the fluorescence of Naphthalene

Fluorescence spectra were recorded with the same experimental conditions at different ion gate voltages. Additionally, the ion has been recorded with the transimpedance amplifier operating in high speed mode with a gain of 10^{10} V A^{-1}.

5.2.3 The effect of the electric field strength on the fluorescence of naphthalene and pyrene

Fluorescence spectra were recorded with the same experimental conditions at different drift voltages. When pyrene was used as the analyte, the injector temperature was increased to 160 ° C and the source temperature was increased to 100° C.

5.2.4 Drift time dependent fluorescence detection of Naphthalene

A mobility spectrum was generated by recording drift time dependent ion current with the transimpedance amplifier operating in high speed mode with a gain of 10^{10} V A^{-1}. The trigger was set on the rising edge of the pulse for the Bradbury Nielsen gate. The pulse generator was set to a pulse width of 200 μs at a frequency of 8 Hz. The ion gate voltage was set to 30 V. 16 averages have been stored with a digital storing oscilloscope in DC mode (Digital Storage Oscilloscope DSO-X 2022A, Agilent Technologies, Santa Clara, CL, USA). Excitation of the approaching ions

was performed with the Nd:YAG laser synchronized with the ion gate pulse and with the ICCD without changes of the parameters. For drift time dependent fluorescence measurements, the delay was manually adjusted by the delay controls of the delay generator.

5.3 *Results and Discussion*

5.3.1 The effect of the photoionization discharge lamp current on the fluorescence of naphthalene

Analogously to [0], the detection of naphthalene via laser-induced fluorescence in electric fields took place between the last ring electrode and the aperture grid of the experimental setup. The total ion current of the photoionization source passing the drift cell was probed with the pulsed laser induced fluorescence detection system. The laser beam enters centered perpendicular to the ion flow axis of the drift cell. The ion transmission was monitored by the DC offset generated by the transimpedance amplifier. When the permeation temperature was constant and the permeated analyte was flowing into the photoionization source continuously and the high voltage was switched on, the DC offset was monitored as a constant value of several volts. This corresponds to several tenths of nano amperes (see Figure 59). The fluorescence emission spectrum of naphthalene at the end of the drift cell is shown in Figure 58. It appears that the photoionization discharge lamp current affects the fluorescence signal of naphthalene in the detection region of the PI-IMS-LIF spectrometer. The effect of the vacuum UV Kr lamp operating current on the fluorescence signal intensity and on the total ion current is shown in the graphs below.
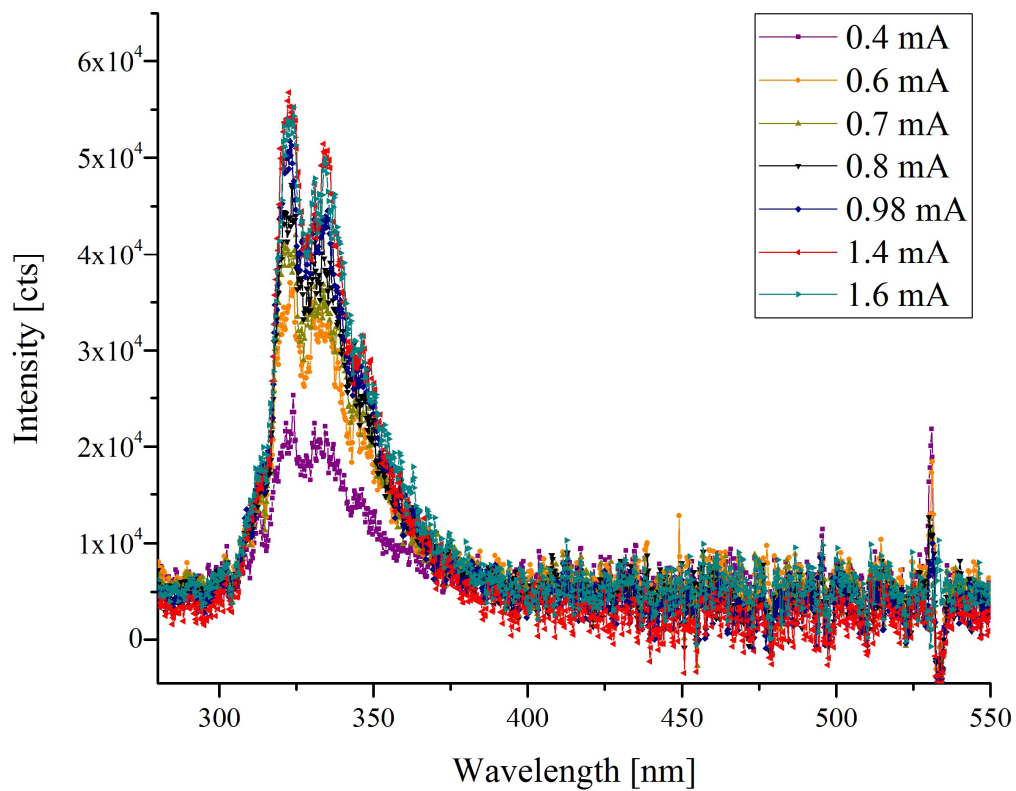
Figure 58 Fluorescence spectra of naphthalene in the gas phase (permeation temperature = 75° C) at different PID lamp currents. Average of n = 3 accumulated spectra, blank subtracted
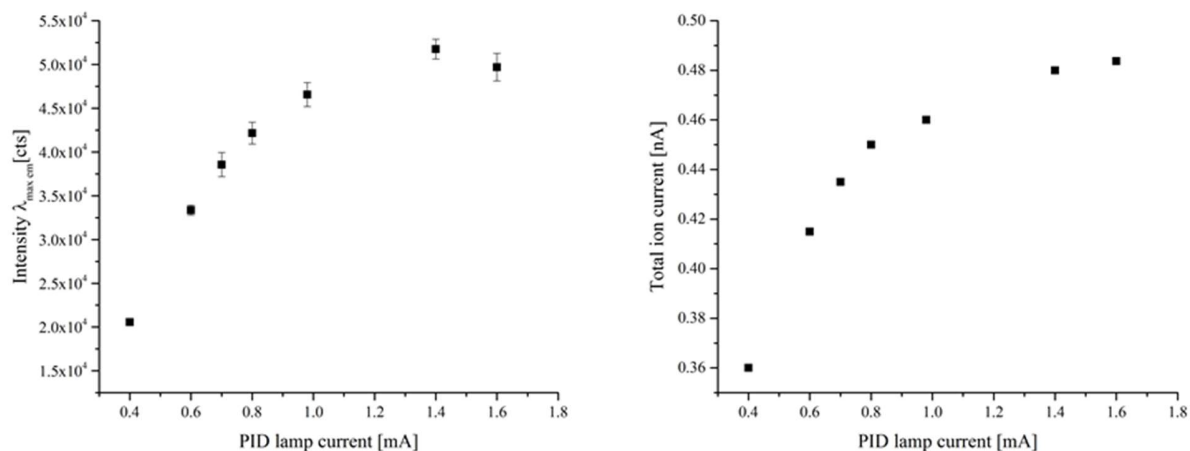
Figure 59 (left) Fluorescence maxima of naphthalene (λ max em = 323 nm) plotted against the PID-lamp current. Smoothed spectra from Figure 58, n=3. (right) Total ion current values plotted against the PID lamp current (transimpedance 10^{10} V/A)

The PID lamp current affects the formation of the ions by photoionization sources in ion mobility spectrometers.[87b] Figure 59 shows the fluorescence maxima at 323 nm and the total ion current with increasing operating current of the photoionization discharge lamp. The fluorescence intensity rises as the PID lamp current rises from 0.4 to 1.6 mA. The total ion current rises with increasing PID lamp current. This can be explained by the increase of the number of emitted photons at increased operating currents of the vacuum UV-Kr lamp. This leads to a more efficient ionization of molecules located in the ion source. Since nothing has been published yet about the laser induced fluorescence detection of PAH in drift tubes of IMS we assume the fluorescence signals can be attributed to the [M+] ions of naphthalene ionized by photoionization. Considering atmospheric pressure and low regime flow rates of nitrogen used as drift gas one has to note the carry over effect of the permeation rate of naphthalene at 75° C. The signal can therefore also be attributed to non-ionized gaseous naphthalene.

5.3.2   The effect of the ion gate voltage on the fluorescence of naphthalene

The effect of ion blocking analogously to section [4.3.3] was also observed in the experimental setup.
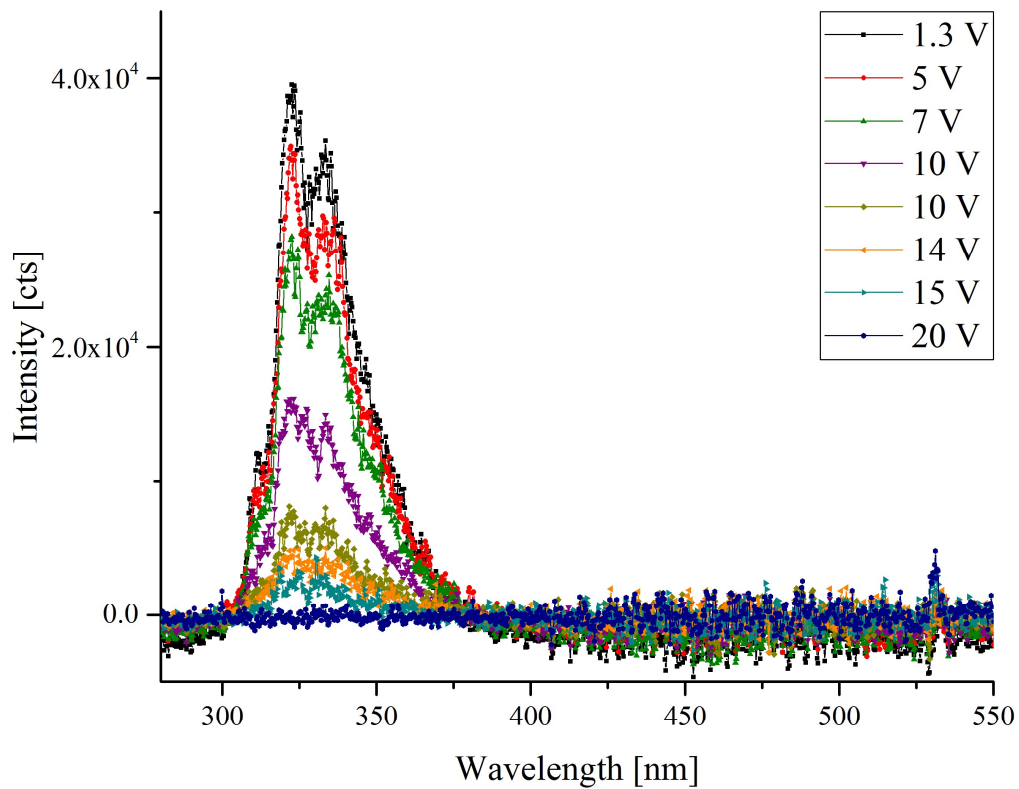
Figure 60 Fluorescence spectra of naphthalene at different ion gate voltages
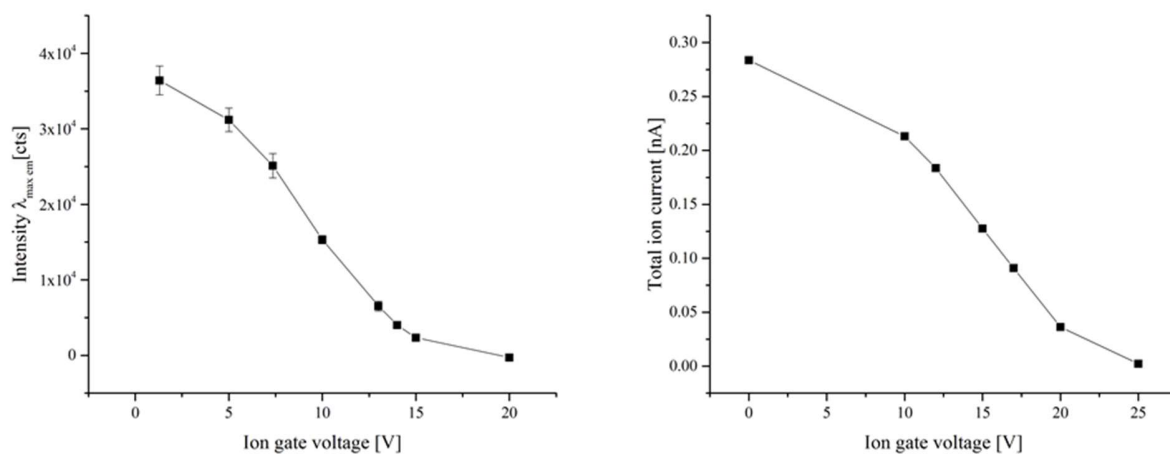
Figure 61 (left) Fluorescence intensity maxima against the ion gate voltage. (right) total ion current against the ion gate voltage (transimpedance 10^{10} V/A)

The electric field strength between the gate wires resulted in the deflection of the transported ions. This can be seen in the changes of the fluorescence intensity when the ion gate bias value is increased from 0 - 20 V. The fluorescence intensity is decreased as penetration of ions is hindered, when the gate voltage is applied. The increased gate voltage results in increase of a deflecting ion shutter field, generated between the gate wires. The gate field deflects the approaching ions, as they pass the wire arrangement. The deflection angle is strongly dependent on the electric field strength between the two wire sets.[102] In general the ions get deflected to a larger extend at higher gate fields. This result can be compared with the experiments in [4.3.3] (see Figure 36, Figure 39, Figure 40).

The change of the fluorescence intensity with increasing ion gate voltage was observable within a time delay in the range of 5-10 minutes. When the fluorescence spectra were recorded immediately after the adjustment of the ion gate voltage, no significant changes of the fluorescence intensity was observable. However, when the fluorescence spectra were recorded ten minutes after the ion gate voltage adjustment, the spectral changes were noticeable. This effect is in contrast to the experimental findings in section [4.3.3].

5.3.3   The effect of the electric field strength on the fluorescence of naphthalene and pyrene

To prove the dependence of naphthalene fluorescence intensity on the electric field, the electric field strength was varied between 0 and 265 V cm^{-1}. The ion gate was switched off in order to analyze the total ion current. The effect of the electric field strength on the fluorescence spectra of the naphthalene at the end of the drift cell at different electric fields is shown in Figure 62. The effect of the electric field strength on the fluorescence emission spectra of naphthalene at different electric fields is shown in Figure 62.
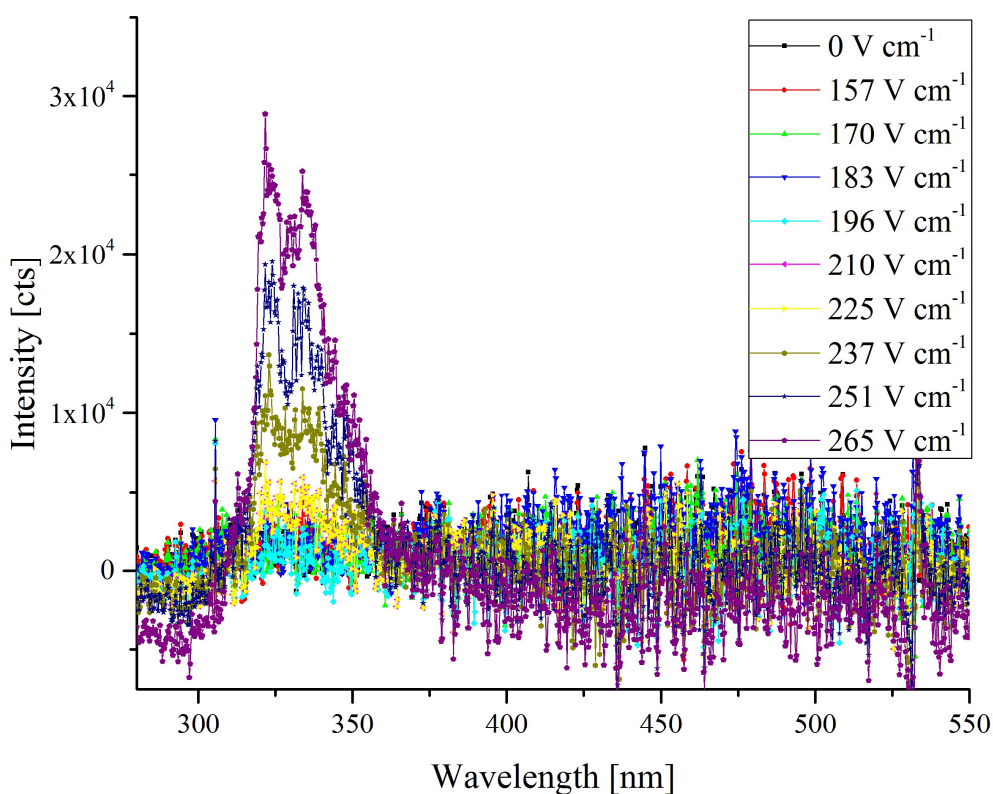
Figure 62 Fluorescence spectra of naphthalene in the PI-IMS-LIF instrument at different electric field strengths, blanc subtracted, average of n=3

In the range of 0-210 V cm^{-1} the fluorescence was not detectable. However, a linear relation was found for the naphthalene fluorescence intensity in the range of 225 – 265 V cm^{-1}.
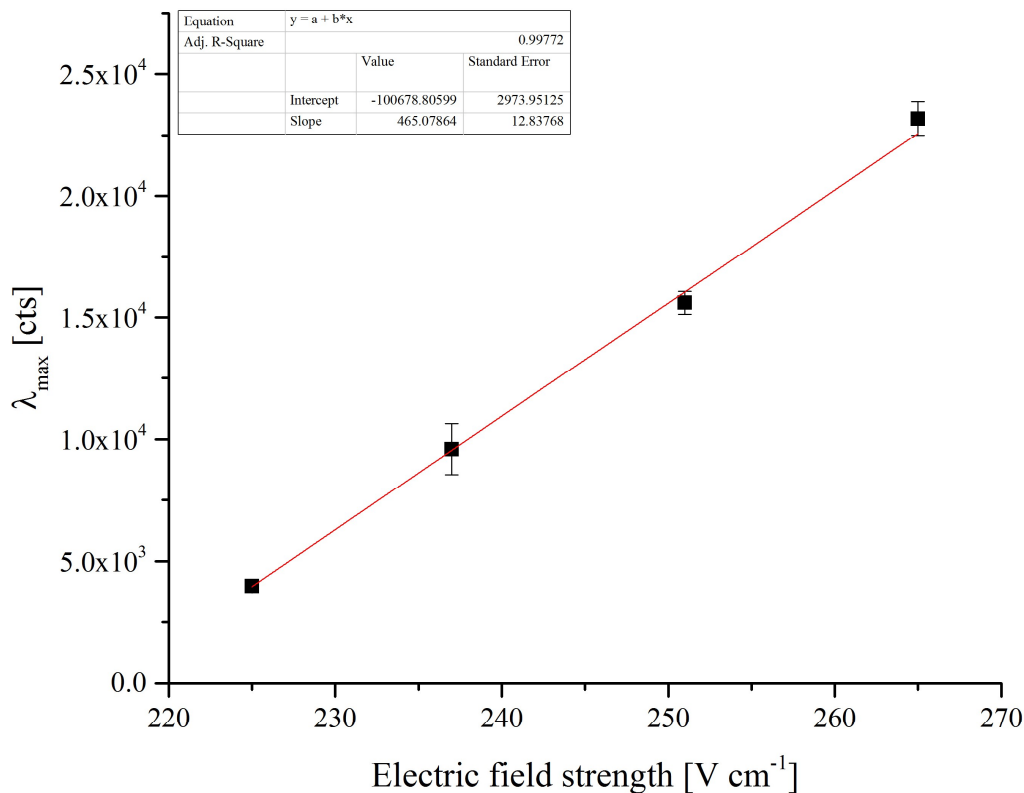
Figure 63 Fluorescence Intensity maxima plottet against the electric field strength. Blanc subtracted, smoothed, average of n=3

This effect can be explained analogously to section [4.3.3] (see Figure 41). The drift time is inversely proportional to the electric field in a drift tube [see equation (7)]. During the drift the diffusion of the ions takes place. The diffusion flux is time-dependent. Therefore, increase of the drift field strength leads to the reduced effect of diffusion. This results in reduced peak width (time scale) and increased intensity. Moreover, due to the reduced drift times the ions have less time for the undesirable reactions (e.g. ion-molecule reactions: charge transfer, recombination) which may lead to the reduced signal intensity. This explains the increasing number of ions that can be detected by laser induced fluorescence emission at increased electric field strengths.

For further increase of the fluorescence intensity the higher values of drift voltage can be applied.

A similar trend was found for pyrene. The effect of the electric field strength on the fluorescence emission spectra of pyrene at different electric fields is shown below.
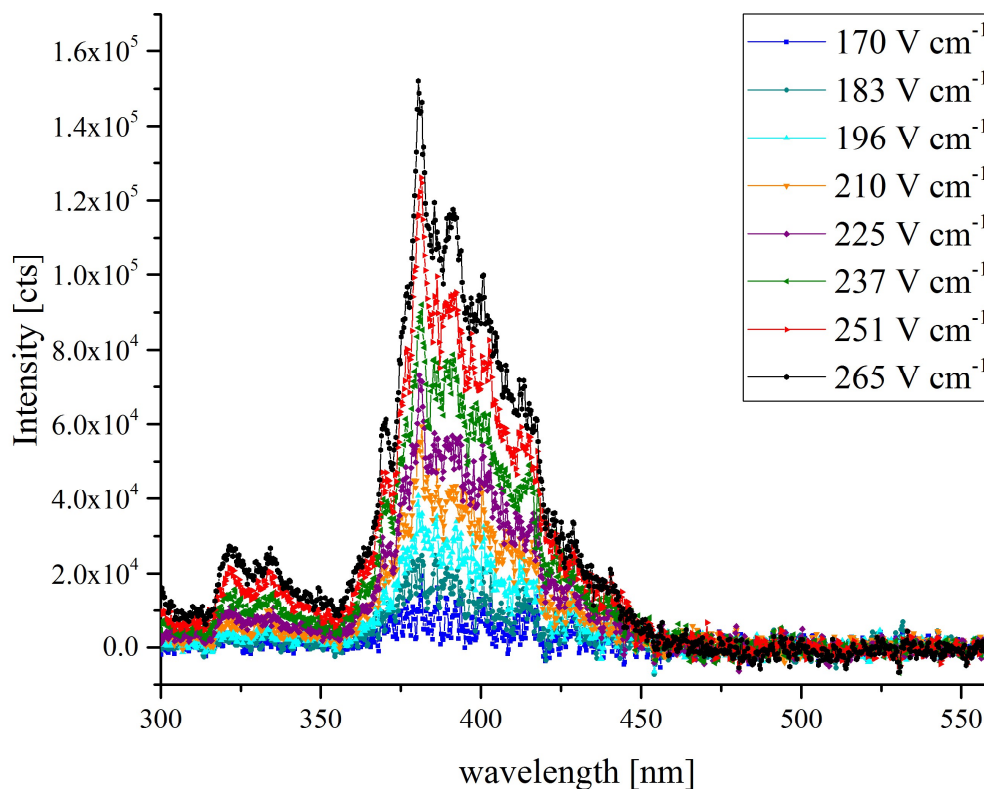
Figure 64 Fluorescence spectra of pyrene in the PI-IMS-LIF instrument at different electric field strengths, blanc subtracted, average of n=3

In the range of 0-183 V cm^{-1} the fluorescence was not detectable or the signal was affected with strong noise. The signal to noise ratio of a single spectrum was < 0.5 at 183 V cm^{-1}. However, a linear relation was found for the pyrene fluorescence intensity in the range of 196 – 265 V cm^{-1}.
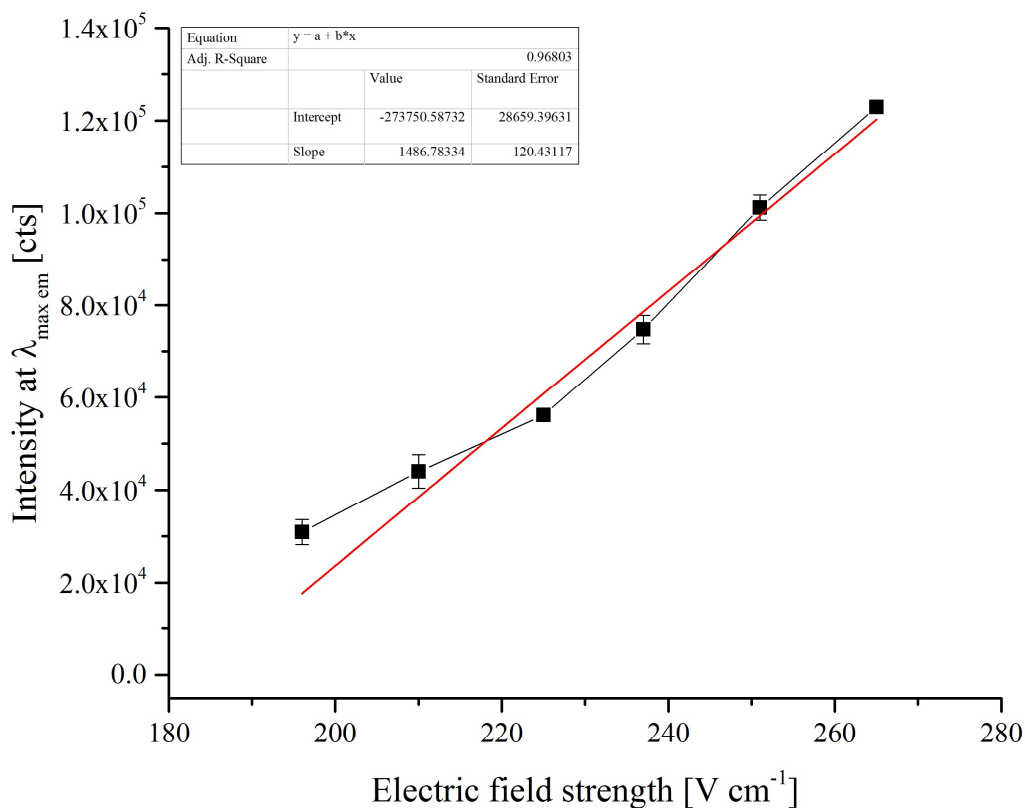
Figure 65 Fluorescence Intensity maxima plotted against the electric field strength. Blanc subtracted, smoothed, average of n=3

The observed dependence of the fluorescence emission intensity on the electric field strength is considered to demonstrate the ion detection of PAH in the photoionization drift time mobility based system. The experiment with pyrene is afflicted with impurities. In the wavelength range of 300 – 350 nm, a second fluorescence signal is detected. Naphthalene was used in the previous experiments and poses a possible source of contamination. This impurity however demonstrates the wavelength discrimination by means of fluorescence of a binary mixture of polycyclic hydrocarbons.

The observed dependencies of naphthalene and pyrene fluorescence intensity on both, the ion gate field and the electric field, point to the feasibility of drift time resolved fluorescence spectra. In

general, the fluorescence needs to be recorded for short periods of time after a defined delay time relatively to the gate pulse.

5.3.4 Drift time dependent fluorescence detection of naphthalene

Analogously to experiments in [4.3.4], drift time dependent fluorescence was performed at different delays relatively to the ion injection pulse on an example of naphthalene (see the insert Figure 66).
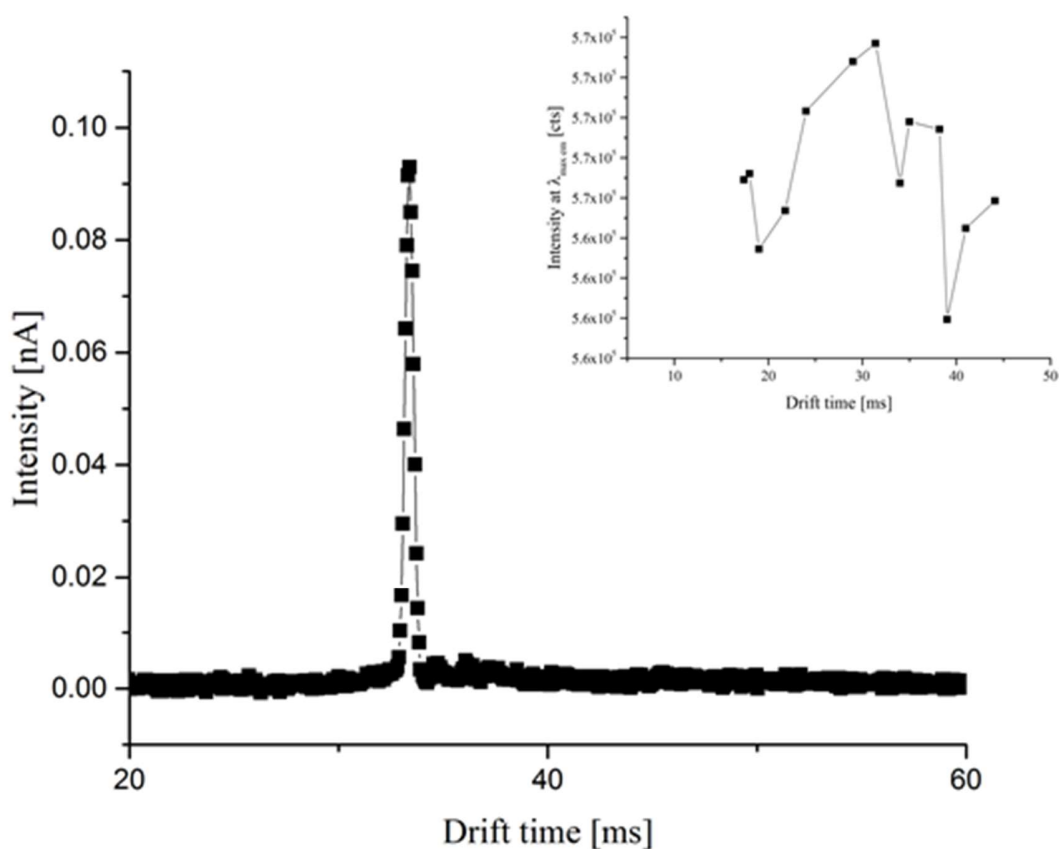
Figure 66 Drift time spectra of naphthalene. The permeation temperature was 40°C. The ion gate voltage and pulse width were 30 V and 200 μs, respectively. The amplifier was working in high mode at 10^{10} V A^{-1}. The carrier gas and drift gas flow rates were 10 mL min^{-1} and 500 mL min^{-1}, respectively. The spectrum represents the average of 16 spectra. The insert demonstrates the fluorescence intensity of naphthalene at $\lambda_{em} = 323$ nm at different drift times. The emission spectra are detected within the range of 15-45 ms.

Analogously to [3.9], single compound spectra of PAH can be generated by placing solid pure substances in the used injector. In this case the method of using permeation tubes poses a suitable method that enables the determination of the analyte concentration in the carrier gas.

The result of drift time resolved fluorescence detection was not as expected (see insert Figure 66). The signal did not show significant differences, when the fluorescence was detected at different drift times. The possible reason is that the concentration of the ions was not sufficient. Numerous attempts have been made to increase the concentration of the analyte ion where the excitation took place. This can be realized by increasing the permeation temperature. Alternatively, it can be performed by increasing the ion gate pulse width and thus increasing the amount of ions travelling through the drift tube. In another attempt, the ion gate voltage was set to 8 V to detect fluorescence intensity differences between the background and the signal.

The drift time spectra in Figure 67 show the broad signal of naphthalene with superimposed signals at different drift times.
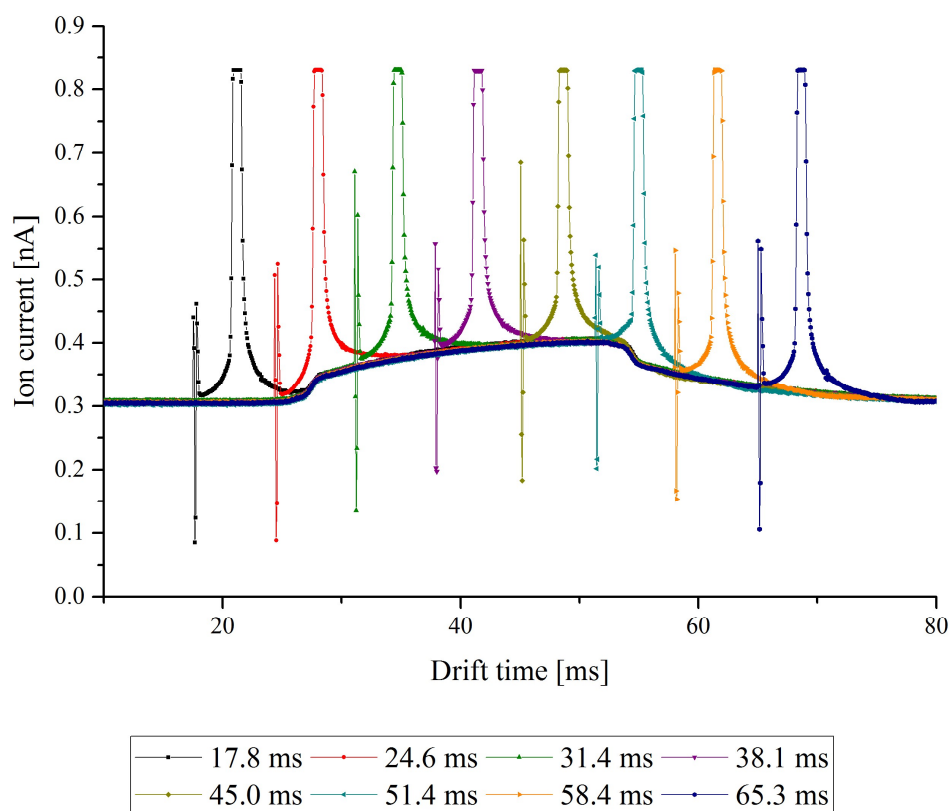
Figure 67 Drift time spectra of naphthalene with laser induced ion current distortions at different delay times. The gate opening time was 20 ms and 8 V ion gate voltage.

Firstly, the broad signal with low intensity is discussed. The signal of interest has a baseline value at 0.3 nA. This offset can be explained by the ion gate voltage. The ion gate voltage was set to a value of 8 V to determine fluorescence intensity differences over the drift time range of 20 – 80 ms. The ion gate does not block the ions to a full extend which results in the increased baseline level. The signal has a not expected peak shape with significant differences to drift time signals that show a normal distributed peak. This can be explained by the high density of ions injected into the IMS at a pulse width of 20 ms. The high ion density leads to a saturation of the drift tube and the separation becomes inefficient. The superimposed signals were originating from the laser pulse. The first signal with smaller band width could be compared with the temporal width of the laser pulse (7 ns). That is possibly the distortion of the pulsing electronics of the Q-switch in the

133

Nd:YAG laser. The second signal with broader bandwidth is most likely from photoionized naphthalene molecules. The temporal difference between the laser pulse and the signal corresponds to the drift time of the laser ionized molecules. Laser ionization ion mobility spectrometry of PAH has been reported in the literature.[48c, 52, 112]

The gas flow settings and the permeation temperatures of the analytes were optimized to achieve the signal to noise ratio $\geq$ 3. This also included reduce of the drift gas flow rate to 50 mL min^{-1}. The fluorescence intensity decreased rapidly, when the drift gas flow rate is increased > 50 mL min^{-1}. These findings indicate the detection of gaseous naphthalene or pyrene in the flow-through cuvette of the IMS. The detected fluorescence signals can originate from neutralized molecules that have lost their charge during the drift towards the faraday plate detector.

It has been reported in the literature that the quantum yield for naphthalene ionization is ~ 0.4 when using vacuum UV Kr lamp.[113] However, no data are available in the literature for the quantum yield of the naphthalene radical cation ionization. The possibly low ionization yield and short lifetime for naphthalene radical cation could be the reason for low fluorescence intensity.

The drift length of 16 cm was chosen for a better separation of the PAH in the drift tube. That is longer as compared to the standard IMS length of 10 cm. However, this results in a higher loss of ions.

The laser pulse width of used in this study Nd:YAG laser is 7 ns. That is too short for the fluorescence monitoring with integration window of 100 ns used in this study. The use of a continuous wave laser can improve the fluorescence intensity.

5.4 *Conclusion and Outlook*

The laser induced fluorescence detection of selected PAH (naphthalene and pyrene) has shown to be possible inside a drift tube ion mobility spectrometer. It was not possible to realize the time resolved IMS-LIF. However, the dependence of the LIF signal intensity on the drift field strength was observed. This demonstrates, that the ions, generated by photoionization can be transported through the drift region and detected with the laser induced fluorescence monitoring system. Despite the reported quantum yield for naphthalene ionization is ~ 0.4, when using vacuum UV Kr lamp, no data are available in the literature for the fluorescence quantum yield of the naphthalene radical cation. The possibly low fluorescence quantum yield and short lifetime for naphthalene radical cation could be the reason for the low fluorescence intensity.

The fluorescence intensity of naphthalene was dependent on the PID lamp current. The observed increased ion current at increased PID lamp current leads to both, the increased fluorescence intensity of naphthalene and the increase of the total ion current. Because the increase of the ion current leads to the increase of the fluorescence signal, it can be concluded that the fluorescence intensity originates from the ionized molecules generated by photoionization. Additional evidence for the relation of the fluorescence signal to the ionized molecules is the simultaneous decrease of both the total ion current and the fluorescence intensity with increase of the ion gate voltage.

This instrumental coupling has the potential to address other specialized fields of research, that require the spatial (and time resolved) ion fluorescence monitoring at atmospheric pressure.

Additional information to the ion current detection can be obtained with the proposed detection method (LIF), namely wavelength of fluorescence maxima and fluorescence lifetime. This was proven on the example of naphthalene and pyrene.

Although the results presented in this chapter point to the detection of ionized PAH species, however the diffusion of the gaseous analytes towards the flow cell at the detector must not be neglected.

There are no excitation and emission spectra available for the ionized PAH species in the gas phase at atmospheric pressure. Therefore, the determination of the absorption and emission maxima of the ionized species is necessary.

6   Summary

The main focus of the study is the realization of drift time resolved fluorescence detection of ions in a drift tube cell. The laser induced fluorescence is proposed as a complimentary/alternative detection system that is potentially faster than a conventional electrometer and provides additional analytical information. The proposed detection method (LIF) can provide additional to usual for IMS drift time information, namely wavelength of fluorescence maxima and fluorescence lifetime. Therefore, the better selectivity/distinguishing can be expected. The coupling of time of flight ion mobility spectrometry with LIF is so far not described in literature.

After the design and development of this novel coupling, the possibility of drift time resolved fluorescence detection was proven on the example of the Xanthene dye Rhodamine 6G ions. The fluorescence of the ionized dye in the gas phase has been investigated in a simplified IMS drift cell of open design. The release and desolvation of R6G ions from the electrospray with following IMS-LIF analysis was demonstrated. The total ion current of the electrospray passing the drift cell was probed with the laser induced fluorescence detection system. The fluorescence spectrum recorded at the exit of the drift cell is identical to that of gaseous dye Rhodamine 6G recorded in the electrospray plume. The decrease of the ion transmission with increase of perpendicular ion gate field was observed by fluorescence of the gaseous ions of dye Rhodamine 6G. The fluorescence intensity of gaseous ionic dye R6G increases with the increase of the drift field gradient.

The improvements of the electrospray source and the excitation source resulted in an increase in both the long-term stability and the fluorescence emission intensity. The optimization of the excitation wavelength resulted in a significant increase of signal intensity. The optimization of electrospray materials and conditions has improved the long-term stability of the electrospray process. With this modified system, signal intensities were improved by one order of magnitude. Therefore, it was possible to reduce the integration time in the LIF measurements to the required for the drift time dependent LIF analysis values of 100 µs.

The drift time resolved LIF detection of Rhodamine 6G ions at ambient conditions was achieved. It was found that the FWHM of the drift time fluorescence signal is dependent on the initial ion gate pulse width. The drift time spectra produced with both, the Faraday plate detector and the laser induced fluorescence detector show the same trends. Besides the peak broadening, a shift of peak maxima towards bigger drift times with increase of the ion gate pulse width was observed.

136

With the increase of electric field strength the peak positions shift towards smaller drift time values. This trend is similar to that observed in the drift time spectra recorded with the electrometer. Remarkably, a difference between the FWHM values derived from drift time resolved spectra with both LIF and Faraday plate detectors was found. The FWHM derived from drift time fluorescence spectra were significantly smaller than those obtained with the electrometer. The main reason for higher FWHM values achieved with electrometer is probably the additional peak broadening caused by the transimpedance amplifier. This demonstrates that the drift time spectra of higher resolution can be potentially achieved with the LIF detection as compared to that with the state of the art electrometer.

The laser induced fluorescence detection of PAH model compounds (naphthalene and pyrene) has shown to be possible inside a drift tube ion mobility spectrometer. It was not possible to realize the time resolved IMS-LIF. However, the dependence of the LIF signal intensity on the drift field strength was observed.

The observed increased ion current at increased PID lamp current leads to both, the increased fluorescence intensity of naphthalene and the increase of the total ion current. The increase of the ion current leads to the increase of the fluorescence signal. Therefore, it can be concluded that the fluorescence intensity originates from the ionized molecules generated by photoionization. The simultaneous decrease of both the total ion current and the fluorescence intensity with increase of the ion gate voltage is an additional evidence for the relation of the fluorescence signal to the ionized molecules.

7 Literature

1.   St. Louis, R. H.; Hill Jr, H. H.; Eiceman, G. A., Ion mobility spectrometry in analytical chemistry. Critical Reviews in Analytical Chemistry 1990, 21 (5), 321-355.

2.   (a) Albritton, D. L.; Miller, T.; Martin, D.; McDaniel, E., Mobilities of mass-identified H 3+ and H+ ions in hydrogen. Physical Review 1968, 171 (1), 94; (b) Karasek, F. W., Plasma chromatography. Analytical Chemistry 1974, 46 (8), 710A-720a.

3.   Borsdorf, H.; Mayer, T.; Zarejousheghani, M.; Eiceman, G. A., Recent developments in ion mobility spectrometry. Applied Spectroscopy Reviews 2011, 46 (6), 472-521.

4.   Baumbach, J. I.; Eiceman, G. A., Ion Mobility Spectrometry: Arriving On Site and Moving Beyond a Low Profile. Applied Spectroscopy 1999, 53 (9), 338A-355A.

5.   McDaniel, E. W.; Mason, E. A., The mobility and diffusion of ions in gases. 1973.

6.   Revercomb, H.; Mason, E. A., Theory of plasma chromatography/gaseous electrophoresis. Review. Analytical Chemistry 1975, 47 (7), 970-983.

7.   Staymates, J. L.; Staymates, M. E.; Lawrence, J., The effect of reusing wipes for particle collection. International Journal for Ion Mobility Spectrometry 2015, 1-9.

8.   Nanji, A. A.; Lawrence, A. H.; Mikhael, N. Z., Use of skin surface sampling and ion mobility spectrometry as a preliminary screening method for drug detection in an emergency room. Journal of Toxicology: Clinical Toxicology 1987, 25 (6), 501-515.

9.   Eiceman, G.; Young, D.; Schmidt, H.; Rodriguez, J.; Baumbach, J.; Vautz, W.; Lake, D.; Johnston, M., Ion mobility spectrometry of gas-phase ions from laser ablation of solids in air at ambient pressure. Applied spectroscopy 2007, 61 (10), 1076-1083.

10.   O'Keeffe, A. E.; Ortman, G. C., Primary Standards for Trace Gas Analysis. Analytical Chemistry 1966, 38 (6), 760-763.

11.   Determination of material resistance to permeation by chemicals –

Part 1: Permeation by liquid chemical under conditions of continuous contact;

German version EN 16523-1:2015.

12.   Borsdorf, H.; Schelhorn, H.; Flachowsky, J.; Döring, H.-R.; Stach, J., Corona discharge ion mobility spectrometry of aliphatic and aromatic hydrocarbons. Analytica chimica acta 2000, 403 (1), 235-242.

13.   Karpas, Z., Ion mobility spectrometry of aliphatic and aromatic amines. Analytical Chemistry 1989, 61 (7), 684-689.

14.   Liu, X.; Nacson, S.; Grigoriev, A.; Lynds, P.; Pawliszyn, J., A new thermal desorption solid-phase microextraction system for hand-held ion mobility spectrometry. Analytica chimica acta 2006, 559 (2), 159-165.

15.   Dole, M.; Mack, L.; Hines, R.; Mobley, R.; Ferguson, L.; Alice, M. d., Molecular beams of macroions. The Journal of Chemical Physics 1968, 49 (5), 2240-2249.

16.   Wilm, M.; Mann, M., Analytical properties of the nanoelectrospray ion source. Analytical chemistry 1996, 68 (1), 1-8.

17.   Budimir, N.; Weston, D. J.; Creaser, C. S., Analysis of pharmaceutical formulations using atmospheric pressure ion mobility spectrometry combined with liquid chromatography and nano-electrospray ionisation. Analyst 2007, 132 (1), 34-40.

18.   Eiceman, G. A.; Karpas, Z., Ion Mobility Spectrometry. Second Edition ed.; CRC: 2009.

19.   (a) Borsdorf, H.; Rämmler, A.; Schulze, D.; Boadu, K.; Feist, B.; Weiss, H., Rapid on-site determination of chlorobenzene in water samples using ion mobility spectrometry. Analytica chimica acta 2001, 440 (1), 63-70; (b) Baumbach, J.; Schmidt, H.; Pilzecker, P., Detection of alcohols using UV-ion mobility spetrometers. Analytica Chimica Acta 2001, 431 (2), 293-301.

20.   Seto, Y., Determination of volatile substances in biological samples by headspace gas chromatography. Journal of Chromatography a 1994, 674 (1), 25-62.

21.   Spangler, G. E.; Carrico, J. P., Membrane inlet for ion mobility spectrometry (plasma chromatography). International journal of mass spectrometry and ion physics 1983, 52 (2), 267-287.

22.   Baim, M. A.; Hill Jr, H. H., Tunable selective detection for capillary gas chromatography by ion mobility monitoring. Analytical Chemistry 1982, 54 (1), 38-43.

23.   Dzidic, I.; Carroll, D.; Stillwell, R.; Horning, E., Comparison of positive ions formed in nickel-63 and corona discharge ion sources using nitrogen, argon, isobutane, ammonia and nitric oxide as reagents in atmospheric pressure ionization mass spectrometry. Analytical Chemistry 1976, 48 (12), 1763-1768.

24.   Carroll, D.; Dzidic, I.; Stillwell, R.; Horning, E., Identification of positive reactant ions observed for nitrogen carrier gas in plasma chromatograph mobility studies. Analytical Chemistry 1975, 47 (12), 1956-1959.

25.   Karasek, F. W.; Kane, D. M., Effect of oxygen on response of the electron-capture detector. Analytical Chemistry 1973, 45 (3), 576-580.

26.   Tanaka, Y.; Zelikoff, M., Continuous emission spectrum of xenon in the vacuum ultraviolet region. JOSA 1954, 44 (3), 254_1-255.

27.   Ševčik, J.; Krýsl, S., A photoionization detector. Chromatographia 1973, 6 (8-9), 375-380.

28.   Spangler, G. E.; Roehl, J. E.; Patel, G. B.; Dorman, A., Photoionization ion mobility spectrometer. 1994.

29.   Hanold, K. A.; Fischer, S. M.; Cormia, P. H.; Miller, C. E.; Syage, J. A., Atmospheric pressure photoionization. 1. General properties for LC/MS. Analytical chemistry 2004, 76 (10), 2842-2851.

30.   Roetering, S.; Nazarov, E. G.; Borsdorf, H.; Weickhardt, C., Effect of dopants on the analysis of pesticides by means of differential mobility spectrometry with atmospheric pressure photoionization. International Journal for Ion Mobility Spectrometry 2010, 13 (2), 47-54.

31.   Tzeng, W.; Wei, S.; Castleman Jr, A., Multiphoton ionization of acetone clusters: metastable unimolecular decomposition of acetone cluster ions and the influence of solvation on intracluster ion-molecule reactions. Journal of the American Chemical Society 1989, 111 (16), 6035-6040.

32.   Baumbach, J. I.; Sielemann, S.; Xie, Z.; Schmidt, H., Detection of the gasoline components methyl tert-butyl ether, benzene, toluene, and m-xylene using ion mobility spectrometers with a radioactive and UV ionization source. Analytical chemistry 2003, 75 (6), 1483-1490.

33.   Cheng, S.; Dou, J.; Wang, W.; Chen, C.; Hua, L.; Zhou, Q.; Hou, K.; Li, J.; Li, H., Dopant-assisted negative photoionization ion mobility spectrometry for sensitive detection of explosives. Analytical chemistry 2012, 85 (1), 319-326.

34.   Kauppila, T. J.; Kersten, H.; Benter, T., The ionization mechanisms in direct and dopant-assisted atmospheric pressure photoionization and atmospheric pressure laser ionization. Journal of The American Society for Mass Spectrometry 2014, 25 (11), 1870-1881.

35.   Gross, J. H., Principles of ionization and ion dissociation. In Mass Spectrometry, Springer: 2011; pp 21-66.

36.   Chapman, S., Carrier mobility spectra of spray electrified liquids. Physical Review 1937, 52 (3), 184.

37.   (a) Shumate, C., Electrospray ion mobility spectrometry. TrAC Trends in Analytical Chemistry 1994, 13 (3), 104-109; (b) Shumate, C. B.; Hill Jr, H. H., Coronaspray nebulization and ionization of liquid samples for ion mobility spectrometry. Analytical chemistry 1989, 61 (6), 601-606.

38.   Wittmer, D.; Chen, Y. H.; Luckenbill, B. K.; Hill Jr, H. H., Electrospray ionization ion mobility spectrometry. Analytical Chemistry 1994, 66 (14), 2348-2355.

39.   Khayamian, T.; Jafari, M., Design for electrospray ionization-ion mobility spectrometry. Analytical chemistry 2007, 79 (8), 3199-3205.

40.   (a) Kurnin, I. V.; Kayumov, A. A.; Muradymov, M. Z.; Krasnov, N. V.; Samokish, A. V., Coupling of liquid chromatograph with ion-mobility spectrometer. International Journal for Ion Mobility Spectrometry 2013, 16 (3), 169-176; (b) Zühlke, M.; Riebe, D.; Beitz, T.; Löhmannsröben, H.-G.; Zenichowski, K.; Diener, M.; Linscheid, M. W., An electrospray ionization-ion mobility spectrometer as detector for HPLC. European Journal of Mass Spectrometry 2015, 21, 0-0.

41.   Cravath, A. M., The Rate of Formation of Negative Ions by Electron Attachment. Physical Review 1929, 33 (4), 605-613.

42.   Bradbury, N. E.; Nielsen, R. A., Absolute Values of the Electron Mobility in Hydrogen. Physical Review 1936, 49 (5), 388-393.

43.   (a) Cotter, R. J.; Gardner, B. D.; Iltchenko, S.; English, R. D., Tandem time-of-flight mass spectrometry with a curved field reflectron. Analytical chemistry 2004, 76 (7), 1976-1981; (b) Beussman, D. J.; Vlasak, P. R.; McLane, R. D.; Seeterlin, M. A.; Enke, C. G., Tandem reflectron time-of-flight mass spectrometer utilizing photodissociation. Analytical chemistry 1995, 67 (21), 3952-3957; (c) Brunner, T.; Mueller, A.; O'Sullivan, K.; Simon, M.; Kossick, M.; Ettenauer, S.; Gallant, A.; Mané, E.; Bishop, D.; Good, M., A large Bradbury Nielsen ion gate with flexible wire spacing based on photo-etched stainless steel grids and its characterization applying symmetric and asymmetric potentials. International Journal of Mass Spectrometry 2012, 309, 97-103.

44.   Tadjimukhamedov, F. K.; Puton, J.; Stone, J. A.; Eiceman, G. A., A study of the performance of an ion shutter for drift tubes in atmospheric pressure ion mobility spectrometry: computer models and experimental findings. Rev Sci Instrum 2009, 80 (10), 103103.

45.   Eiceman, G. A.; Karpas, Z.; Hill Jr, H. H., Ion mobility spectrometry. CRC press: 2013.

46.   Puton, J.; Knap, A.; Siodłowski, B., Modelling of penetration of ions through a shutter grid in ion mobility spectrometers. Sensors and Actuators B: Chemical 2008, 135 (1), 116-121.

47.   Carr, T. W., Plasma chromatography. Plenum Pub Corp: 1984.

48.   (a) An, Y.; Aliaga-Rossel, R.; Choi, P.; Gilles, J.-P., Development of a short pulsed corona discharge ionization source for ion mobility spectrometry. Review of scientific instruments 2005, 76 (8), 085105; (b) Jenkins, A., Ion mobility spectrometers. Google Patents: 1993; (c) Phillips, J.; Gormally, J., The laser desorption of organic molecules in ion mobility spectrometry. International journal of mass spectrometry and ion processes 1992, 112 (2), 205-214.

49.   Cohen, M. J.; Karasek, F., Plasma chromatography™—a new dimension for gas chromatography and mass spectrometry. Journal of Chromatographic science 1970, 8 (6), 330-337.

50.   (a) Soppart, O.; Baumbach, J., Comparison of electric fields within drift tubes for ion mobility spectrometry. Measurement Science and Technology 2000, 11 (10), 1473; (b) Eiceman, G. A.; Nazarov, E. G.; Rodriguez, J. E.; Stone, J. A., Analysis of a drift tube at ambient pressure: Models and precise measurements in ion mobility spectrometry. Review of Scientific Instruments 2001, 72 (9), 3610.

51.   Liu, X.; Li, S.; Li, M., Optimization design of drift tube for ion mobility spectrometer based on simulation of drift electric field. International Journal for Ion Mobility Spectrometry 2012, 15 (4), 231-237.

52.   Gormally, J.; Phillips, J., The performance of an ion mobility spectrometer for use with laser ionization. International Journal of Mass Spectrometry and Ion Processes 1991, 107 (3), 441-451.

53.   (a) Carrico, J.; Sickenberger, D.; Spangler, G.; Vora, K., Simple electrode design for ion mobility spectrometer. Journal of Physics E: Scientific Instruments 1983, 16 (11), 1058; (b) Spangler, G. E.; Vora, K. N.; Carrico, J. P., Miniature ion mobility spectrometer cell. Journal of Physics E: Scientific Instruments 1986, 19 (3), 191.

54.   Laprade, B., Use of conductive glass tubes to create electric fields in ion mobility spectrometers. Google Patents: 2006.

55.   Spangler, G. E., Expanded theory for the resolving power of a linear ion mobility spectrometer. International Journal of Mass Spectrometry 2002, 220 (3), 399-418.

56.   McDaniel, E.; Martin, D.; Barnes, W., Drift tube-mass spectrometer for studies of low-energy ion-molecule reactions. Review of Scientific Instruments 1962, 33 (1), 2-7.

57.   McKnight, L.; McAfee, K.; Sipler, D., Low-field drift velocities and reactions of nitrogen ions in nitrogen. Physical Review 1967, 164 (1), 62.

58.   McDaniel, E., Possible Sources of Large Error in Determinations of Ion–Molecule Reaction Rates with Drift Tube–Mass Spectrometers. The Journal of Chemical Physics 1970, 52 (8), 3931-3935.

59.   Karasek, F.; Kim, S.; Hill Jr, H., Mass identified mobility spectra of p-nitrophenol and reactant ions in plasma chromatography. Analytical Chemistry 1976, 48 (8), 1133-1137.

60.   Steiner, W. E.; Clowers, B. H.; Fuhrer, K.; Gonin, M.; Matz, L. M.; Siems, W. F.; Schultz, A. J.; Hill, H. H., Electrospray ionization with ambient pressure ion mobility separation and mass analysis by orthogonal time-of-flight mass spectrometry. Rapid Communications in Mass Spectrometry 2001, 15 (23), 2221-2226.

61.   Kaplan, K.; Graf, S.; Tanner, C.; Gonin, M.; Fuhrer, K.; Knochenmuss, R.; Dwivedi, P.; Hill Jr, H. H., Resistive Glass IM-TOFMS. Analytical chemistry 2010, 82 (22), 9336-9343.

62.   Dwivedi, P.; Wu, P.; Klopsch, S. J.; Puzon, G. J.; Xun, L.; Hill Jr, H. H., Metabolic profiling by ion mobility mass spectrometry (IMMS). Metabolomics 2008, 4 (1), 63-80.

63.   (a) Coy, S. L.; Krylov, E. V.; Schneider, B. B.; Covey, T. R.; Brenner, D. J.; Tyburski, J. B.; Patterson, A. D.; Krausz, K. W.; Fornace, A. J.; Nazarov, E. G., Detection of radiation-exposure biomarkers by differential mobility prefiltered mass spectrometry (DMS–MS). International journal of mass spectrometry 2010, 291 (3), 108-117; (b) Schneider, B. B.; Covey, T. R.; Coy, S. L.; Krylov, E. V.; Nazarov, E. G., Planar differential mobility spectrometer as a pre-filter for atmospheric pressure ionization mass spectrometry. International journal of mass spectrometry 2010, 298 (1), 45-54.

64.   Davila, S. J.; Hadjar, O.; Eiceman, G. A., Ion profiling in an ambient drift tube-ion mobility spectrometer using a high pixel density linear array detector ionCCD. Analytical chemistry 2013, 85 (14), 6716-6722.

65.   Johnson, G. E.; Hadjar, O.; Laskin, J., Characterization of the ion beam focusing in a mass spectrometer using an IonCCD™ detector. Journal of the American Society for Mass Spectrometry 2011, 22 (8), 1388-1394.

66.   Hadjar, O.; Johnson, G.; Laskin, J.; Kibelka, G.; Shill, S.; Kuhn, K.; Cameron, C.; Kassan, S., IonCCD™ for direct position-sensitive charged-particle detection: from electrons and keV ions to hyperthermal biomolecular ions. Journal of the American Society for Mass Spectrometry 2011, 22 (4), 612-623.

67.   Montalti, M.; Credi, A.; Prodi, L.; Gandolfi, M. T., Handbook of photochemistry. CRC press: 2006.

68.	Lakowicz, J. R.; Masters, B. R., Principles of fluorescence spectroscopy. Journal of Biomedical Optics 2008, 13 (2), 9901.

69.	Engelking, P. C.; Smith, A. L., Tunable laser fluorescence spectroscopy of the molecular nitrogen cation at 390 nm. Chemical Physics Letters 1975, 36 (1), 21-22.

70.	(a) Bondybey, V.; Miller, T. A., Laser excitation spectra of the CO+ 2 molecular ion A 2Πu→ X 2Πg fluorescence. The Journal of Chemical Physics 1977, 67 (4), 1790-1792; (b) Miller, T. A.; Bondybey, V., Laser induced fluorescence and vibrational relaxation in CO+. Chemical Physics Letters 1977, 50 (2), 275-277.

71.	Sears, T.; Miller, T. A.; Bondybey, V., Laser excitation and emission spectra of the hexafluorobenzene cation in the gas phase. Journal of the American Chemical Society 1981, 103 (2), 326-329.

72.	Grieman, F.; Mahan, B.; O'Keefe, A., Laser induced fluorescence spectrum of trapped CD/sup+. J. Chem. Phys.;(United States) 1980, 72 (7).

73.	Mahan, B. H.; Martner, C.; O'Keefe, A., Laser induced fluorescence studies of the charge transfer reactions of N2+ with Ar and N2. The Journal of Chemical Physics 1982, 76 (9), 4433-4438.

74.	Wang, Y.; Hendrickson, C. L.; Marshall, A. G., Direct optical spectroscopy of gas-phase molecular ions trapped and mass-selected by ion cyclotron resonance: laser-induced fluorescence excitation spectrum of hexafluorobenzene (C 6 F 6+). Chemical physics letters 2001, 334 (1), 69-75.

75.	Cage, B.; McFarland, M. A.; Hendrickson, C. L.; Dalal, N. S.; Marshall, A. G., Resolution of individual component fluorescence lifetimes from a mixture of trapped ions by laser-induced fluorescence/ion cyclotron resonance. The Journal of Physical Chemistry A 2002, 106 (42), 10033-10036.

76.	Cage, B.; Friedrich, J.; Little, R. B.; Wang, Y.-S.; McFarland, M. A.; Hendrickson, C. L.; Dalal, N.; Marshall, A. G., Wavelength resolved laser-induced fluorescence emission of trapped in an ion cyclotron resonance cell. Chemical physics letters 2004, 394 (1), 188-193.

77.	Friedrich, J.; Fu, J.; Hendrickson, C. L.; Marshall, A. G.; Wang, Y.-S., Time resolved laser-induced fluorescence of electrosprayed ions confined in a linear quadrupole trap. Review of scientific instruments 2004, 75 (11), 4511-4515.

78.	Khoury, J. T.; Rodriguez-Cruz, S. E.; Parks, J. H., Pulsed fluorescence measurements of trapped molecular ions with zero background detection. Journal of the American Society for Mass Spectrometry 2002, 13 (6), 696-708.

79.	Forbes, M. W.; Jockusch, R. A., Gas-phase fluorescence excitation and emission spectroscopy of three xanthene dyes (rhodamine 575, rhodamine 590 and rhodamine 6G) in a quadrupole ion trap mass spectrometer. Journal of the American Society for Mass Spectrometry 2011, 22 (1), 93-109.

80.   Duncan, M. A.; Bierbaum, V. M.; Ellison, G. B.; Leone, S. R., Laser-induced fluorescence studies of ion collisional excitation in a drift field: Rotational excitation of N+ 2 in helium. The Journal of chemical physics 1983, 79 (11), 5448-5456.

81.   (a) Frankevich, V.; Barylyuk, K.; Sinues, P. M.-L.; Zenobi, R., Ion mobility spectrometry coupled to laser-induced fluorescence for probing the electronic structure and conformation of gas-phase ions. Journal of Analytical Chemistry 2014, 69 (13), 1215-1219; (b) Frankevich, V.; Martinez-Lozano Sinues, P.; Barylyuk, K.; Zenobi, R., Ion mobility spectrometry coupled to Laser-Induced fluorescence. Analytical chemistry 2012, 85 (1), 39-43.

82.   Danell, A. S.; Parks, J. H., FRET measurements of trapped oligonucleotide duplexes. International Journal of Mass Spectrometry 2003, 229 (1), 35-45.

83.   Chingin, K.; Frankevich, V.; Balabin, R. M.; Barylyuk, K.; Chen, H.; Wang, R.; Zenobi, R., Direct access to isolated biomolecules under ambient conditions. Angewandte Chemie International Edition 2010, 49 (13), 2358-2361.

84.   Kirk, A. T.; Allers, M.; Cochems, P.; Langejuergen, J.; Zimmermann, S., A compact high resolution ion mobility spectrometer for fast trace gas analysis. Analyst 2013, 138 (18), 5200-5207.

85.   (a) Leasure, C.; Fleischer, M.; Anderson, G.; Eiceman, G., Photoionization in air with ion mobility spectrometry using a hydrogen discharge lamp. Analytical Chemistry 1986, 58 (11), 2142-2147; (b) Tabrizchi, M.; Bahrami, H., Improved design for the atmospheric pressure photoionization source. Analytical chemistry 2011, 83 (23), 9017-9023.

86.   Stach, J.; Baumbach, J., Ion mobility spectrometry-basic elements and applications. Int J Ion Mobility Spectrom 2002, 5, 1-21.

87.   (a) Bahrami, H.; Tabrizchi, M., Combined corona discharge and UV photoionization source for ion mobility spectrometry. Talanta 2012, 97, 400-405; (b) Chen, C.; Dong, C.; Du, Y.; Cheng, S.; Han, F.; Li, L.; Wang, W.; Hou, K.; Li, H., Bipolar ionization source for ion mobility spectrometry based on vacuum ultraviolet radiation induced photoemission and photoionization. Analytical chemistry 2010, 82 (10), 4151-4157.

88.   Smith, D. P., The electrohydrodynamic atomization of liquids. IEEE Transactions on Industry Applications 1986, (3), 527-535.

89.   Taylor, G. In Disintegration of water drops in an electric field, Proceedings of the Royal Society of London A: Mathematical, Physical and Engineering Sciences, The Royal Society: 1964; pp 383-397.

90.   Ikonomou, M. G.; Blades, A. T.; Kebarle, P., Electrospray-ion spray: a comparison of mechanisms and performance. Analytical Chemistry 1991, 63 (18), 1989-1998.

91.   Cole, R. B., Electrospray and MALDI mass spectrometry: fundamentals, instrumentation, practicalities, and biological applications. John Wiley & Sons: 2010.

92.   Salleras, M.; Kalms, A.; Krenkow, A.; Kessler, M.; Goebel, J.; Müller, G.; Marco, S., Electrostatic shutter design for a miniaturized ion mobility spectrometer. Sensors and Actuators B: Chemical 2006, 118 (1), 338-342.

93.   (a) Kimmel, J. R.; Engelke, F.; Zare, R. N., Novel method for the production of finely spaced Bradbury–Nielson gates. Review of scientific instruments 2001, 72 (12), 4354-4357; (b) Szumlas, A. W.; Rogers, D. A.; Hieftje, G. M., Design and construction of a mechanically simple, interdigitated-wire ion gate. Review of scientific instruments 2005, 76 (8), 086108.

94.   Wu, C.; Siems, W. F.; Asbury, G. R.; Hill, H. H., Electrospray ionization high-resolution ion mobility spectrometry-mass spectrometry. Analytical chemistry 1998, 70 (23), 4929-4938.

95.   Moore, J. H.; Davis, C. C.; Coplan, M. A.; Greer, S. C., Building scientific apparatus. Cambridge University Press: 2009.

96.   Eichler, H. J.; Eichler, J., Laser: Bauformen, Strahlführung, Anwendungen. Springer-Verlag: 2015.

97.   Whitaker, T.; Bushaw, B., Laser-induced fluorescence analysis of vapor-phase pyrene. The Journal of Physical Chemistry 1981, 85 (15), 2180-2182.

98.   Jandris, L. J.; Forcé, R. K., Determination of polynuclear aromatic hydrocarbons in vapor phases by laser-induced molecular fluorescence. Analytica Chimica Acta 1983, 151, 19-27.

99.   Jandris, L. J.; Force, R. K., Determination of the fluorescence properties of polynuclear aromatic hydrocarbons in the vapor phase and adsorbed on solid supports by laser-induced molecular fluorescence. Analytica Chimica Acta 1985, 175, 333-337.

100.   Niessner, R.; Robers, W.; Krupp, A., Detection of particulate polycyclic aromatic hydrocarbons by laser-induced time-resolved fluorescence. Fresenius' journal of analytical chemistry 1991, 341 (3-4), 207-213.

101.   Riebe, D.; Zühlke, M.; Zenichowski, K.; Beitz, T.; Dosche, C.; Löhmannsröben, H.-G., Characterization of Rhodamine 6G Release in Electrospray Ionization by Means of Spatially Resolved Fluorescence Spectroscopy. Zeitschrift für Physikalische Chemie International journal of research in physical chemistry and chemical physics 2011, 225 (9-10), 1055-1072.

102.   Yoon, O. K.; Zuleta, I. A.; Robbins, M. D.; Barbula, G. K.; Zare, R. N., Simple template-based method to produce Bradbury-Nielsen gates. Journal of the American Society for Mass Spectrometry 2007, 18 (11), 1901-1908.

103.   Spangler, G. E.; Collins, C. I., Peak shape analysis and plate theory for plasma chromatography. Analytical Chemistry 1975, 47 (3), 403-407.

104.   Nagy, A. M.; Talbot, F. O.; Czar, M. F.; Jockusch, R. A., Fluorescence lifetimes of rhodamine dyes in vacuo. Journal of Photochemistry and Photobiology A: Chemistry 2012, 244, 47-53.

105.   Ilbeigi, V.; Tabrizchi, M., Peak–peak repulsion in ion mobility spectrometry. Analytical chemistry 2012, 84 (8), 3669-3675.

106.   Rokushika, S.; Hatano, H.; Baim, M. A.; Hill Jr, H. H., Resolution measurement for ion mobility spectrometry. Analytical Chemistry 1985, 57 (9), 1902-1907.

107.   (a) Shih, T.; Rong, Y.; Harmon, T.; Suffet, M., Evaluation of the impact of fuel hydrocarbons and oxygenates on groundwater resources. Environmental science & technology 2004, 38 (1), 42-48; (b) Zakaria, M. P.; Takada, H.; Tsutsumi, S.; Ohno, K.; Yamada, J.; Kouno, E.; Kumata, H., Distribution of polycyclic aromatic hydrocarbons (PAHs) in rivers and estuaries in Malaysia: a widespread input of petrogenic PAHs. Environmental science & technology 2002, 36 (9), 1907-1918; (c) Booij, K.; Hoedemaker, J. R.; Bakker, J. F., Dissolved PCBs, PAHs, and HCB in pore waters and overlying waters of contaminated harbor sediments. Environmental Science & Technology 2003, 37 (18), 4213-4220.

108.   (a) Bjorseth, A.; Becher, G., Polycyclic aromatic hydrocarbons in workplace atmospheres: occurrence and determination. 1986; (b) Vo-Dinh, T., Chemical analysis of polycyclic aromatic compounds. Wiley: 1989; (c) Grimmer, G.; Brune, H.; Dettbarn, G.; Jacob, J.; Misfeld, J.; Mohr, U.; Naujack, K.-W.; Timm, J.; Wenzel-Hartung, R., Relevance of polycyclic aromatic hydrocarbons as environmental carcinogens. Fresenius' journal of analytical chemistry 1991, 339 (10), 792-795.

109.   (a) Smalley, M. B.; McGown, L. B., Limits of detection and resolution for on-the-fly fluorescence lifetime detection in HPLC. Analytical Chemistry 1995, 67 (8), 1371-1376; (b) Giger, W.; Blumer, M., Polycyclic aromatic hydrocarbons in the environment. Isolation and characterization by chromatography, visible, ultraviolet, and mass spectrometry. Analytical chemistry 1974, 46 (12), 1663-1671.

110.   (a) Sagoo, S. K.; Jockusch, R. A., The fluorescence properties of cationic rhodamine B in the gas phase. Journal of Photochemistry and Photobiology A: Chemistry 2011, 220 (2), 173-178; (b) Bian, Q.; Forbes, M. W.; Talbot, F. O.; Jockusch, R. A., Gas-phase fluorescence excitation and emission spectroscopy of mass-selected trapped molecular ions. Physical Chemistry Chemical Physics 2010, 12 (11), 2590-2598.

111.   Kumke, M.; Löhmannsröben, H.-G.; Roch, T., Fluorescence spectroscopy of polynuclear aromatic compounds in environmental monitoring. Journal of fluorescence 1995, 5 (2), 139-152.

112.   (a) Illenseer, C.; Löhmannsröben, H.; Schultze, R., Application of laser-based ion mobility (IM) spectrometry for the analysis of polycyclic aromatic compounds (PAC) and petroleum products in soils. Journal of Environmental Monitoring 2003, 5 (5), 780-785; (b) Eiceman, G.; Anderson, G.; Danen, W.; Ferris, M.; Tiee, J., Laser desorption and ionization of solid polycyclic aromatic hydrocarbons in air with analysis by ion mobility spectrometry. Analytical letters 1988, 21 (4), 539-552.

113.   Jochims, H.; Baumgärtel, H.; Leach, S., Photoionization quantum yields of polycyclic aromatic hydrocarbons. Astronomy and Astrophysics 1996, 314, 1003-1009.

8 Appendix

8.1 *List of abbreviations and symbols*

e	elementary charge [As]
μ	reduced mass
ν_d	drift velocity [m s^{-1}]
Ω	collision cross section [nm²]
φ	quantum yield
$M\Omega$	Mega ohm
μF	micro Farads
ΔV	bias Voltage [V]
D	Diffusion coefficient
E	electric field strength [V cm^{-1}]
f	focal length [mm]
F	focal point
fA	femto ampere
Hz	Hertz [1 s^{-1}]
K	ion mobility coefficient [cm^{-1} Vs^{-1}]
K_0	reduced mobility coefficient
k_f	fluorescence rate constant
k_{nr}	non radiative transition constant
kV	kilovolts

L_d	drift length
mA	milli ampere
ms	milli seconds
nm	nano meters
ns	nano seconds
N	Number density [molecules per cm^{-3}]
nA	nano ampere
P	Pressure [Torr]
pA	pico ampere
T	Temperature [K]
Td	Townsend [10^{-21} V m²]
t_d	drift time [ms]
t_r	rise time [μs]
T_{eff}	effective Temperature [K]
V	Voltage [V]
V_{ref}	reference Voltage [V]
VA	Volt Ampere
z	charge

BNC	Bajonett Neill-Concelman
BNG	Bradbury-Nielsen-Gate

CCD	charge coupled device
cw	continuous wave
DC	direct current
DMS	differential ion mobility spectrometry
ESI	electrospray ionization
FAIMS	field asymmetric high field ion mobility spectrometry
FWHM	full width at half maximum
GC	Gas chromatography
HV	High Voltage
HPLC	high performance liquid chromatography
ICCD	intensified charge coupled device
IMS	Ion mobility spectrometer
IM MS	Ion mobility mass spectrometry
IMS-LIF	Ion mobility spectrometry laser induced fluorescence detection
I.D.	Inner Diameter
IP	Ionization potential [eV]
LIF	laser induced fluorescence
KDP	Pottasiumdihydrogenphosphate
LASER	light amplification by stimulated emission of radiation
MCP	microchannel plate
MS	Mass spectrometry/Mass spectrometer

O.D.	Outer diameter
PA	proton affinity
PEEK	polyether ether ketone
PI	Photoionization
PAH	polycyclic aromatic hydrocarbons
PID	photo ionization discharge
Q-switch	Quality-switch
RF	radio frequency
RIP	reactant ion positive
SEM	secondary electron multiplier
SPME	solid phase microextraction
TIC	Total ion current
TTL	transistor-transistor logic
TOF	time of flight
TOF-MS	time of flight mass spectrometry
nESI	nano electrospray ionization
VUV	vacuum ultraviolet
VOC	volatile organic compounds

8.2 *List of figures*

8.3 *List of tables*

8.4 *List of publications*

1. 2013, Klaus Kerpen, Andriy Kuklya, Robert Marks, Florian Uteschil, Ursula Telgheder, Development of an ESI-FAIMS/DMS system for rapid water analysis, 5th Water Contamination Emergencies: managing the threats

2. 2014, Andriy Kuklya, Florian Uteschil, Klaus Kerpen, Robert Marks, Ursula Telgheder, Development of an electrospray-63Ni-differential ion mobility spectrometer for the analysis of aqueous samples, Talanta

3. 2015, Andriy Kuklya, Florian Uteschil, Klaus Kerpen, Robert Marks, Ursula Telgheder, Non-polar modifier assisted analysis of aromatic compounds by means of planar differential ion mobility spectrometry with 63Ni ionization source, Analytical methods

4. 2015, Andriy Kuklya, Florian Uteschil, Klaus Kerpen, Robert Marks, Ursula Telgheder, Effect of the humidity on analysis of aromatic compounds with planar differential ion mobility spectrometry, International Journal for Ion Mobility Spectrometry

5. 2015, Andriy Kuklya, Carsten Engelhard, Florian Uteschil, Klaus Kerpen, Robert Marks, Ursula Telgheder, Low-temperature plasma ionization differential ion mobility spectrometry, Analytical Chemistry

6. 2016, Andriy Kuklya, Sasho Joksimoski, Klaus Kerpen, Florian Uteschil, Robert Marks, Ursula Telgheder, Analysis of gasoline contaminated water samples by means of dopant assisted atmospheric pressure photoionization differential ion mobility spectrometry, International Journal for Ion Mobility Spectrometry

7. 2017, Andriy Kuklya, Tobias Reinecke, Florian Uteschil, Klaus Kerpen, Stefan Zimmermann, Ursula Telgheder, X-Ray ionization differential ion mobility spectrometry, Talanta

8.5 *Presentations*

1. 2013, Klaus Kerpen, Andriy Kuklya, Florian Uteschil, Robert marks, Ines Schäfer, Ursula Telgheder, Entwicklung eines ESI-FAIMS-Systems zur schnellen Wasseranalyse, IMS Anwendertreffen, Berlin, oral presentation, Poster

2. 2013, Florian Uteschil, Klaus Kerpen, Andriy Kuklya, Robert Marks, Ursula Telgheder, Analyse von wässrigen Proben mit Elektrospray-63Ni-FAIMS, Anakon 2013, oral presentation

3. 2013, Florian Uteschil, Andriy Kuklya, Klaus Kerpen, Robert Marks, Ursula Telgheder, Design and Development of a desolvation unit for the ESI FAIMS coupling, ISIMS, Boppard, oral presentation

4. 2014, Florian Uteschil, Andriy Kuklya, Klaus Kerpen, Robert Marks, Ursula Telgheder, Design and Development of a desolvation unit for the ESI FAIMS coupling, IMS Anwendertreffen, Essen, oral presentation

5. 2015, Florian Uteschil, Jan Peters, Robert Marks, Klaus Kerpen, Andriy Kuklya, Ursula Telgheder Stir bar sorptive extraction (SBSE) of selected polyaromatic hydrocarbons (PAHs) in combination with thermal desorption - fluorescence spectrometry, (ANAKON) oral presentation, Poster

6. 2015, Florian Uteschil, Klaus Kerpen, Andriy Kuklya, Robert Marks, Ursula Telgheder Dopant assisted Photoionization Ion Mobility Spectrometry (IMS) for Determination of PAH in Aqueous Samples, (ICCE) oral presentation, Poster

7. 2016, Florian Uteschil, Klaus Kerpen, Andriy Kuklya, Robert Marks, Ursula Telgheder, Photoionisations-Ionenmobilitätsspektrometrie in Kombination mit laserinduzierter Fluoreszenzdetektion (IMS-LIF) für die Bestimmung von PAK in wässrigen Proben IMS Anwendertreffen, Hannover, oral presentation

8.6 *Erklärung*

Hiermit versichere ich, dass ich die vorliegende Arbeit mit dem Titel

„Drift tube ion mobility spectrometry laser induced fluorescence detection"

selbst verfasst und keine außer den angegebenen Hilfsmitteln und Quellen benutzt habe, und dass die Arbeit in dieser oder ähnlicher Form noch bei keiner anderen Universität eingereicht wurde.

Essen im Dezember 2016